1-1-2008

Structure and thermodynamics of polyelectrolyte complexes : simulation and experiment.

Zhaoyang Ou
University of Massachusetts Amherst

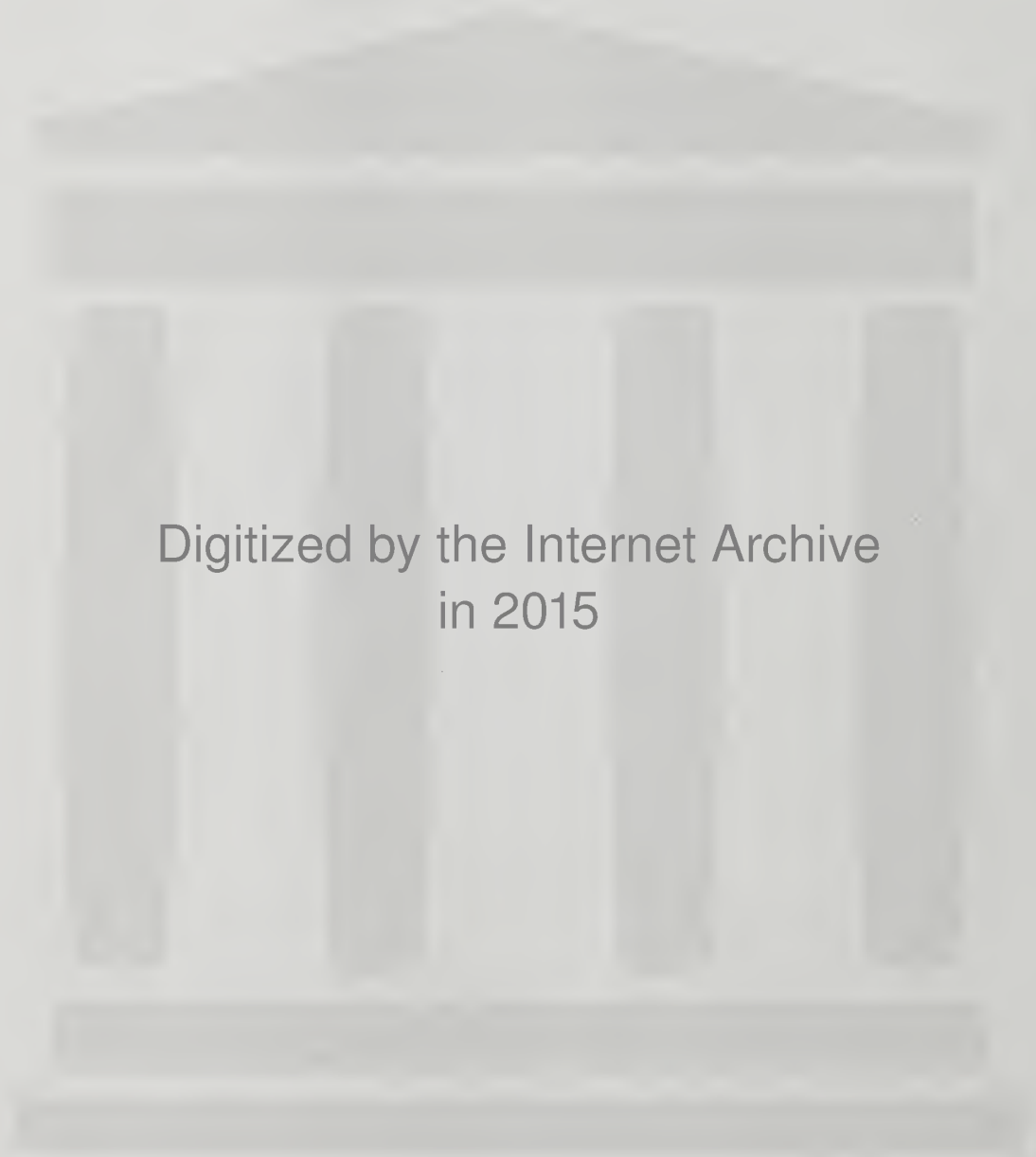

STRUCTURE AND THERMODYNAMICS OF POLYELECTROLYTE COMPLEXES: SIMULATION AND EXPERIMENT

A Dissertation Presented

by

ZHAOYANG OU

Submitted to the Graduate School of the
University of Massachusetts Amherst in partial fulfillment
of the requirements for the degree of

DOCTOR OF PHILOSOPHY

FEBRUARY 2008

Polymer Science and Engineering

STRUCTURE AND THERMODYNAMICS OF POLYELECTROLYTE COMPLEXES: SIMULATION AND EXPERIMENT

A Dissertation Presented

by

ZHAOYANG OU

Approved as to style and content by:

Murugappan Muthukumar, Chair

Todd Emrick, Member

Anthony D. Dinsmore, Member

Shaw Ling Hsu, Department Head
Department of Polymer Science and Engineering

STRUCTURE AND THERMODYNAMICS OF POLYELECTROLYTE COMPLEXES: SIMULATION AND EXPERIMENT

A Dissertation Presented

by

ZHAOYANG OU

Approved as to style and content by:

Murugappan Muthukumar, Chair

Todd Emrick, Member

Anthony D. Dinsmore, Member

Shaw Ling Hsu, Department Head
Department of Polymer Science and Engineering

DEDICATION

To my grandparents Yuliu Ou and Lanmei He

ACKNOWLEDGMENTS

I am most thankful to my thesis advisor, Professor Muthukumar, for his guidance, support, patience and encouragement throughout these years. His unparalled knowledge about polyelectrolytes and his passion for the pursuits of fundamental understandings have been a strong source of motivation for me. I have been very fortunate to have the opportunities to explore some intriguing aspects of polyelectrolytes. I am very grateful for having had the honor of working with him.

I would like to thank my thesis committee members, Professor Todd Emrick and Professor Tony Dinsmore, for their valuable time, insightful questions and suggestions.

I want to thank Professor Todd Emrick and his student, Rebecca B. Breitenkamp, for their collaborations on the project of comb polyelectrolytes. I appreciate their support and patience. It has been a rewarding experience for me.

My sincere appreciations to past and present students and postdocs of the Muthu's group for many discussions, activities and helps: Shulan Liu, Sonoko Kanai, Joe McNamara, Joey Kong, Chi-lun Lee, Jiafang Wang, Vladimir Belyi, Ryan Murphy, Joanna Pool, Arindam Kundagrami, Ajay Panwar, Erica Saltzman, Deniz Kaya, Jianing Zhang, Chris Forrey, Jessica McCoy, Rajeev Kumar, Stephen Mirigian, Mark Kelly, Andrew Wong, Deniz Civay, JP Mahalik, Eliseev Alexander and Xiangdong Gu. I am most indebted to Shulan Liu for his resourcefulness and unselfish helps in computer simulations. I also want to express my sincere gratitude to Sonoko Kanai for leading me her expertise in light scattering experiments on polyelectrolytes.

My life in PSE and Amherst has been made most enjoyable and unforgettable by the people I have met and befriended. Thanks very much to all of you my friends:

Jianing Zhang, Qingling Zhang, Jong-Young Lee, Jiafang Wang, Liming Ding, Zhixiang Lu, Xiaoming Pan, Shujun Chen, Jiayu Wang, Jiangshui Huang, Xiaolin Pu, Cheng Xu, and Bo Pan.

Last and not the least, I would like to thank my family here and in China for their unwavering loves and supports throughout these years. I thank my wife, Liyuan Huang, for her love and care for me and for having given me the most precious gift, our son, Andrew Ou. I would like to dedicate this thesis to my grandparents whose courage, perseverance and optimism are always an inspiring force in my life.

ABSTRACT

STRUCTURE AND THERMODYNAMICS OF POLYELECTROLYTE COMPLEXES: SIMULATION AND EXPERIMENT

FEBRUARY 2008

ZHAOYANG OU, B.E. TSINGHUA UNIVERSITY

M.S. GEORGIA INSTITUTE OF TECHNOLOGY

M.S. UNIVERSITY OF MASSACHUSETTS AMHERST

Ph.D. UNIVERSITY OF MASSACHUSETTS AMHERST

Directed by: Professor Murugappan Muthukumar

Ionic complexes of polyelectrolytes with molecules of opposite polarity are ubiquitous and important in both nature and synthetic arenas. DNA condensation by multivalent counterions enables long stiff DNA chains to be condensed for storage in small volumes such as nuclei and virus capsids. Applications of synthetic polyelectrolytes as complexation (or encapsulation) agents for proteins and nucleic acids have proliferated in recent decades in quest for more effective drug and gene delivery.

This dissertation investigated several aspects of the structure and thermodynamics of polyelectrolyte complexes, using both computer simulation and experimental characterization. We applied a Langevin dynamic simulation to the complexation of a semiflexible polyelectrolyte with multivalent counterions. The central issue is the interplay of polyelectrolyte intrinsic stiffness and counterion valency in shaping ordered structures such as toroid and folded-chain bundles as seen in DNA condensation studies. Also in accordance with experiments, our simulation has uncovered multiple kinetic

pathways leading from disordered to ordered states. The simulation is extended to the complexation by polyelectrolytes of opposite polarities. The major issue is to differentiate enthalpic and entropic contributions to complexation in both weak and strong electrostatic coupling systems. Two regimes of complexation are delineated: (1) enthalpy-driven in weak polyelectrolytes where mutual Coulombic attraction between polycations and polyanions drives complexation; (2) entropy-driven in strong polyelectrolytes where although polycations and polyanions still attract each other strongly, a large entropy gain from releasing condensed counterions during complexation becomes dominant. We have also studied conformational properties of comb polyelectrolytes and their complexes. Static and dynamic light scattering studies reveal that polycyclooctene-g-pentalysine adopts an extended rodlike conformation due to strong electrostatic repulsion of the oligolysine side chains. It is demonstrated that rigid polycyclooctene-g-pentalysine could self-assemble with dsDNA to generate stable nanosized particles whose dimension can be finely adjusted by pH and polyelectrolyte/DNA mixing ratio. In conjunction with experiments, we also set forth to simulate electrostatic-mediated rigidity of comb polyelectrolytes. Interestingly, comb polyelectrolytes of greatest rigidity are those grafted with modestly charged side chains (like oligolysines) which could maximize inter-side chain repulsion without significant disruption from the counterions.

TABLE OF CONTENTS

LIST OF TABLES

LIST OF FIGURES

CHAPTER 1

INTRODUCTION

1.1. Polyelectrolyte

A polyelectrolyte is a polymer that bears many ionizable groups that could readily dissociate into one polyion and many small counterions in water or other polar solvents. Polyelectrolytes play critical biological functions in nature. Nucleic acids, DNA and RNA, are probably the most famous biologically important polyelectrolytes. Proteins, polypeptides, and polysaccharides are several other examples of the essential functions of polyelectrolytic macromolecules in living systems. In addition to natural biological functions, polyelectrolytes have found many important applications in polymer and colloidal solutions, surface modification and analytical chemistry. Polyelectrolytes have been used as thickening reagents and rheology modifiers in health and personal care industry, and as flocculating and coagulating agents in water treatment and the pulp and paper industry. Recently, interests in developing synthetic polyelectrolytes have grown rapidly due to large potential of applying these functional polymers as non-viral encapsulation and delivery vehicles of corrective nucleic acids in gene therapy.

Many applications of polyelectrolytes rely on controlling electrostatic interaction of polyelectrolytes among themselves as well as with other charged objects. Compared to other interactions such as van deer force which act in short range, electrostatic interaction is long-ranged and in polyelectrolyte case is further complicated by long chain architecture. Structure, dynamics, and thermodynamic properties of

polyelectrolytes in water remain one of the least understood systems in polymer science. Yet, many important biological and non-biological applications of polyelectrolytes are continuing to be identified and polyelectrolyte field remains one of the most active areas for both academic and industrial research.

1.2. Polyelectrolyte complexes

Electrostatic complexation between oppositely charged molecules has been long exploited in nature for generating highly-structured functional materials. Crystallization of small salt ions (Na^+ and Cl^-, Cu^{2+} and SO_4^{2-}, etc) from aqueous solution is one elegant example of electrostatic-mediated ionic self-assembly (Figure 1.1(a)). Complexation of polyelectrolyte with molecules carrying opposite charges is implicated in many important biological processes. Chromosome in cell nucleus is known to be made of a long negatively charged DNA molecule wrapping around many positively charged histone proteins. The complexation and condensation of RNA by proteins is critical for successful transport of nucleic acid (and its genetic information) into and out of nucleus membrane. Remarkably, when DNA itself is mixed with simple multivalent ions ($\geq 2+$) *in vitro*, this highly charged rigid chain (average $1e^-$ per 1.7Å in its double-helix backbone) wraps itself into a compacted toroidal condensate with a diameter comparable to DNA persistence length (l_p=50nm) (Figure 1.1(b)). [1, 2] DNA also binds strongly with synthetic cationic polyelectrolytes. In fact, polyelectrolyte/DNA complex (*"polyplex"*) has attracted intense interest in developing highly-efficient low-toxic non-viral DNA delivery vehicles.[3-6] In recent decade, the complexation of oppositely charged synthetic polyelectrolytes has fueled an increasingly important material

innovation, whereby positively and negatively charged polyelectrolytes are alternately adsorbed on a substrate to produce multilayered thin films with tailored functionalities (Figure 1.1(c)).[7]

Synthetic polyelectrolytes offer greater structural variability compared to naturally occurring polyelectrolytes. The charge density of a polyelectrolyte chain can be systematically adjusted by copolymerizing charged and neutral monomers, therefore affecting its binding strength with oppositely charged molecules. Besides linear chains, polyelectrolytes with dendritic and grafted chain architectures can be readily designed and synthesized.[8-13]

The importance of polyelectrolyte complexation is clearly shown in its ubiquitous presence in natural assembly systems and materials science. The challenge in unraveling the fundamental principles of polyelectrolyte complexation is its large parameter space that is shaping the structure, stability and kinetics of polyelectrolyte complex. Polyelectrolyte charge density and architecture, solvent characteristics, ionic strength and temperature all play important roles in the formation of polyelectrolyte complexes. In assessing structures and thermodynamics in polyelectrolyte complexation, two complexities are particularly notable. The first one concerns the spatial correlation between a polyelectrolyte chain and its counterions. Electrostatic repulsion among charged monomers favors an expanded conformation of a polyelectrolyte chain. The repulsion and chain expansion of a polyelectrolyte chain is, however, strongly moderated by counterions drawn to the neighborhood of the chain through the celebrated *"counterion condensation"* mechanism.[14-16] A polyelectrolyte chain in solution is typically enshrouded by a counterion cloud; the number of condensed

counterions within such cloud increases with polyelectrolyte charge density but decreases with the polarity (dielectric constant) of solvent. During complexation with a polyelectrolyte chain, incoming molecules have to compete with and displace condensed counterions. Such ionic exchange process is the key to the understanding of free energy changes (enthalpy and entropy contributions) of polyelectrolyte complexation and ultimately the stability of polyelectrolyte complexes formed. The second one is the roles of the intrinsic stiffness and chain architecture of a polyelectrolyte chain in shaping the structure of polyelectrolyte complex. Due to its multivalent nature, polyelectrolyte chain shows strong attraction for any oppositely charged molecules, particularly so when encountering another polyelectrolyte. The majority of vinyl-based linear synthetic polyelectrolytes are inherently flexible (l_p in the range of 1-5nm). Hence, with strong electrostatic attraction, a polyelectrolyte complex made of synthetic polymers resembles a scrambled-egg like amorphous globule. Intriguing ordered structures (toroid, rod, "tennis racket" morphologies) arise with the use of biologically originated polyelectrolytes (DNA[1, 2], Actin filament,[17, 18] Xthantan,[19-21] etc) which possess a much higher intrinsic stiffness (l_p from 25nm to several μm). Recently, synthetic polyelectrolytes densely grafted with charged side chains have become increasingly accessible[22-25]. The conformation rigidity of such comb-like polyelectrolyte is driven by both steric and electrostatic repulsions among charged side chains. This class of polyelectrolyte has been developed in the polymer chemist Professor Todd Emrick's group in efforts to develop novel non-viral gene therapy vehicles. It is therefore both fundamentally and practically important to

understand the how a conformationally rigid comb-like polyelectrolyte interacts electrostatically with oppositely charged molecules.

1.3. Langevin dynamics simulation of polyelectrolytes

Despite of many excellent experimental and theoretical works on polyelectrolytes, establishing structure-property correlation in a multi-component polyelectrolyte system remains a daunting challenge. With the advent of faster computation facility and maturing coarse-grained molecular models, computer simulation has offered a new and powerful way to understand the intriguing behaviors of polyelectrolytes. It is in principle possible to parameterize all the essential elements of a real system in a computation study. For example, a molecular dynamic simulation of a polyelectrolyte solution can include representations of the polyelectrolyte chain, all its counterions, salt ions (if present) and water molecules, with explicit molecular details. However, simulation of such a large system is currently limited by its short time scale, typically in the nanosecond scale. This is in contrast with the microsecond scale that characterizes most of the interesting dynamic processes in polyelectrolytes. It is necessary to develop and use effective and efficient simulation methodologies in order to capture the essential physics in desirable length and time scale.

Many variations of coarse-grained polymer models have been proposed with different levels of treatments of molecular interactions. Bond-spring model has been one of the most successful simulation methods in many neutral polymer systems.[26] A polyelectrolyte chain will be modeled as a *bead-spring* chain. Monomer(s) is

represented by a bead with certain diameter. These beads are connected by elastic springs (bonds) to generate a linear chain. Each bead carries one negative electrical charge in its center. Chain intrinsic stiffness is approximated by introducing a bending penalty for two successive bonds in a chain to deviate from equilibrium bond angle. The higher the bending penalty is, the stiffer the chain behaves. By adjusting this bending penalty level, polyelectrolytes with a spectrum of stiffness, from completely flexible to rod-like, can be investigated. Neutralizing counterion of a polyelectrolyte chain is modeled by a sphere of certain diameter and mass. The electrical charge(s) (1, 2, or 3) of counterions are located in the center of the sphere. Figure 1.2 is a cartoon of a bead-spring chain model and spherical counterions.

Polyelectrolyte and its counterions are immerged in a solvent that is inexplicitly modeled as a dielectric continuum of certain dielectric constant, ε. Having built the molecular models, we use the Langevin equation (Eq. (1.1)) to simulate the motions of a chain and counterions in the solution.

$$m\frac{d^2\mathbf{r}_i}{dt^2} = -\zeta \boldsymbol{v}_i - \nabla_{\mathbf{r}_i} U + \mathbf{F}_i(t). \tag{1.1}$$

where $\mathbf{m}$ and ξ are the mass and the friction coefficient, respectively, of the i^{th} particle. $\boldsymbol{U}$ is the total potential energy acting on the i^{th} particle. $\mathbf{F}_i(t)$ is the random force from the dielectric medium acting on the i^{th} particle. The value of $\mathbf{F}_i(t)$ is randomly generated in the simulation within the restriction of Fluctuation-Dissipation theorem,

$$\langle \mathbf{F}_i(t) \cdot \mathbf{F}_j(t') \rangle = \delta_{ij} 6 k_B T \zeta \delta(t - t') \quad \textbf{(1.2)}$$

where k_BT is the Boltzmann constant times the absolute temperature, and δ represents a delta function. The total potential energy, U, in Eq. (1.2) experienced by a particle (bead, or counterion) in a solution is the sum of several contributions: (1) Bond stretching; (2) Bond angle bending potential; (3) Excluded volume interaction; (4) more importantly, Columbic interaction. Various models and formulations have been put forward to calculate these contributions and will depend on the system to be simulated on (for detailed models and parameters, see the chapters below). On the start of simulation, one polyelectrolyte chain and an exact number of neutralizing counterions are generated randomly inside a cubic box (with periodical boundaries). Then, the motion of each particle is simulated by integrating the Eq. (1.1) with the potential energy, U, calculated from the coordinates of all the particles within the simulation box. The coordinates of each particle within then box is updated after each simulation step(δt), which leads to new interaction potential energy, U, for each particle at next simulation step. The simulation is carried out until the system reaches its equilibrium state. During a simulation run, data on position and velocity of all particles are saved. Interesting physical quantities such as radius of gyration and system Columbic energy are then computed from stored data.

The rest of the dissertation will be organized as follows: Chapter 2 describes a Langevin dynamic simulation study on the complexation of semiflexible polyelectrolyte with multivalent counterions. Chapter 3 contains the results from a systematic simulation study on the free energy changes (enthalpy and entropy) in complexation of

oppositely charged flexible polyelectrolytes. Chapter 4 first describes static and dynamic light scattering studies on conformational properties of novel oligopeptide-*g*-polycyclooctenes in water. This is followed by the formation and characterizations of dsDNA complexes with pentalysine-*g*-polycyclooctene. Last, a computer simulation study is reported on conformational properties of a general comb polyelectrolyte model, with emphasis on correlating structural and environmental parameters with electrostatic-mediated rigidity of comb polyelectrolytes.

1.4 References

1. V. A. Bloomfield, Current Opinion In Structural Biology 6, 334 (1996).

2. N. V. Hud and K. H. Downing, Proceedings Of The National Academy Of Sciences Of The United States Of America 98, 14925 (2001).

3. O. Boussif, F. Lezoualch, M. A. Zanta, M. D. Mergny, D. Scherman, B. Demeneix, and J. P. Behr, Proceedings Of The National Academy Of Sciences Of The United States Of America 92, 7297 (1995).

4. F. D. Ledley, Human Gene Therapy 6, 1129 (1995).

5. D. Luo and W. M. Saltzman, Nature Biotechnology 18, 33 (2000).

6. M. Nishikawa and L. Huang, Human Gene Therapy 12, 861 (2001).

7. G. Decher, Science 277, 1232 (1997).

8. Nisato, R. Ivkov, and E. J. Amis, Macromolecules 33, 4172 (2000).

9. P. Welch and M. Muthukumar, Macromolecules 31, 5892 (1998).

10. S. Forster, I. Neubert, A. D. Schluter, and P. Lindner, Macromolecules 32, 4043 (1999).

11. V. Percec, C. H. Ahn, G. Ungar, D. J. P. Yeardley, M. Moller, and S. S. Sheiko, Nature 391, 161 (1998).

12. J. K. Wolterink, J. van Male, M. Daoud, and O. V. Borisov, Macromolecules 36, 6624 (2003).

13. B. Zhang, F. Grohn, J. S. Pedersen, K. Fischer, and M. Schmidt, Macromolecules 39, 8440 (2006).

14. G. S. Manning, Quarterly Reviews Of Biophysics 11, 179 (1978).

15. S. Liu and M. Muthukumar, Journal Of Chemical Physics 116, 9975 (2002).

16. M. Muthukumar, Journal Of Chemical Physics 120, 9343 (2004).

17. J. X. Tang, J. A. Kas, J. V. Shah, and P. A. Janmey, European Biophysics Journal With Biophysics Letters 30, 477 (2001).

18. J. X. Tang, S. E. Wong, P. T. Tran, and P. A. Janmey, Berichte Der Bunsen-Gesellschaft-Physical Chemistry Chemical Physics 100, 796 (1996).

19. G. Maurstad and B. T. Stokke, Current Opinion In Colloid & Interface Science 10, 16 (2005).

20. G. Maurstad, S. Danielsen, and B. T. Stokke, Journal Of Physical Chemistry B 107, 8172 (2003).

21. G. Maurstad and B. T. Stokke, Biopolymers 74, 199 (2004).

22. R. Djalali, S. Y. Li, and M. Schmidt, Macromolecules 35, 4282 (2002).

23. T. Stephan, S. Muth, and M. Schmidt, Macromolecules 35, 9857 (2002).

24. B. Zhang, K. Fischer, and M. Schmidt, Macromolecular Chemistry And Physics 206, 157 (2005).

25. N. Gunari, M. Schmidt, and A. Janshoff, Macromolecules 39, 2219 (2006).

26. A. Milchev, W. Paul, and K. Binder, Journal Of Chemical Physics 99, 4786 (1993).

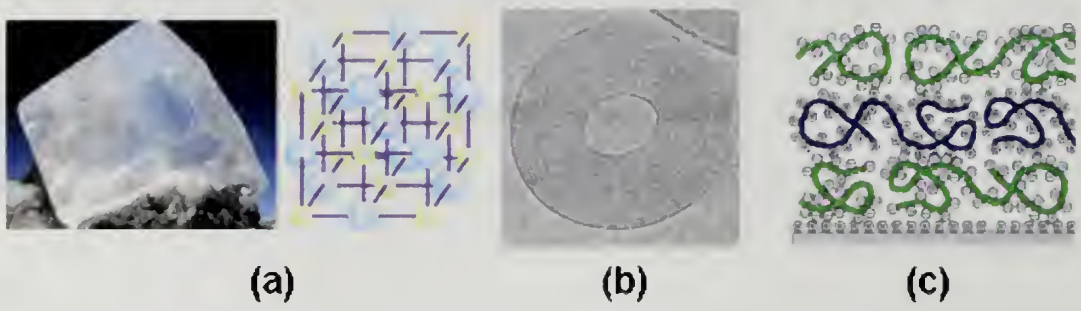

Figure 1.1 Examples of electrostatic-mediated self-assembly. (a) Left: sodium chloride salt crystal; right: cubic lattice model for NaCl salt. Blue sphere is the chloride ion and yellow one is the sodium ion. (b) Toroidal DNA condensate[2]; (c) Layer-by-layer alternate adsorption of cationic and anionic polyelecrolytes on a charged substrate.

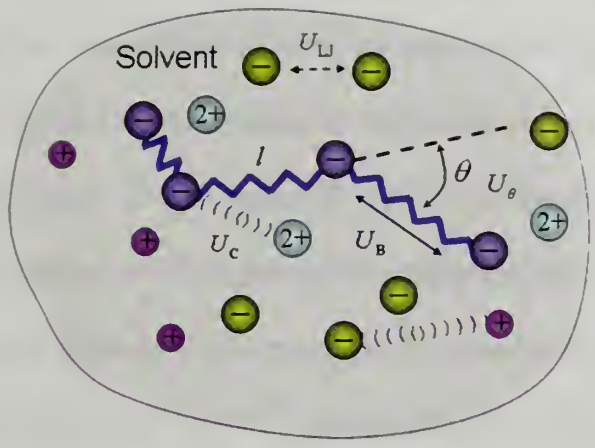

Figure 1.2 The bead-spring representation of a polyelectrolyte chain. Counterions are modeled as spheres. The meanings of various interaction potentials can be found in the text.

CHAPTER 2

COMPLEXATION OF SEMIFLEXIBLE POLYELECTROLYTES WITH MULTIVALENT COUNTERIONS

2.1 Introduction

The analogs of the coil-globule and rod-coil transitions of uncharged polymer molecules for polyelectrolytes are yet to be understood. The main challenge arises from the difficulties in the experimental characterization of polyelectrolytes in terms of their structures and net electric charge. However, there is a converging description for isolated flexible polyelectrolyte molecules, as to the nature of electrostatic expansion and counterion distribution. This progress has been made by a combination of experimentation,[1-8] analytical theory,[9-21] and computer simulations.[22-29] In this study, we extend previous studies of flexible polyelectrolyte chains[27,28] to semiflexible polyelectrolytes.

It is known experimentally that semiflexible polyelectrolytes with intrinsic chain stiffness exhibit several intriguing phenomena, not seen with flexible polymer molecules. For example, dsDNA[30-39] and other stiff biomacromolecules[40,41] undergo a transition from extended chain configuration to compacted toroidal structure, upon addition of multivalent condensing ions. Sometimes, bundle-like folded-chain structures are also seen along with toroidal ones. The transition between toroid and folded-chain bundle has been directly followed by real-time *in situ* atomic force microscopy (AFM) study,[42] pointing to the dynamic nature of these condensed structures. Computer simulations have been previously used to investigate the stability of toroids for

semiflexible uncharged polymers with prescribed short-range attraction.[43-49] In addition, there has been a preliminary molecular dynamics simulation of toroids formed by semiflexible DNA molecules in the presence of counterions of valency greater than or equal to 3.[26]

In the present chapter we address several fundamental issues pertinent to the configurations of semiflexible polyelectrolyte chains, which are yet to be understood. First we report systematic simulations of counterion distribution around semiflexible polyelectrolyte chains and compute the degree of counterion adsorption (condensation) as a function of chain stiffness, counterion valency, and the strength of electrostatic interaction. Using the results of simulations, we represent the effect of intrachain electrostatic excluded volume interactions in terms of an electrostatic persistence length parameter l_p, with its definition in line with ongoing discussions on this topic. The dependence of l_p on electrostatic strength and chain stiffness is explored systematically. We also find, in our simulations, the compactified structures of stiff polyelectrolyte chains in the presence of multivalent counterions, as seen in experiments with biomacromolecules. Our simulations show in vivid detail the kinetic pathways of formation of compact structures such as toroids and folded-chain states, and challenge the existing theoretical attempts on toroids formed by stiff polymer chains.

We have simulated uniformly charged polymers of N segments in a neutralizing dielectric bath (dielectric constant, ε) of volume L^3 containing N/Z_c counterions, each with valency of Z_c. The intrinsic chain stiffness is modeled by a harmonic bending potential between two adjacent bonds with a force constant K. In the present simulations,

electrostatic interactions follow the Coulomb law with counterions described explicitly. The strength of electrostatic interaction among ions is parameterized by the Coulomb strength parameter, Γ, proportional to $1/(\varepsilon T)$, where T is the absolute temperature. We have investigated systematically the role of N, L, Z_c, K, and Γ in determining the various structural properties of the polymer and counterion distribution. In the following results, temperature appears only through Γ with the multiplicative combination of T and the temperature-dependent ε. As an example, for the case of water and the charge separation distance along the chain being 0.17 nm (roughly corresponding to that of dsDNA), Γ changes from about 4.18 at 20 °C to about 4.81 at 70 °C. The values of Γ explored outside this range of Γ for water are envisaged for other polar solvents and to seek a fundamental understanding of compactification of semiflexible polyelectrolyte chains by counterions.

The present simulations show that the degree of ionization of semiflexible polyelectrolytes in salt-free solutions decreases continuously with the Coulomb strength parameter Γ ($\sim 1/\varepsilon T$). For a given value of εT, the degree of ionization is higher for stiffer chains. On the other hand, the radius of gyration increases first with Γ and then decreases as the counterions progressively adsorb to the polymer as εT is decreased. For very stiff chains, R_g is independent of Γ. At larger values of Γ and with multivalent counterions, sufficiently stiff polyelectrolyte (but not rigid rodlike) chains form toroidal structures in contrast with the disordered globules formed by flexible polyelectrolytes. The formation of toroids follows very complex kinetic pathways involving diverse set of metastable structures. The average radius of toroids is found to be roughly

proportional to chain length, in contrast with other simulations and scaling results for toroids from uncharged stiff chains.

2.2 Simulation Method

We model the polyelectrolyte molecule as a freely rotating chain of N spherical beads, each with point unit electric charge $-e$. The counterion is treated as a sphere with point electric charge of $Z_c e$, where Z_c is the valency of the counterion. One polyelectrolyte molecule and N/Z_c counterions are placed in a medium of uniform dielectric constant ε and the medium is taken to be a cubic box of volume L^3. Periodic boundary conditions are applied in our simulations.

The total potential energy of the system consists of the following four parts:

(i) Bond stretch. The potential energy associated with bond stretching of each bond of the chain is taken to be

$$U_{\text{bond}} = k_b(l - l_0)^2, \tag{2.1}$$

where l is the bond length and l_0 is the equilibrium bond length. We have used l_0 as the unit of length. The spring constant k_b is taken to be high enough (i.e., $5000\,\varepsilon_{\text{LJ}}/l_0^2$) to allow fluctuation of the bond length within 10% of l_0.

(ii) Excluded volume. The excluded volume interaction between non-bonded beads of the chain is taken as a purely repulsive Lennard-Jones (LJ) potential

$$U_{\mathrm{LJ}} = \begin{cases} \epsilon_{\mathrm{LJ}}\left[\left(\frac{\sigma}{r}\right)^{12} - 2\left(\frac{\sigma}{r}\right)^{6} + 1\right], & r \leq \sigma \\ 0, & r > \sigma, \end{cases} \tag{2.2}$$

where $\varepsilon_{\mathrm{LJ}}$ is the interaction strength, σ is the distance at which force is zero, and r is the distance between two beads. $\varepsilon_{\mathrm{LJ}}$ is used as the unit of energy in our system. We have used the same form of potential as in Eq. (2.2) to capture the nonelectrostatic excluded volume interactions between polymer beads and counterions. The values of σ are taken as $1.0l_0$, $0.8l_0$, and $0.6l_0$ for bead–bead, bead–counterion, and counterion–counterion, respectively. The values of σ parameters depend on the extent of excluded volume interactions mediated by solvent molecules. Due to the absence of *ab initio* calculations of the pair potentials and the lack of knowledge on the sizes of hydrated ions near polymer chains, we have considered here only a model system.

(iii) Bending. The bending energy between two successive bonds is taken as

$$U_{\mathrm{bend}} = K(\theta - \theta_0)^2, \tag{2.3}$$

where θ is the bond angle between two adjacent bond vectors at any given configuration and θ_0 is the equilibrium bond angle for the model stiff chain, which is taken as 180°. K is the bending force constant and is varied from 0 to 3000 to study the effect of chain stiffness.

(iv) Electrostatic interaction. The electrostatic interaction among charged beads and counterions is taken to be the Coulomb energy

$$U_C(r_{ij}) = \frac{Z_i Z_j e^2}{4\pi\epsilon_0 \epsilon r_{ij}}, \tag{2.4}$$

where r_{ij} is the distance between ions i and j, and Z_k is the valency of the kth ion (Z_k=Z_c=−1 for the bead and Z_k=Z_c for the counterion). e is the unit electric charge, ε_0 is the permittivity of vacuum, and ε is the relative dielectric constant of the medium.

In this paper, the key parameters of electrostatic interaction are the Bjerrum length, l_B, and Coulomb strength parameter Γ defined by

$$l_B = \frac{e^2}{4\pi\epsilon_0 \epsilon k_B T}, \tag{2.5}$$

$$\Gamma = \frac{l_B}{l_0}, \tag{2.6}$$

with $k_B T$ being the Boltzmann constant times the absolute temperature T. In our simulations, we studied the effect of temperature and Coulomb interaction strength through Eqs. (2.5) and (2.6). We have adopted Ewald summation technique[50] to compute the electrostatic interaction potential U_C.

The solvent of uniform dielectric constant ε is modeled as a Langevin thermostat. The dynamics of the i^{th} particle (either bead or counterion) is taken as

$$m\frac{d^2\mathbf{r}_i}{dt^2} = -\zeta \boldsymbol{v}_i - \nabla_{\mathbf{r}_i} U + \mathbf{F}_i(t), \tag{2.7}$$

where m and ξ are the mass and the friction coefficient, respectively, of the i^{th} particle. U is the total potential energy ($U=U_{LJ}+U_{bond}+U_{bend}+U_C$) acting on the i^{th} particle. $\mathbf{F}_i(t)$ is the random force from the bath acting on the i^{th} particle and is stipulated to satisfy the fluctuation-dissipation theorem

$$\langle \mathbf{F}_i(t) \cdot \mathbf{F}_j(t') \rangle = \delta_{ij} 6 k_B T \zeta \delta(t - t') \tag{2.8}$$

The velocity-Verlet finite-differencing scheme has been used for integration of Eq. (2.7). In the present simulations, we have taken the mass of polymer beads as unit mass, and m=0.5 for the mass of counterions. Friction coefficient is chosen as constant τ^{-1} where $\tau=\sqrt{m\sigma^2/\varepsilon_{LJ}}$ is the time unit of the system. In defining this time unit, we have taken m and δ to be 1 and l_0, respectively. Given the multidimensionality of the parameter space, we have extensively experimented with different choices of the integration time step δt. For the ranges of values of parameters studied here, all choices of δt from 0.0002 to 0.007 gave equivalent results for radius of gyration, radial distribution functions, etc. The only place where the choice of δt affects is the initial time for the approach of equilibrium which is usually about 500 time steps. In the interest of saving computational time, we set δt to be 0.007 in units of τ. The total duration of each simulation run takes from 10^7 to 2×10^8 time steps, depending on the selection of system parameter sets, N, Γ, Z_c, and L. The ranges of values studied in the current work are N=30–180, Γ =0.1–7.0, $L=60l_0$–$250l_0$, K=0–3000, and Z_c=1–3. The range of monomer density $\rho=Nl_0^3/L^3$ is 1.92×10^{-6}–8.3×10^{-4}. Although we have investigated a wider range of parameter values in the hope of addressing the role of arbitrary chain stiffness, only

particular values are relevant to particular systems. As an example, Γ changes from about 4.18 at 20 °C to about 4.81 at 70 °C for an aqueous solution of dsDNA.

In a typical simulation run, one polyelectrolyte chain and an exact number of neutralizing counterions are randomly generated inside the simulation box. Then, the Langevin dynamics simulation [Eq. (2.7)] is carried out for the prescribed total time steps. During the simulation run, data on position and velocity of all particles are saved at every 1000 time steps. Physical quantities discussed below are then computed from the stored data on simulations.

2.3 Results and Discussion

2.3.1 Uncharged Semiflexible Polymer

Before a consideration of electrostatic effects on a stiff polymer molecule, we present the results on the size and shape of an uncharged stiff polymer in the parameter space used in this paper. Taking U_C=0, we have calculated the mean-square end-to-end distance $\langle R^2 \rangle$, average radius of gyration, R_g, and hydrodynamic radius, R_h, defined by

$$\langle R^2 \rangle = \sum_{i=1}^{N-1} \sum_{j=1}^{N-1} \langle \mathbf{r}_{i+1,i} \cdot \mathbf{r}_{j+1,j} \rangle, \tag{2.9}$$

$$\langle R_g^2 \rangle = \frac{1}{N} \sum_{i=1}^{N} \langle r_i^2 \rangle, \tag{2.10}$$

$$\frac{1}{R_h} = \frac{1}{N^2}\sum_{i=1}^{N}\sum_{j=1, j\neq i}^{N}\left\langle \frac{1}{r_{ij}} \right\rangle. \tag{2.11}$$

for different values of N, K, and Γ. In Eqs. (2.9),(2.10), and (2.11), $\mathbf{r}_i$ is the distance of the ith bead from the center of mass of the chain, $\mathbf{r}_{i+1,i}=\mathbf{r}_{i+1}-\mathbf{r}_i$, and the angular brackets indicate the averaging over chain configurations. All lengths are expressed in units of l_0.

The effect of the stiffness parameter K on the N dependence of the root-mean-square end-to-end distance $R_e=\langle R^2\rangle^{1/2}$, and R_g is given in Figs. 1.(a) and 1.(b). The data in Fig. 1(b) are replotted in the double-logarithmic plot of Fig. 1(c) to identify the effective size exponent, defined through $R_g \sim N^{\nu}$. In the flexible chain limit, K=5.0, ν =0.62±0.01 corresponding to the self-avoiding walk limit. In the stiff chain limit, K=3000.0, ν=0.93±0.01 corresponding to the approach of the rodlike limit. Perfect rods are not investigated in this paper. The results were obtained at the reduced temperature (k_BT/ε_{LJ}) of 1.1 and $L=1.5Nl_0$ corresponding to $\rho=8/27N^2$. For the repulsive Lennard-Jones interaction used in calculating the above statistics, R_e and R_g are insensitive to the temperature as shown extensively for the case of flexible chains in Ref. 27. To put our simulation results in the context of recent extensive interest in the electrostatic persistence length of polyelectrolyte chains, we have calculated the persistence length l_p in two nonidentical ways. In the first, l_p is fitted to the Kratky–Porod result relating $\langle R^2\rangle$ and N, [51]

$$\langle R^2\rangle = 2Nl_p - 2l_p^2\left[1-\exp\left(-\frac{N}{l_p}\right)\right]. \tag{2.12}$$

where all lengths are in units of l_0. In the second method[52]

$$l_p = \frac{1}{2} \sum_{i=1}^{(N/2)-1} \langle \mathbf{a}_0 \cdot (\mathbf{a}_i + \mathbf{a}_{-i}) \rangle, \tag{2.13}$$

where $\mathbf{a}_i = \mathbf{r}_{N/2+i} - \mathbf{r}_{N/2+i+1}$. The values of l_p are plotted against N in Fig. 2 for different values of K. For the flexible limit, l_p is essentially independent. For the semiflexible region, l_p is strongly N dependent reflecting the nature of crossover between flexible and rod limits. It must be noted that the value of l_p for semiflexible chains depends very strongly on its definition. The value of l_p obtained by fitting with the Kratky–Porod formula of Eq. (2.12), as typically done in experimental investigations, is significantly higher (filled symbols) than that obtained from the correlation function of Eq. (2.13) (open symbols). We give below both values of l_p when we report the effects of electrostatic interaction. One of the experimental measures of the shape of the chain is the ratio R_g/R_h. This ratio is plotted in Fig. 3 against N for different values of K. The ratio increases from about 1.25 (corresponding to self-avoiding-walk configurations) to about 2.25 (corresponding to slender-rodlike configurations) as the chain stiffness increases.

2.3.2 Size and Shape of the Polyelectrolyte with Monovalent Counterion

We have calculated $\langle R^2 \rangle$, R_g, R_h, and l_p for different values of N, L, K, Γ, and Z_c (=1, 2, and 3, corresponding to the monovalent, divalent, and trivalent, respectively). First, we consider Z_c=1 and typical results for the various structural quantities. R_g for

N=90 and L=105l_0 (or monomer density ρ=7.8×10^{-5}), is plotted against Γ in Fig. 4 for K=0, 10, 50, and 3000. Snapshots of typical polymer configurations are included for K=0, and K=3000 at Γ =3.0. The result for the flexible limit K=0 is fully consistent with the previous results.[22,23,27,28] For a flexible polyelectrolyte chain, R_g depends nonmonotonically on Γ. For very stiff polyelectrolyte chains, R_g is essentially independent of Γ, due to the negligible intrachain electrostatic repulsion in comparison with the intrinsic chain stiffness energy. The crossover between these two limiting behaviors is depicted in Fig. 4 for intermediate values of K. The nonmonotonic dependence of R_g on Γarises from a combination of temperature-dependent Coulomb interaction strength between polymer beads and adsorption strength of counterions on the polymer.[16,22,23,27] For Γ up to about 0.5, intrachain electrostatic repulsion is progressively manifest as $1/(\varepsilon T)$ increases. But for Γ larger than 0.5, this repulsion is mitigated by adsorption of counterions, which then leads to chain shrinkage. The overall effect of these contributions is the nonmonotonic dependence of R_g on Γ. The extent of chain shrinkage due to the counterion adsorption gets weaker as the chain gets stiffer. As an example, while the flexible polyelectrolyte chain is globular at Γ =6.5 (i.e., at K=0.0, R_g=6.0, more dense than its uncharged counterpart R_g=7.1), the stiff chain with K=50 is still more expanded (R_g=17.5) than the size with only LJ interactions (R_g=15.0).

As mentioned above, there is considerable interest in describing the consequences of intrachain electrostatic interactions in terms of an electrostatic persistence length. The values of the parameter l_p as defined through Eqs. (2.12) and (2.13) are presented in Fig. 5(a) in terms of Γ for N=90 and K=50. For these values of N and K, l_p=10 for the

uncharged chain. The effective persistence length of the charged semiflexible polyelectrolyte chain is higher than that for the uncharged polymer, due to electrostatic expansion in the salt-free case. For example, for $\Gamma \rightarrow 0$ (i.e., 0.1), l_p [as obtained by local tangent vector correlation, Eq. (3.5)] is about 20 in units of l_0 (N=90, K=50, and Z_c=1), in comparison to about 10 for the uncharged chain. It is to be noted that the actual value of l_p depends on the definition of l_p. In general, l_p as defined through the Kratky–Porod formula of Eq. (2.12) is higher than that defined through correlations of bond orientations. Nevertheless, l_p is seen to depend on Γ nonmonotonically, reflecting the non-monotonicity of R_g on Γ (Fig. 4). The expansion of the polymer size due to electrostatic interaction can equivalently be described as chain swelling due to electrostatic excluded volume effect. The shape ratio R_g/R_h, of interest in light-scattering studies of dilute polyelectrolyte solutions, is plotted against Γ in Fig. 5(b) for N=90, K=50, and Z_c=1. The polyelectrolyte chain is more anisotropic than the uncharged polymer ($R_g/R_h \simeq 1.7$), especially for intermediate values of Γ, due to the additional electrostatic contribution.

2.3.3 Size and Shape of the Polyelectrolyte with Multivalent Counterion

In marked contrast with the case of monovalent counterions for high Coulomb strength parameter Γ, where disordered globules form, divalent and trivalent counterions lead to the formation of toroidal and folded-chain structures if the stiffness parameter K is sufficiently high (i.e., $K \geq 50$ for N=90). The dependence of R_g on Γ is given in Figs. 6(a) and 6(b) for divalent and trivalent counterions, respectively.

Snapshots of typical configurations at selected values of Γ are also included in these figures. The generic dependence of R_g on Γ is similar to that in Fig. 4, except that more ordered toroids and fold-chain bundles are seen at high Γ values (i.e., lower εT). We discuss the details of these ordered structures in Sec. III E.

2.3.4 Counterion Distribution

As mentioned above, when εT is low enough such that $\Gamma \geqslant 0.5$, the attraction between the beads and counterions begins to take effect. Close examination of the position of counterions reveals that the counterion distribution around the polyelectrolyte is dynamic and that the average density of counterions near the polymer is higher than that in the bulk. Following the procedure in Ref. 27, we construct a tube around the chain backbone in a given chain configuration. The tube is a non-overlapping superposition of spheres of fixed radius r_c centered at each bead position. The cutoff parameter r_c is set at $2l_0$ at which the electrostatic energy $l_B k_B T/r_c$ between two monovalent charges equals the kinetic energy $3k_B T/2$. In this setting, l_B is assumed to be roughly $3l_0$. More details on the consequences of the choice of r_c are given in Ref. 27. We then count the number n_c of all counterions inside the tube, and by averaging over all chain configurations, we calculate the effective degree of ionization α of the polyelectrolyte chain,

$$\alpha = \frac{N - \langle n_c \rangle}{N} \tag{2.14}$$

The dependence of α on Γ is shown in Fig. 7. The shape of all the curves is qualitatively the same for different counterion valencies and chain stiffness. A significant drop in α occurs around $\Gamma \cong 1.0$ as counterions begin to adsorb on the chain.[9-11] Naturally, for the same set of $\Gamma$and K values, multivalent counterions are more effective in neutralizing the polymer charge than monovalent counterions. It is also obvious from the curves in Fig. 7 that stiffer chains have a higher degree of ionization, in agreement with the predictions of a recent theory of counterion condensation on flexible polyelectrolytes.[16] The primary reason for this effect is due to the diminished local monomer charge density for stiffer chains with a consequent gain in the translational entropy of unabsorbed counterions. It is of interest that when toroidal and folded-chain structures are formed, the degree of ionization is essentially zero, in agreement with the results of Ref. 53.

To emphasize the adsorption mechanism of counterion condensation along the polymer chain, we have varied the volume of the simulation, whereby varying the translational entropy of counterions. If the polymer concentration is low, translational entropy favors more spreading of counterions so that α is higher. This argument is supported by our simulation results as depicted in Fig. 8, where α is plotted against C_P/C_P^* for different values of N and Z_c. Γ is fixed at 1.5. Here, C_P^* is the overlapping concentration of polymer, defined as $2(3)^{5/2}/\pi N^2 l_0^3$ by assuming the chain to be rodlike.

2.3.5 Toroid

As seen in Fig. 6, for a stiff chain with bending force constant K=50, the toroidal and folded-chain condensates appear only above a certain threshold value of Γ, Γ^*. Γ^* is

about 2 and 3, respectively, for trivalent and divalent counterions. No such ordered structures are seen in our simulations for monovalent counterion. These results are in agreement with the general trends found in experiments.[32, 54-57] For a long dsDNA in aqueous solutions, counterions of valence $\geqslant 3$ are required to form toroids. Divalent cations are also effective in condensing dsDNAs into toroids in mixed solvents with lower dielectric constant (stronger electrostatic interaction, or large Γ).[31,33,58] Thus the minimal model presented here is able to capture the essential features of DNA toroid formation.[59,60]

As seen in our simulations, the kinetic pathway of formation of toroids involves several metastable states. An example is the case of N=180, Γ=2.0, K=70, and Z_c=3. The time evolution of toroid formation for this case is given in Fig. 9 as a series of snapshots where the values of reduced time are 200, 1530, 1940, 4100, 5210, 5500, 6140, 8200, and 10 000, respectively for (1)–(9), starting from a random configuration at t=0. A nucleus is formed first, which consists of a looplike structure containing continuously bending portion of the chain and a few multivalent counterions. The nucleation can occur at essentially any point along the chain contour. This nucleus then grows by circumferentially wrapping other beads until all beads are in the toroid. During this growth stage, the radius of the original looplike nucleus changes (sometimes by expanding and other times by shrinking) to reach an optimum radius at later times. For example, the toroid has four loops right after all the beads have adsorbed on the nucleus and then, through dynamic cooperative sliding segment motion, it relaxes to a three-loop structure. These snapshots are complementary to the experimental micrographs observed for DNA condensation.[38,39,42,55]

The formation of a toroid does not always involve the nucleation of one loop, as also seen in Ref. 61. Sometimes, multiple nuclei appear along one chain as shown in Fig. 10 for the case of N=180, Γ=4.0, K=70, and Z_c=3. As seen in this figure, nucleation of loops starts near both ends at different times, and these two nuclei grow by accumulating segments until eventually the two toroids are adjacent. This metastable state ultimately evolves into a single toroid by a cooperative sliding motion of segments. Several metastable shapes, such as "*tennis racket*," are seen as intermediate states, as also seen in other simulations.[43,44]

The randomness associated with the location of the nucleating loop along the chain can play a crucial role in the kinetics. For example, for a given set of parameter values, the kinetic pathway for the formation of toroid is strongly dependent on the initial random configuration. By thermal motion, if the internal angle of contact between segments of the nucleating loop is obtuse, then a toroid grows. If the angle is acute, then a folded-chain structure dominates. The toroidal and folded-chain structures are typically separated by huge barriers. However, if the chain length is small, this barrier could be surmounted. As an example, the dynamic interchange between toroidal and folded-chain structures is illustrated in Fig. 11 for the case of N=60, Z_c=2, K=50, and Γ =4.0. Both R_g and the net Coulomb energy are plotted as a function of time. The toroidal and folded-chain structures flip back and forth. For certain conditions, the metastable folded-chain structure evolves into a stable toroid as exemplified in Fig. 12 for the case of N=120, Γ=4.0, K=70, and Z_c=3. From the snapshots, a four-folded chain is seen to split into a pair of two-stranded loops, which evolves into a toroid by sliding of segments. Again, many metastable shapes such as tennis racket are seen as intermediate

states. Several of the shapes seen in our simulations have been observed in many experiments on DNA condensation.[54-58] Our simulations provide the kinetic dimension to the experimentally observed cryo-transmission electron microscopy (TEM) micrographs.

Finally, we have monitored the N dependence of the radius of the toroid. Defining the inner radius R_i, outer radius R_o, and the average radius R_0, according to the sketch in Fig. 13(a), these are plotted against N for Γ=3.0 and K=70. There have been varying predictions on the N dependence of R_0. Writing $R_0 \sim N^{\beta}$, β has been predicted to be 0, 1/5, and 1/3, respectively, by Park *et al.*,[62] Stukan *et al.*,[63] and Kuznetsov *et al.*[64] Our simulation results, as shown in Fig. 13, indicate that $\beta \cong 1$. Although simulations[63] of toroid-forming uncharged semiflexible chains show that $\beta \cong 1/4$, close to the value of 1/5, our simulations with electrostatic interactions clearly give much more sensitive dependence of R_0 on N. This discrepancy in β is beyond error bars and demands a theoretical resolution.

2.4 Conclusions

We have investigated the structures of isolated semiflexible polyelectrolyte molecules and counterion distributions, using Langevin dynamics simulations with explicit counterions. Similar to the behavior of fully flexible polyelectrolytes, R_g increases first and then continuously decreases, as the Coulomb strength parameter Γ is increased. In the limit of extremely stiff polyelectrolytes, R_g is independent of Γ.

The persistence length calculated by fitting with the wormlike chain model and directly by tangent vector correlation is larger for polyelectrolytes than the value

corresponding to the uncharged semiflexible chains, effectively due to the electrostatic expansion of the chain. Reflecting the behavior of the Γ dependence of R_g, both the persistence length and the shape factor R_g/R_h are nonmonotonic in Γ.

The degree of ionization decreases continuously with Γ, as in the case of fully flexible chains. The intrinsic stiffness of the polymer increases the degree of ionization, consistent with the predictions of the adsorption model of counterion condensation.[16]

At low values of εT (large Γ), flexible and weakly semiflexible chains form disordered globules which are more compact than Gaussian coil dimensions, due to multipole-multipole attractions arising from condensed counterions (see Ref. 27 for more details). For monovalent counterions, as the chain stiffness is increased, the chain is more expanded than the uncharged polymer. If the counterion is multivalent, moderately semiflexible chains form toroids, provided Γ is greater than a certain threshold value.

The formation of toroids follows complex kinetic pathways with many metastable structures, such as "tennis racket," folded chain, double toroid, etc. However, the generic pathway involves the nucleation of one loop somewhere along the chain contour, followed by a growth process where the rest of the chain is folded continuously on top of the primary loop. The average radius of the toroid is found to be a sensitive function of chain length for small toroids studied here, in disagreement with existing scaling predictions.

2.5 References

1. K.S. Schmitz, Macroions in Solution and Colloidal Suspension (Springer, Berlin, 1993).

2. S. Förster and M. Schmidt, Adv. Polym. Sci. 120, 51 (1995).

3. M. Sedlák, J. Chem. Phys. 105, 10123 (1996).

4. M. Beer, M. Schmidt, and M. Muthukumar, Macromolecules 30, 8375 (1997).

5. B. D. Ermi and E. J. Amis, Macromolecules 31, 7378 (1998).

6. Y. B. Zhang, J. F. Douglas, B. D. Ermi, and E. J. Amis, J. Chem. Phys. 114, 3299 (2001).

7. V. M. Prabhu, M. Muthukumar, G. D. Wignall, and Y. B. Melnichenko, Polymer 42, 8935 (2001).

8. V. M. Prabhu and M. Muthukumar, J. Chem. Phys. 119, 4085 (2003).

9. F. Oosawa, Biopolymers 6, 1633 (1968).

10. G. S. Manning, J. Chem. Phys. 51, 924 (1969).

11. G. S. Manning, Q. Rev. Biophys. 11, 179 (1978).

12. M. Fixman and J. Skolnick, Macromolecules 11, 863 (1978).

13. T. Odijk, Macromolecules 12, 688 (1979).

14. M. Muthukumar, J. Chem. Phys. 105, 5183 (1996).

15. K. Ghosh, G. A. Carri, and M. Muthukumar, J. Chem. Phys. 115, 4367 (2001).

16. M. Muthukumar, J. Chem. Phys. 120, 9343 (2004).

17. P. Gonzalez-Mozuelos and M. Olvera de la Cruz, J. Chem. Phys. 103, 3145 (1995).

18. F. J. Solis and M. Olvera de la Cruz, J. Chem. Phys. 112, 2030 (2000).

19. A. V. Dobrynin, R. H. Colby, and M. Rubinstein, Macromolecules 28, 1859 (1995).

20. R. M. Nyquist, B. Y. Ha, and A. J. Liu, Macromolecules 32, 3481 (1999).
21. T. Hofmann, R. G. Winkler, and P. Reineker, J. Chem. Phys. 118, 2406 (2003).
22. M. J. Stevens and K. Kremer, J. Chem. Phys. 103, 1669 (1995).
23. R. G. Winkler, M. Gold, and P. Reineker, Phys. Rev. Lett. 80, 3731 (1998).
24. C. Y. Shew and A. Yethiraj, Phys. Rev. Lett. 77, 3937 (1996).
25. A. Yethiraj, Phys. Rev. Lett. 78, 3789 (1997).
26. M. J. Stevens, Biophys. J. 80, 130 (2001).
27. S. Liu and M. Muthukumar, J. Chem. Phys. 116, 9975 (2002).
28. S. Liu and M. Muthukumar, J. Chem. Phys. 119, 1813 (2003).
29. J. M. G. Sarraguca, M. Skepö, A. A. C. C. Pais, and P. Linse, J. Chem. Phys. 119, 12621 (2003).
30. J. Widom and R. L. Baldwin, J. Mol. Biol. 144, 431 (1980).
31. H. Votavová, D. Kucerová, J. Felsberg, and J. Sponar, J. Biomol. Struct. Dyn. 4, 477 (1986).
32. V. A. Bloomflied, Curr. Opin. Struct. Biol. 6, 334 (1996).
33. P. G. Arscott, C. L. Ma, J. R. Wenner, and V. A. Bloomfield, Biopolymers 36, 345 (1995).
34. P. G. Arscott, A. Z. Li, and V. A. Bloomfield, Biopolymers 30, 619 (1990).
35. N. V. Hud and K. H. Downing, Proc. Natl. Acad. Sci. U.S.A. 98, 14925 (2001).
36. C. C. Conwell, I. D. Vilfan, and N. V. Hud, Proc. Natl. Acad. Sci. U.S.A. 100, 9296 (2003).
37. C. Böttcher, C. Endisch, J. H. Fuhrhop, C. Catterall, and M. Eaton, J. Am. Chem. Soc. 120, 12 (1998).
38. M. Ueda and K. Yoshikawa, Phys. Rev. Lett. 77, 2133 (1996).
39. M. Takahashi, K. Yoshikawa, V. V. Vasilevskaya, and A. R. Khokhlov, J. Phys. Chem. B 101, 9396 (1997).

40. J. X. Tang, J. A. Kas, J. V. Shah, and P. A. Janmey, Eur. Biophys. J. 30, 477 (2001).

41. G. Maurstad, S. Danielsen, and B. T. Stokke, J. Phys. Chem. B 107, 8172 (2003).

42. A. L. Martin, M. C. Davies, B. J. Rackstraw, C. J. Roberts, S. Stolnik, S. J. B. Tendler, and P. M. Williams, FEBS Lett. 480, 106 (2000).

43. B. Schnurr, F. C. Mackintosh, and D. R. M. Williams, Europhys. Lett. 51, 279 (2000).

44. B. Schnurr, F. Gittes, and F. C. Mackintosh, Phys. Rev. E 65, 061904 (2002).

45. V. A. Ivanov, W. Paul, and K. Binder, J. Chem. Phys. 109, 5659 (1998).

46. V. A. Ivanov, M. R. Stukan, V. V. Vasilevskaya, W. Paul, and K. Binder, Macromol. Theory Simul. 9, 488 (2000).

47. H. Noguchi, S. Saito, S. Kidoaki, and K. Yoshikawa, Chem. Phys. Lett. 261, 527 (1996).

48. H. Noguchi and K. Yoshikawa, J. Chem. Phys. 109, 5070 (1998).

49. H. Noguchi and K. Yoshikawa, J. Chem. Phys. 113, 854 (2000).

50. P. Ewald, Ann. Phys. (Paris) 64, 253 (1921).

51. M. Doi and S.F. Edwards, The Theory of Polymer Dynamics (Oxford University Press, New York, 1986).

52. G. A. Christos and S. L. Carnie, J. Chem. Phys. 91, 439 (1989).

53. Y. Yamasaki, Y. Teramoto, and K. Yoshikawa, Biophys. J. 80, 2823 (2001).

54. S. Q. He, P. G. Arscott, and V. A. Bloomfield, Biopolymers 53, 329 (2000).

55. D. D. Dunlap, A. Maggi, M. R. Soria, and L. Nucleic, Nucleic Acids Res. 25, 3095 (1997).

56. H. G. Hansma, R. Golan, W. Hsieh, C. P. Lollo, P. Mullen-Ley, and D. Kwoh, Nucleic Acids Res. 26, 2481 (1998).

57. D. Liu, C. Wang, J. W. Li, Z. Lin, Z. K. Tan, and C. L. Bai, J. Biomol. Struct. Dyn. 18, 1 (2000).

58. C. Ma and V. A. Bloomfield, Biophys. J. 67, 1678 (1994).

59. R. W. Wilson, D. C. Rau, and V. A. Bloomfield, Biophys. J. 30, 317 (1980).

60. V. A. Bloomfield, Biopolymers 31, 1471 (1991).

61. T. Sakuue, J. Chem. Phys. 120, 6299 (2004).

62. S. Y. Park, D. Harries, and W. M. Gelbart, Biophys. J. 75, 714 (1998).

63. M. R. Stukan, V. A. Ivanov, A. Yu. Grosberg, W. Paul, and K. Binder, J. Chem. Phys. 118, 3392 (2003).

64. Yu. A. Kuznetsov, E. G. Timoshenko, and K. A. Dawson, J. Chem. Phys. 105, 7116 (1996).

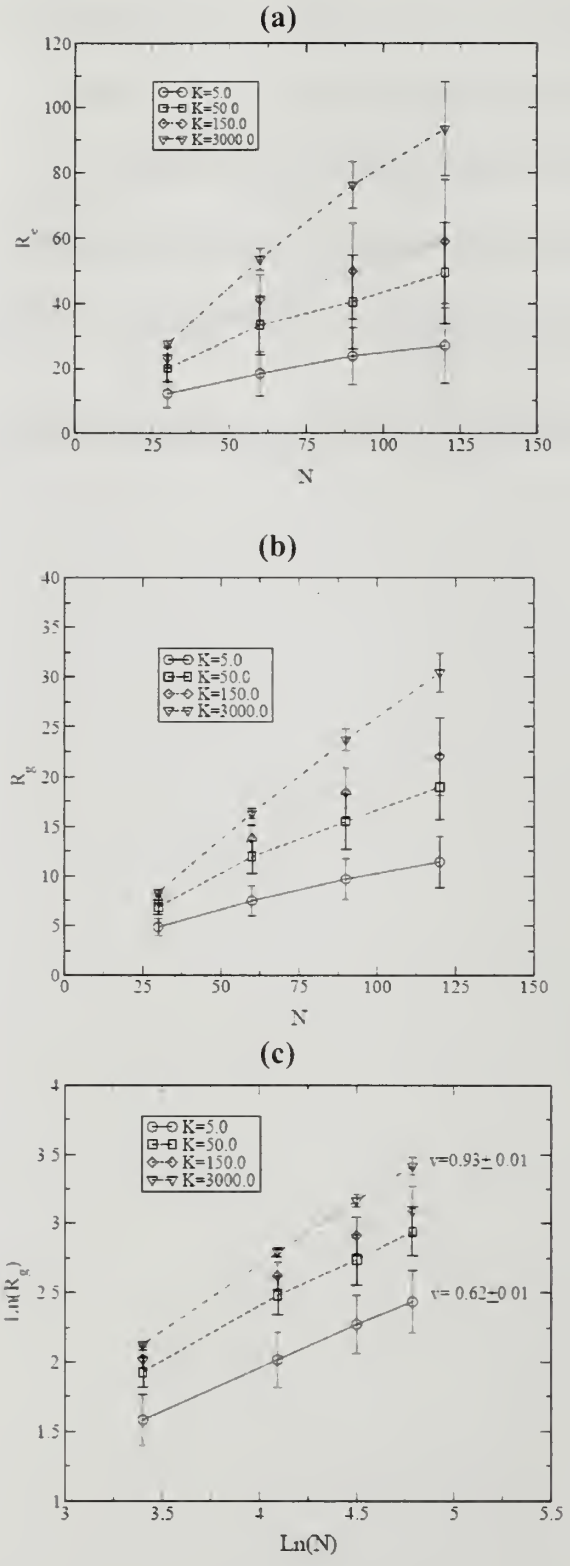

Figure 2.1 Effect of K on conformational properties of uncharged polymer. (a) R_e vs N; (b) R_g vs N; (c) double logarithmic plot of R_g vs N.

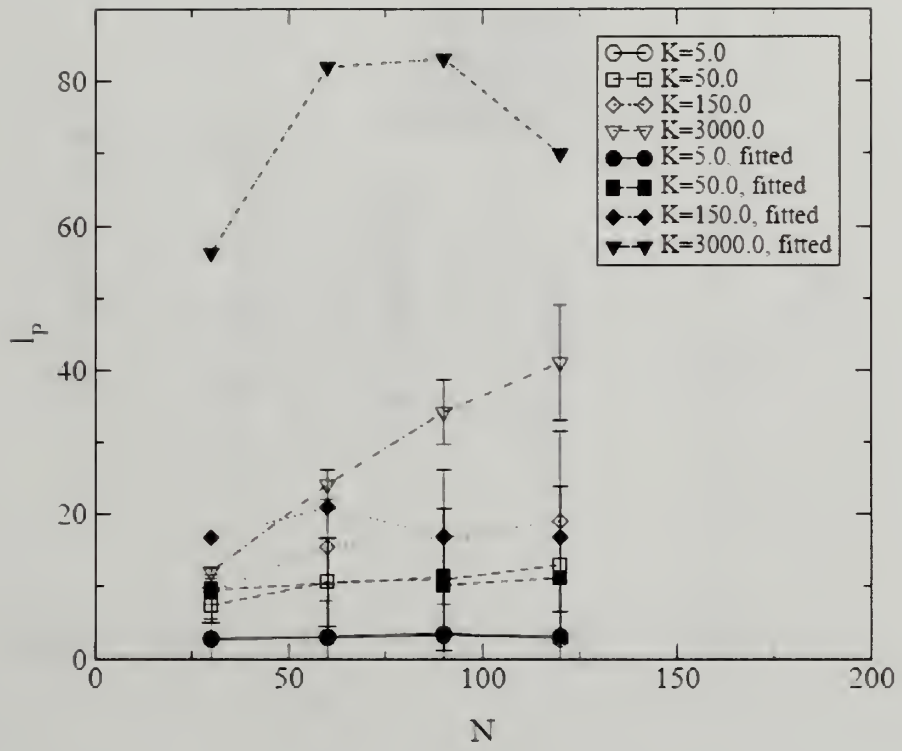

Figure 2.2 Dependence of persistence length l_p on N for K=5 (**O**), 50 (□), 150 (◊), and 3000 (∇), as calculated with Eq. (2.5). Filled symbols correspond to Eq. (2.4).

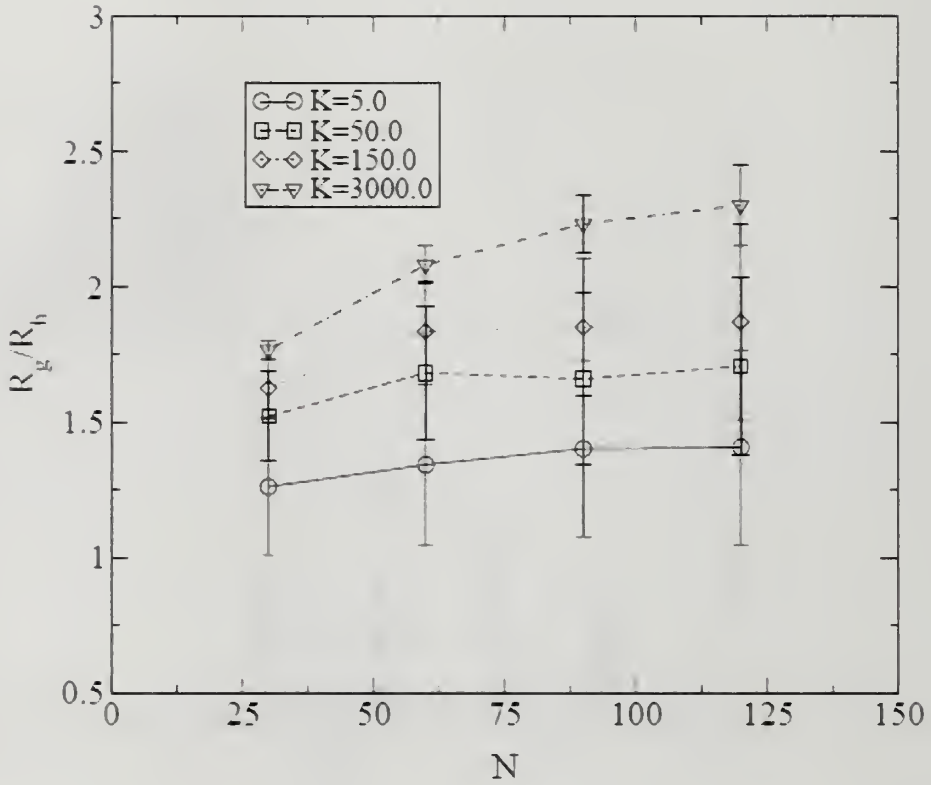

Figure 2.3 The shape factor R_g/R_h as a function of N for different chain stiffness, K.

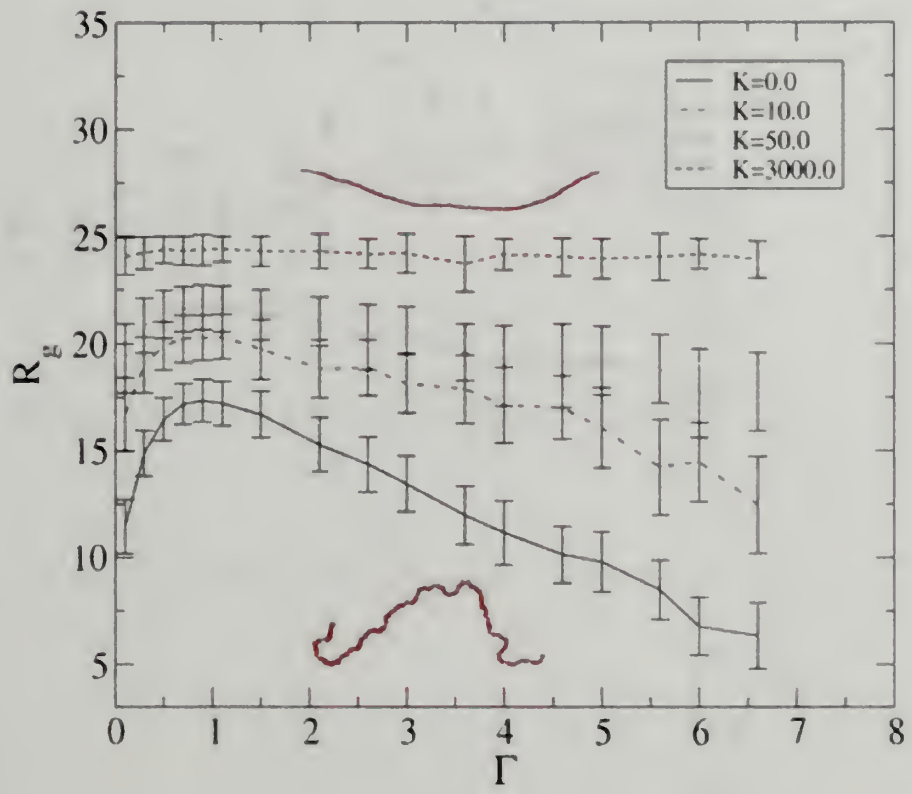

Figure 2.4 Radius of gyration, R_g for a charged stiff polymer with N=90, Z_c=1, and different K. Monomer density ρ=7.8×10^{-5}.

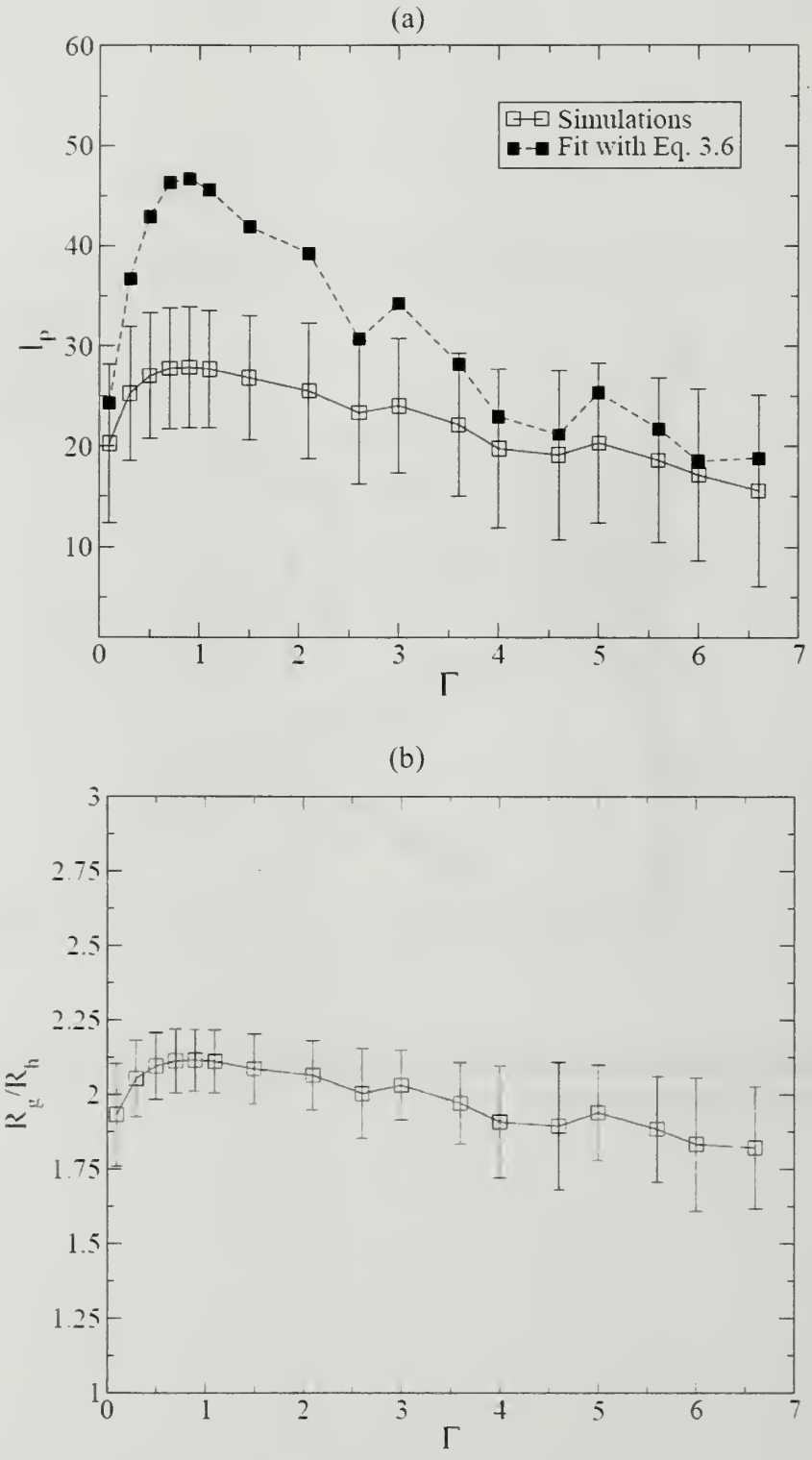

Figure 2.5 For a chain of N=90, Z_c=1, K=50.0, and $\rho=7.8\times10^{-5}$; (a) l_p vs. Γ [filled, Eq. (2.4); open, Eq. (2.5)]; (b) the shape factor R_g/R_h vs. Γ

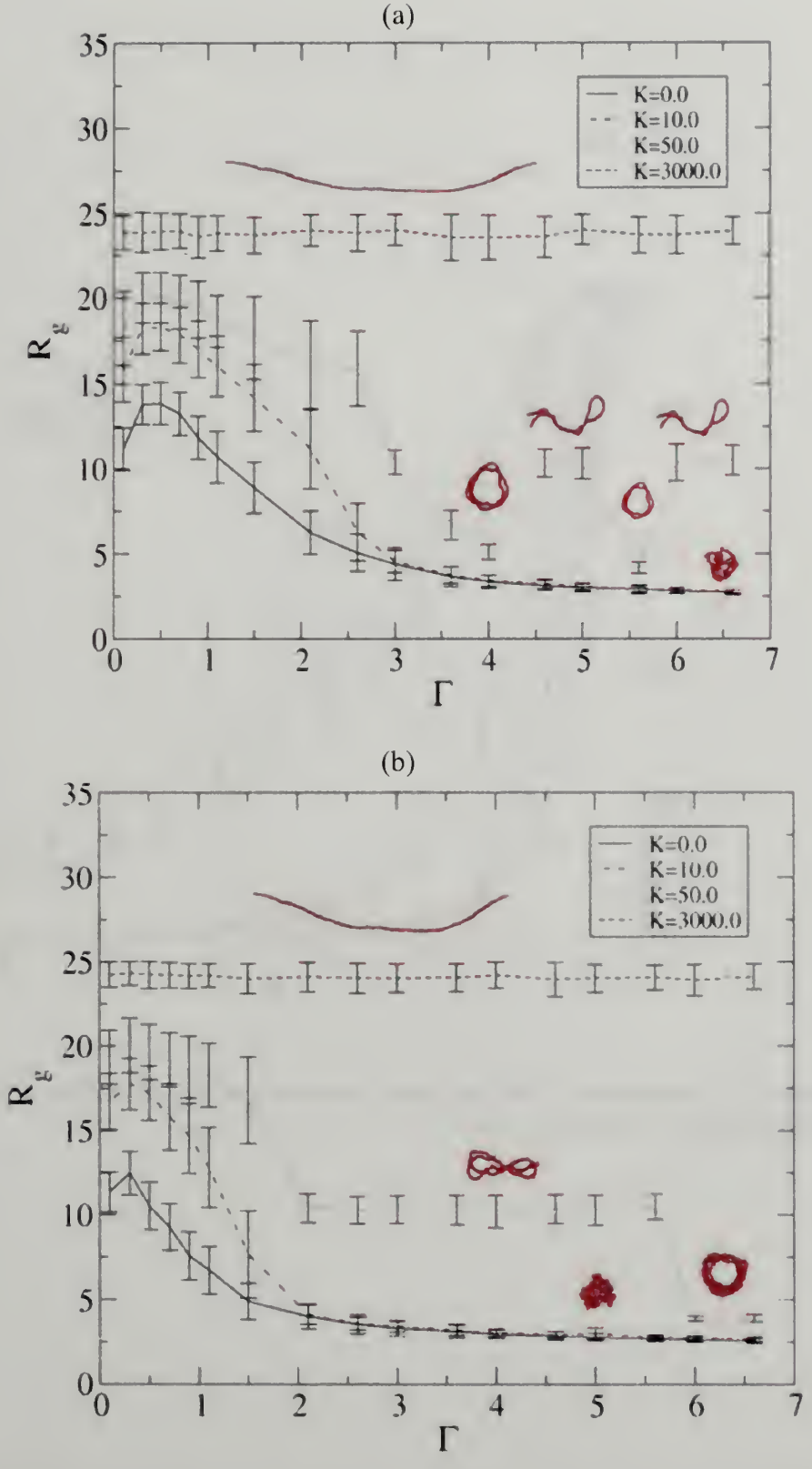

Figure 2.6 Radius of gyration R_g for a chain of length N=90 and some values of bending force constant K; monomer density $\rho=7.8\times10^{-5}$. (a) Z_c=2; (b) Z_c=3. Typical configurations are included for K=0, K=50, and K=3000 at different Γ.

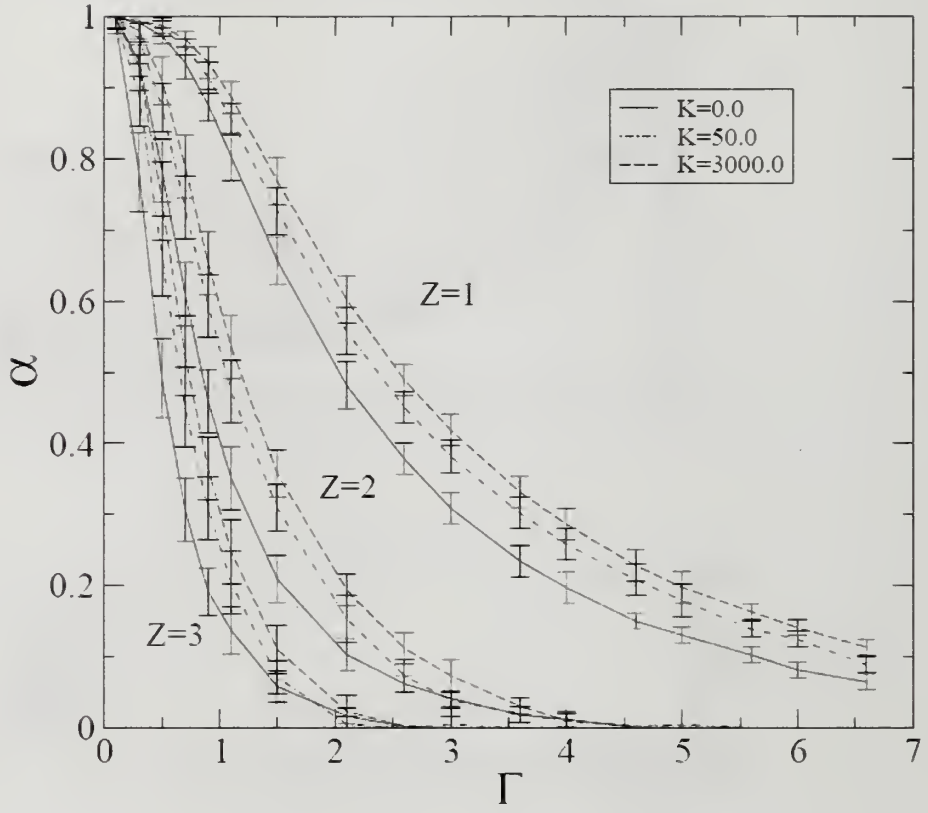

Figure 2.7 Dependence of the degree of ionization α on Γ for different K and Z_c values; the chain length N=90 and $\rho=7.8\times10^{-5}$.

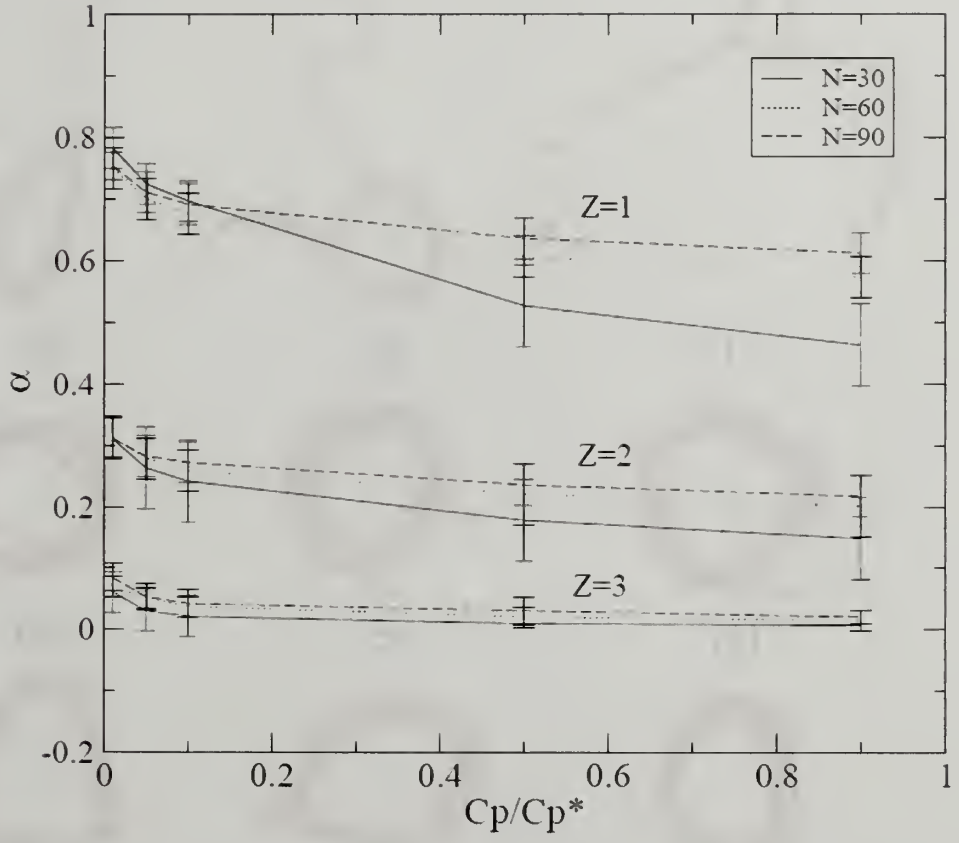

Figure 2.8 Dependence of degree of ionization α on the polymer concentration. N=30–90, K=20.0, and Γ=1.5. The C^* corresponds to the overlapping concentration assuming that the chain is rodlike.

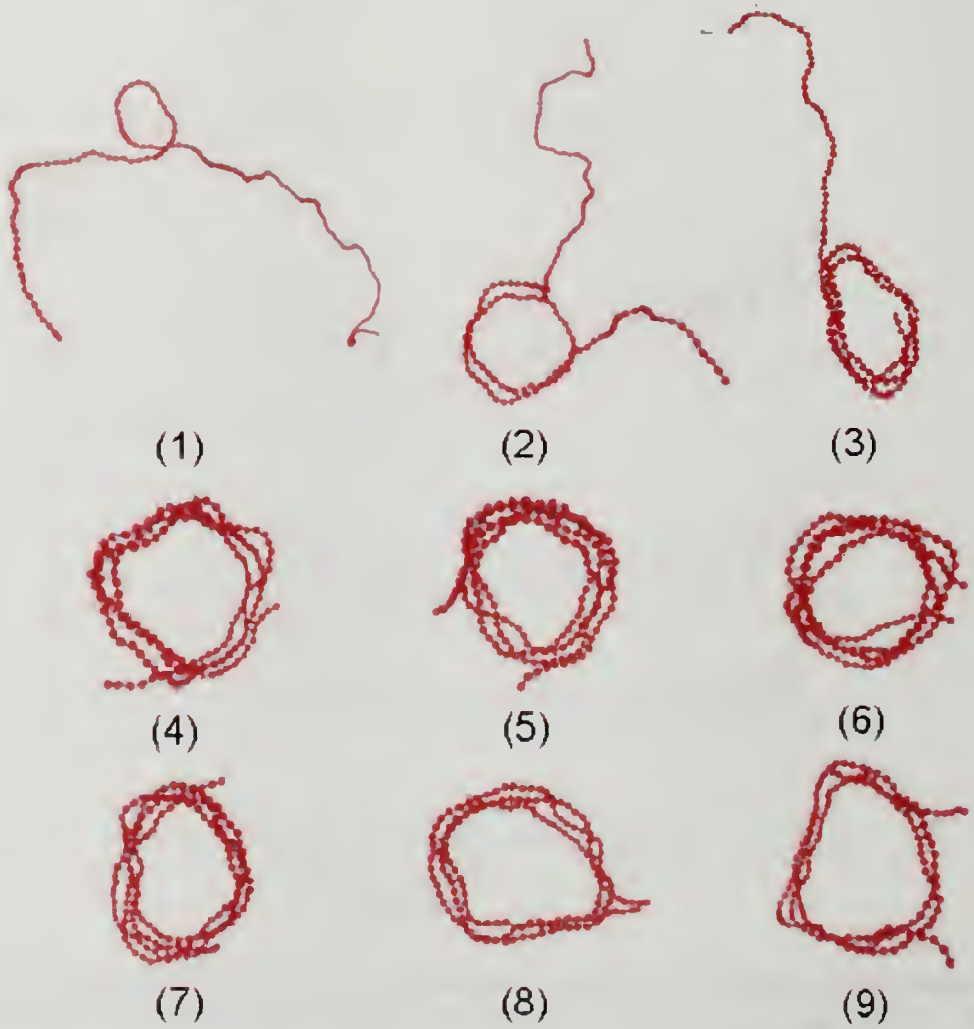

Figure 2.9 Snapshots of the formation of a toroid with one nucleus. N=180, K=70, Γ=2.0, Z_c=3, and ρ=1.2×10^{-5}. (1)–(9) correspond to time steps 200, 1530, 1940, 4100, 5210, 5500, 6140, 8200, and 10 000, respectively.

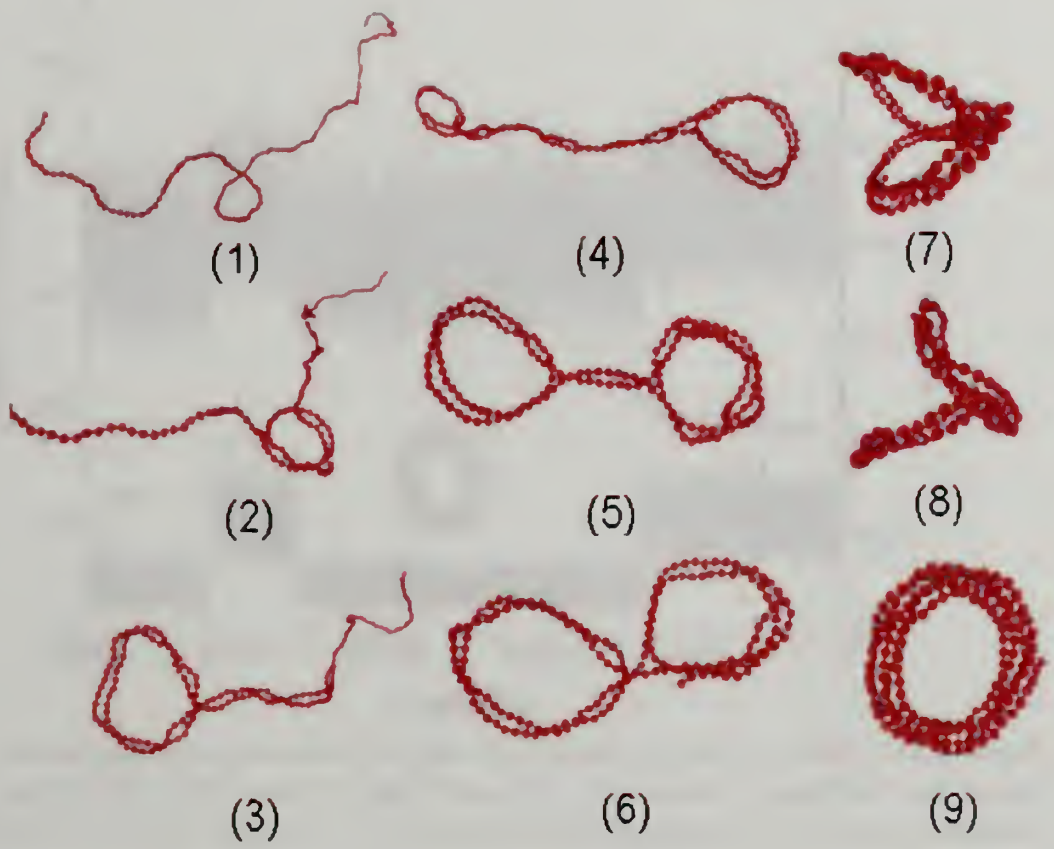

Figure 2.10 Snapshots of formation of a toroid with multiple nuclei. N=180, Γ=4.0, K=70, Z_c=3, and $\rho=1.2\times10^{-5}$. (1)–(9) correspond to time steps 200, 1450, 1800, 2300, 3400, 3850, 3900, 3970, and 10 000, respectively.

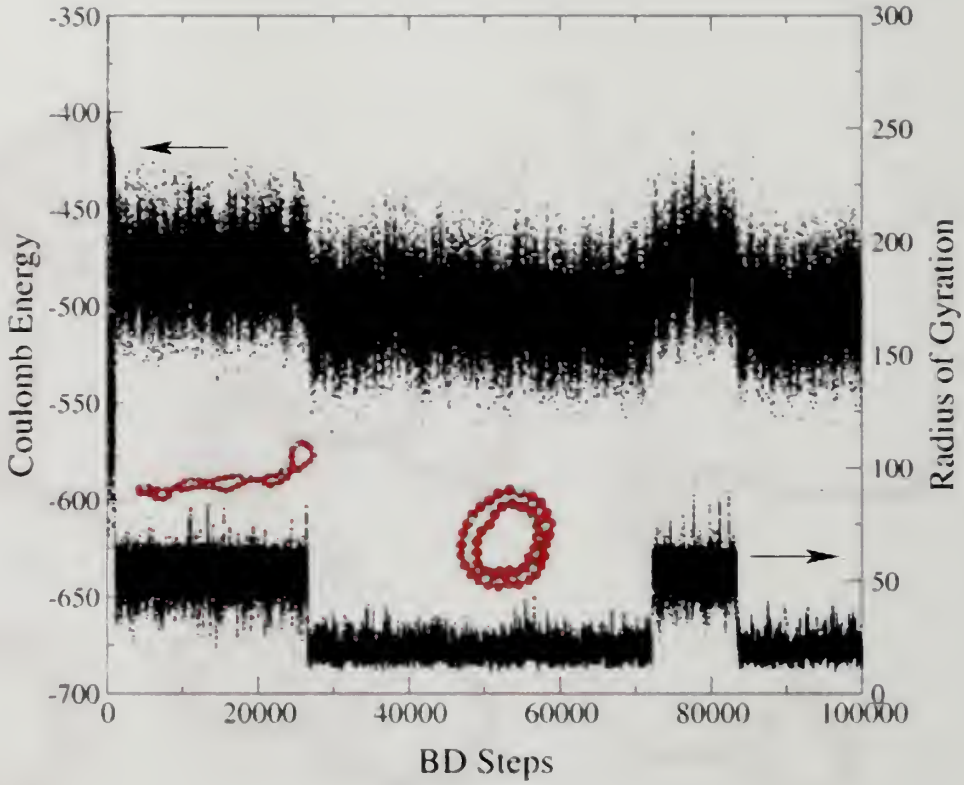

Figure 2.11 Dynamic exchange between toroidal and folded-chain structures in a typical run. The trace of radius of gyration and Coulomb energy were plotted as a function of time. Total simulation time steps are 2×10^{8}. N=60, K=50, Z_c=2, Γ=4.0, and $\rho=6.0\times10^{-5}$.

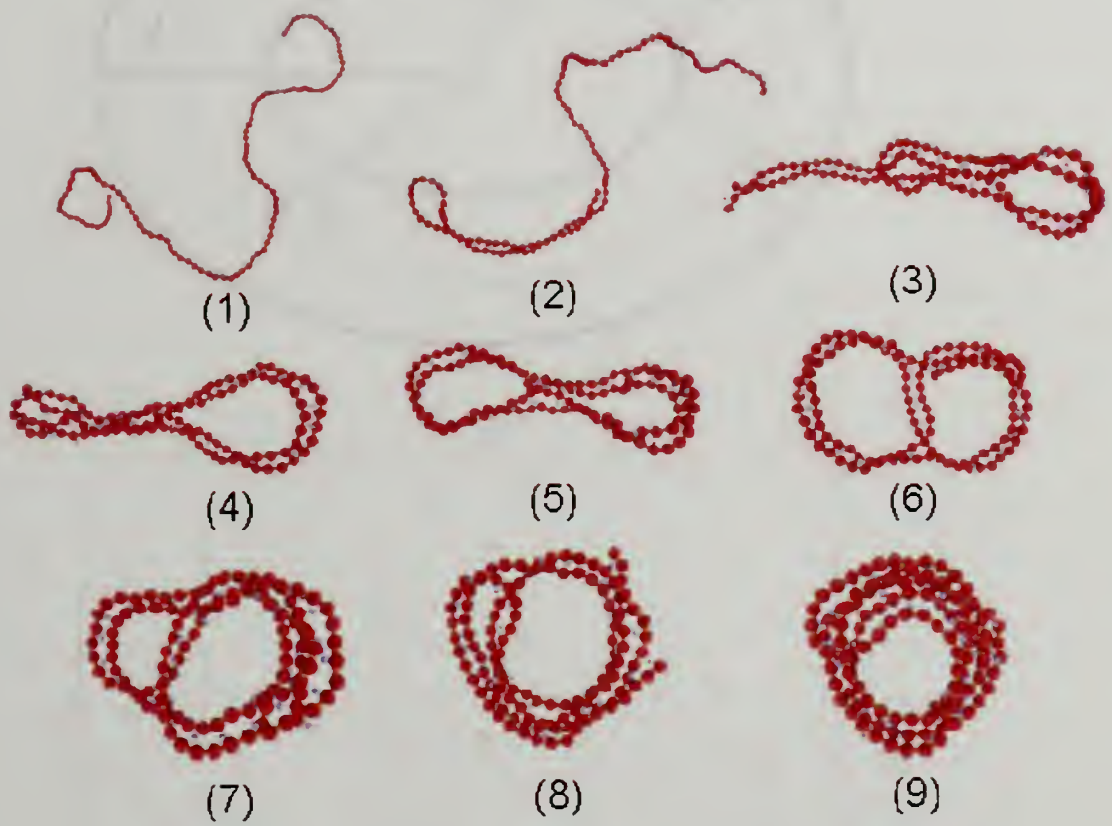

Figure 2.12 The evolution of transitions among coil, folded-chain, and toroid states for a stiff chain of N=120 and K=70 for Γ=4.0, Z_c=3, and ρ=1.5×10^{-5}. (1)–(9) correspond to time steps 200, 2160, 2900, 3080, 6100, 8100, 8200, 8300, and 10 000, respectively.

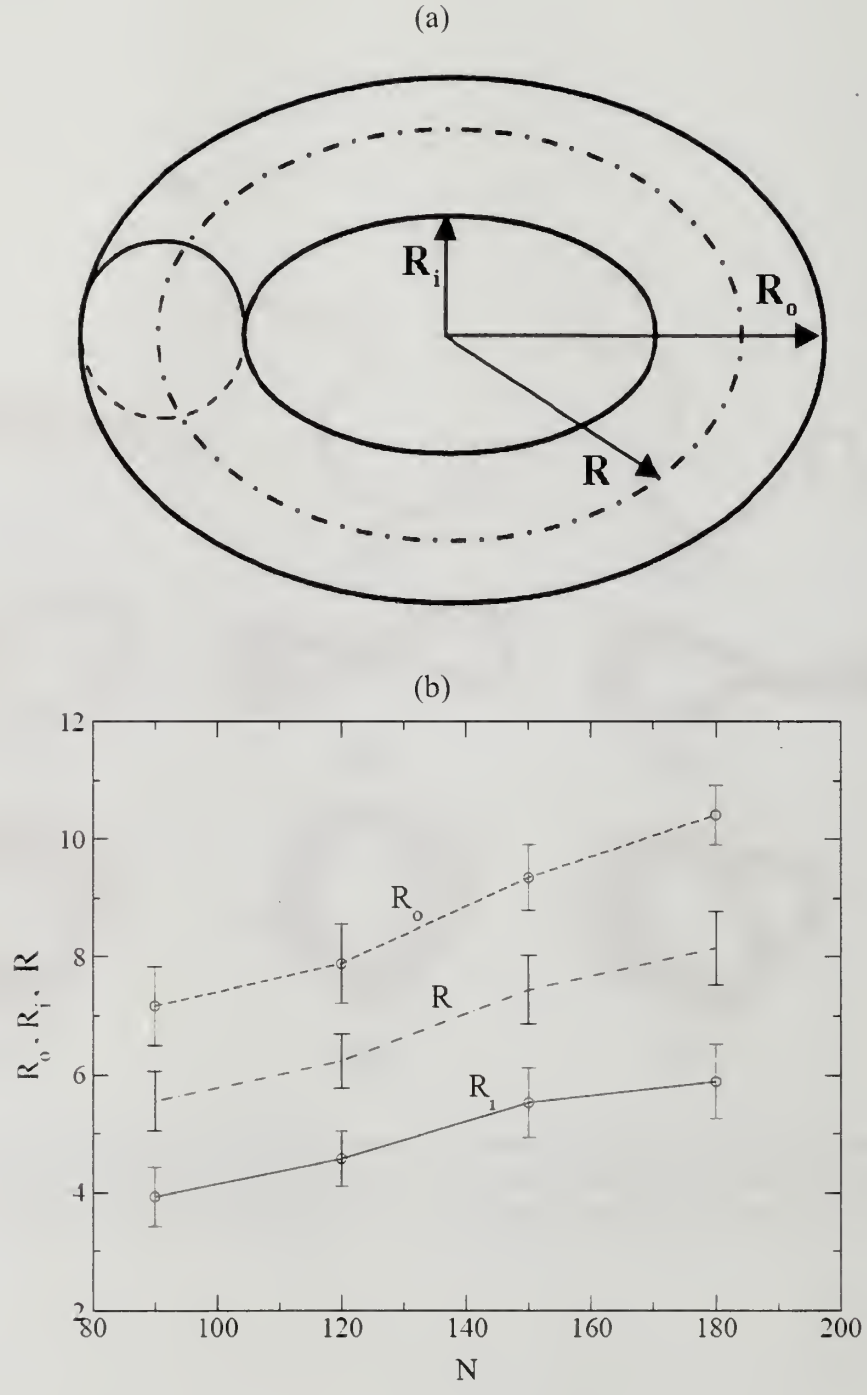

Figure 2.13 Scaling of toroid dimension with polyelectrolyte length. (a) Sketch of a toroid. (b) N dependence of R_i, R_o, and R. Γ=3.0, K=70, and Z_c=3.

CHAPTER 3

ENTROPY AND ENTHALPY OF POLYELECTROLYTE COMPLEXATION: A LANGEVIN DYNAMIC SMULATION STUDY

3.1 Introduction

Electrostatic attraction between two oppositely charged polyelectrolytes results in polyelectrolyte complexes widely used for flocculation, coating, and coacervation.[1] Recently, polyelectrolyte complexes have attracted considerable interest in the design of cationic polymers as non-viral synthetic vectors for gene therapy purposes.[2,3] Cationic polymers ("vectors") interact electrostatically with negatively charged DNA molecules, condensing them into a globule that facilitates the transportation to targeted cells. Another rapidly growing use for polyelectrolyte complexes has been to fabricate multilayered functional materials by sequentially adsorbing positive and negative charged polymers on charged surfaces of different geometries.[4]

A lot of experimental investigations have focused on the structural characteristics of polyelectrolyte complexes and their stability in response to environmental changes such as temperature and solution ionic strength.[5-13] In general, the morphology of a polyelectrolyte complex resembles a compacted globule, with an interpenetrating internal structure of no apparent long-range order. A polyelectrolyte complex usually has 1:1 stoichiometry of positive and negative charged polymers, regardless of their molecular characteristics such as charge density and chain length.[1, 5, 6] As such, a complete exclusion of counterions of both signs is expected in a polyelectrolyte complex. Stability studies of polyelectrolyte complexes have shown that complexes

made of highly charged polymers such as double-stranded DNA (dsDNA) are typically stable to the change of solution ionic strength while those from weak polyelectrolytes such as polyacrylic acid could undergo complete dissociation at elevated salt concentrations.[10] In contrast to intensive studies in structure-property relationship of polyelectrolyte complexes, the energetics of polyelectrolyte complexation has received much less attention.[14-18] In titration microcalorimetry study of polycation-DNA interactions, it was concluded that electrostatic interaction constitutes approximately 90% of total binding free energy at low salt concentration.[16] Moreover, a small positive enthalpy was reported in a study of DNA complex with a cationic copolymer,[14] while a negative one was measured in complexation of DNA with another cationic copolymer.[17] In both cases, polyelectrolyte complexation was driven by a large entropy gain, presumably due to the release of adsorbed counterions.[18] Salt effects on the enthalpy and entropy of polyelectrolyte complexation were also investigated.[19-22] It was observed that the driving force for polyelectrolyte complexation tends to decrease with salt concentration. But the enthalpy and entropy components respond differently to the addition of salt: a weak salt dependence for the enthalpy of complexation and a large variation in the entropy with salt concentration.

Theoretical and simulation efforts were also made to study the formation and structural characteristics of polyelectrolyte complexes. Theories on polyelectrolyte complexation have dealt primarily with weakly charged polyelectrolytes; free energy of complexation was formulated and phase diagrams of polyelectrolyte complexes were constructed.[23-26] Monte Carlo simulation was first applied to study the interpenetrating aggregates formed by two oppositely charged polymers; the radii of gyration of a chain

in an aggregate and of aggregates were examined at different chain lengths.[27] Similar system was later investigated by molecular dynamics simulation; the radii of gyration and the densities of the polyelectrolyte complexes were discussed at different Coulomb interaction strengths.[28] Polyelectrolyte complexes formed in solutions of multiple chains were recently systematically studied on effects of asymmetric chain lengths[29-31] and different salt contents.[32] Simple rules for cluster formation by oppositely charged polymers were proposed. Lately, Monte Carlo and molecular dynamics simulations were also applied to study the multilayering of oppositely charged polyelectrolytes at charged surfaces of different geometries.[33,34] Globules of oppositely charged polymers were obtained in the first few layers,[33] while strongly intermixing structures were observed for multilayers when adsorbed chains were allowed to equilibrate for a long period of time.[34]

Most of the theoretical and computational studies above have so far focused on different structures of polyelectrolyte complexes. A systematic study of energetics for polyelectrolyte complexation is lacking. Experimental works have, however, provided a wealth of enthalpy data for complex formation by polyelectrolytes of vastly different molecular characteristics, but they were often compounded by contributions from hydrophobic interaction, hydrogen bonding, hydration force, etc., making it hard to discern from others the electrostatic contribution, which is of foremost interest for any charged systems. It is desirable to have a prior knowledge of how the electrostatic interaction will affect complexation behavior before designing new polyelectrolyte architectures. In this chapter, by using Langevin dynamics simulation, we attempt to systematically examine the energetics profile of complex formation by two oppositely

charged polyelectrolytes in both weakly and strongly interacting systems and with different salt concentrations.

We model uniformly charged flexible polymers of N monomers immersed in a dielectric continuum characterized by dielectric constant, ε. In salt-free solutions, N/Z_c counterions each with valency of Z_c are included for electrostatic neutrality. Variation of salt concentrations is made through addition of a given amount of salt cations and anions into the solution.

3.2 Simulation Method

In the current study, flexible polyelectrolytes are modeled as freely jointed chains; each chain has N spherical beads connected by a harmonic stretching bond. Each bead carries charge of either e or $-e$ where e is unit electric charge. The counterion is treated as a sphere with point electric charge of either 1 or -1. The salt ions are chosen to be made of the same positive and negative counterions of polyelectrolyte chains used. Two oppositely charged chains together with their neutralizing counterions and prescribed amount of salt ions are placed in a dielectric medium of uniform dielectric constant, ε. The system is taken to be a cubic box of volume L^3 with periodic boundary conditions in all three dimensions.

In our system, two consecutive beads in each chain are connected by a harmonic stretching spring whose potential is taken to be

$$U_{\text{bond}} = k_b(l - l_0)^2, \tag{3.1}$$

where l is the bond length and l_0 is the equilibrium bond length. We have used l_0 as the unit of length throughout the simulations. The spring constant k_b is chosen to be high enough (i.e., $5000\varepsilon_{LJ}/l_0^2$) to allow fluctuation of the bond length within 10% of l_0. Consecutive bonds are freely jointed together and the polyelectrolyte chain is intrinsically flexible in the current study.

The excluded volume interaction between nonbonded beads of the chain is taken as a purely repulsive Lennard-Jones potential

$$U_{LJ} = \begin{cases} \epsilon_{LJ}\left[\left(\frac{\sigma}{r}\right)^{12} - 2\left(\frac{\sigma}{r}\right)^{6} + 1\right], & r \leq \sigma \\ 0, & r > \sigma, \end{cases} \tag{3.2}$$

where ε_{LJ} is the interaction strength, σ is the distance at which the potential is zero, and r is the distance between two particles. ε_{LJ} is used as the unit of energy in our system. Same form of potential is used for the excluded volume interactions of polymer beads-ions and ions-ions where ions are either counterions or salt ions. So we have simulated charged polymers in a good solvent condition. The values of σ are taken as $1.0l_0$, $0.8l_0$, and $0.6l_0$ for bead-bead, bead-ion, and ion-ion, respectively. Here, the choices of σ are considered only as a model system due to the lack of complete knowledge on sizes of hydrated ions near charged polymers.

The electrostatic interaction among charged beads and ions follows the Coulomb law

$$U_C(r_{ij}) = \frac{Z_i Z_j e^2}{4\pi\epsilon_0\epsilon r_{ij}}, \tag{3.3}$$

where r_{ij} is the distance between charged species i and j and Z_k is the valency of the kth ion (Z_k=Z_p for the polymer bead, Z_k=Z_c for counterion, and Z_k=Z_s for salt ion). ε_0 is the permittivity of vacuum and ε is the relative dielectric constant of the medium. We have adopted Ewald summation technique[35] to compute the electrostatic interaction potential U_C.

In current simulations, the strength of electrostatic interaction among charged groups is parameterized by the Coulomb strength parameter Γ defined as

$$\Gamma = \frac{l_B}{l_0}, \tag{3.4}$$

where l_0 is the charge separation distance along a chain or, in uniformly charged chains, the equilibrium bond length and l_B is the Bjerrum length defined by

$$l_B = \frac{e^2}{4\pi\epsilon_0\epsilon k_B T}, \tag{3.5}$$

with k_BT being the Boltzmann constant times the absolute temperature T. In the following results, temperature appears only through Γ with the multiplicative combination of T and the temperature dependent $\varepsilon(T)$ which is characteristic of specific solvent used. For instance, in the case of water and dsDNA (l_0=0.17nm), Γ increases from 4.18 at 20 °C to 4.81 at 70 °C. In experimental systems, Γ could be tuned

continually by changing charge separation distance l_0, e.g., using polymers of different charge densities.

The solvent of uniform dielectric constant ε is modeled as a Langevin thermostat. The dynamics of the ith particle (either bead or ion) is given by the Langevin equation

$$m\frac{d^2\mathbf{r}_i}{dt^2} = -\zeta\mathbf{v}_i - \nabla_{\mathbf{r}_i}U + \mathbf{F}_i(t), \tag{3.6}$$

where m and ξ are the mass and the friction coefficient, respectively, of the ith particle. The mass of polymer beads is set as unit mass, and that of counterions and salt ions is half unit mass. Friction coefficient is chosen as constant τ^{-1} where $\tau=\sqrt{m\sigma^2/\varepsilon_{LJ}}$ is the unit of time in the system. In defining this time unit, m=1 and $\sigma=l_0$. $\vec{r}_i$ and $\vec{v}_i$ are the position and velocity vector of the ith particle, respectively. U is the total potential energy ($U=U_{\text{bond}}+U_{\text{LJ}}+U_C$) acting on the ith particle. $\vec{F}_i(t)$ is the random force from the solvent acting on the ith particle and satisfies the following fluctuation-dissipation theorem:

$$\langle \mathbf{F}_i(t)\cdot\mathbf{F}_j(t')\rangle = \delta_{ij}6k_BT\zeta\delta(t-t') \tag{3.7}$$

To integrate Eq. (3.6), we have used the velocity-Verlet finite-differencing scheme. The integration time step δt is set at 0.001 in units of τ. Different values of δt from 0.0001 to 0.01 were found to give equivalent results for radius of gyration, Coulomb energy, etc. The only place where the choice of δt affects is the initial time for the approach of

equilibrium. The total duration of each simulation run takes from 10^6 to 10^7 time steps, depending on the choices of system parameters such as Γand salt concentration.

The ranges of values studied in current work are N=60, Z_c=1, L=129, and Γ=0.01–6.0. From Eqs. (3.4) and (3.5), a low value of Γ could be due to high dielectric constant, high temperature, or large charge separation distance as with polymers of low charge density. We have investigated polyelectrolyte complexation in a wide range of Γ to cover both weakly and strongly interacting Coulomb systems. The concentration of salt is varied from $0.1M$ to $0.5M$ by adding corresponding amount of salt ions to the system. Simulations on systems with even higher salt concentrations are presently hindered by prohibitively long computational time required for large Coulomb systems.

A typical simulation protocol is as follows: Two oppositely charged chains are first randomly generated in a large simulation box, the distance between them being half of the length of the simulation box. Counterions and salt ions are randomly distributed throughout the rest of the simulation box. In the first stage, Langevin dynamics simulation is carried out for prescribed time steps, ensuring that each chain reaches its equilibrium state. In the second stage, the pre-equilibrated chains together with their adsorbed counterions are translated to a center-of-mass separation distance of twice the average radius of gyration of each chain and Langevin dynamics simulation is further carried out. During each simulation, the position and velocity data of each particle are stored every 1000 time steps, from which physical quantities such as radius of gyration and Coulomb energy are computed and analyzed.

3.3 Results and Discussion

3.3.1 Properties of isolated polyelectrolyte chains

Before considering the energetics of polyelectrolyte complexation, we first note the reference properties of isolated polyelectrolytes. The dynamics and structures of polyelectrolytes in solutions have been the subjects of intense research in the past few decades.[36-46] Here, we will focus on only two aspects: chain configuration as measured by its radius of gyration R_g and the interaction of single polyelectrolyte chain with its counterions, i.e., counterion adsorption. Here, we simulated single polyelectrolyte in salt-free solution at different Coulomb interaction strengths.

3.3.1.1 Radius of gyration

A polyelectrolyte chain differs considerably from its neutral analog because of its highly charged backbone and long-ranged nature of electrostatic interaction.[36-38, 42-44] The size and shape of a polyelectrolyte chain depend on the strength of electrostatic interaction, which in the current study is characterized by a Coulomb interaction strength Γ. We have simulated polyelectrolyte chains at a broad range of Γ, in efforts to study the behavior of a polyelectrolyte chain in both weakly and strongly interacting systems. As a measure of chain configuration, the average radius of gyration of a polyelectrolyte chain, R_g, is monitored as a function of Γ in Figure 3.1. A nonmonotonic dependence on Γ is apparent for R_g: At the lowest range of Γ where Coulomb interaction is considerably weaker than thermal energy, a polyelectrolyte chain behaves more like a neutral self-avoiding chain; with increasing Γ, intrachain monomer-monomer repulsion

becomes stronger and chain size expands to minimize the repulsion; at high enough Γ, there is increasing attraction between counterions and charged monomers, and chain size starts to fall down when Γ >1.0; finally, at the highest value of Γ, R_g is comparable to that at the lowest Γ value. Previous simulation studies have also observed similar behavior of radius of gyration of single polyelectrolyte.[28,44,46,47]

3.3.1.2 Counterion adsorption

The highly charged backbone of a polyelectrolyte chain creates a considerable attraction for its counterions. According to polyelectrolyte theories,[48,49] such attraction amounts to territorially adsorbing a fraction of counterions onto the chain when Γ becomes large enough, e.g., Γ >1.0. In the current simulation study, a counterion is considered as adsorbed if it falls within a cutoff distance (l_0) to the chain backbone. The choice of the cutoff distance is to ensure that the Coulomb attraction experienced by a counterion at that distance is equal to or larger than thermal energy k_BT. It is also evident from direct visualizations of chain and counterion configurations that at large enough Γ, there are some certain numbers of counterions clustering around the chain. The total number of such adsorbed counterions is counted and averaged over different configurations after the chain establishes its equilibrium state. The fraction of adsorbed counterions is plotted as a function of Γ in Figure 3.1 for a single polyelectrolyte. It assumes a sigmoidal shape: the fraction of adsorbed counterions is negligible until Γ reaches about 1, after which it increases steadily and saturates toward 100% at the highest Γ studied. It shall be pointed out that Γ in aqueous solutions is 2.8 and 4.1 for

sodium polystyrene sulfonate (NaPSS) and dsDNA, respectively; in other words, for these highly charged polyelectrolytes, over 70% of charges are already neutralized by monovalent counterions at room temperature. It is no wonder that the actual charges of a strong polyelectrolyte in aqueous solutions could be significantly lower than that from its chemical structure. By associating with charged monomers, adsorbed counterions neutralize intrachain monomer-monomer repulsion. Such counterion-monomer association, however, does not resemble frozen ion pairs as found in ionic crystals; it is, in fact, very dynamical in nature: adsorbed counterions are able to move along the contour length of the chain and frequently exchange with free counterions in the solution (see Refs. 45,47).

3.3.2 Polyelectrolyte complexation in salt-free solutions

We first examine the complex formation by two oppositely charged polymers in salt-free solutions where only polymers and their exact number of neutralizing counterions are present. Two oppositely charged chains are first introduced in a dilute solution where the distance between these two chains is much larger ($\sim 10R_g$) than either their radii of gyration or Debye screening length. These individual chains are equilibrated for a sufficiently long period of time during which each chain could have diffused a distance of the length of a simulation box without encounter with each other. Chain size, counterion adsorption, and Coulomb energy of the system are monitored at the same time to ensure that polyelectrolyte chains indeed reach their equilibrium states. After the equilibration stage, two chains are translated, together with their adsorbed

counterions, to a center-of-mass separation distance of $2R_g$. This translation is used only to facilitate the encounter between two otherwise widely separated chains; we have systematically experimented with different separation distances and found the same results as obtained from the situation where two chains freely diffuse into each other. The close encounter of two oppositely charged chains typically leads to a fast overlapping and complexation. The resultant complex is further allowed to equilibrate with the rest of the solution until the Coulomb energy of the system stabilizes.

3.3.2.1 Kinetics and structures of polyelectrolyte complexes

Figure 3.2 shows snapshots from computer simulations of typical chain configurations at different stages during the complexation between two oppositely charged polymers at Γ=2.0. From Figure 3.2, two significant changes are obvious: Those counterions which are previously associated with polyelectrolyte chains are displaced during the course of complexation, and extended chains collapse into a compacted globule after complexation. These changes have to do with the cooperative interaction between two oppositely charged polyelectrolytes whose topologically connected charged monomers present a stronger affinity to its analog of opposite sign than discrete counterions do. The solution after polyelectrolyte complexation consists of counterions of both signs and a complex made of two oppositely charged chains. In experiments, mixing of solutions containing oppositely charged polymers often leads to a macrophase separation of polyelectrolyte complexes from the rest of the solution, or precipitation. In the current study, the interaction between solvent molecules and

polyelectrolyte beads is not explicitly accounted for; polyelectrolytes are envisaged to be in a good solvent condition by ascribing a purely repulsive excluded volume interaction between two polymer beads (see Sec. II). So, polyelectrolyte complexation studied here would correspond to that in dilute solutions with good solvent, and the resultant polyelectrolyte complex is in equilibrium with the rest of the solution, without precipitation.

Figure 3.3 follows dynamic evolution of the radii of gyration for both positive and negative polyelectrolyte chains participating in complexation. Upon approaching, two oppositely charged chains quickly overlap with each other in a cooperative fashion as seen in a quick drop of chain size. Similar observations were made in Monte Carlo[27] and molecular dynamics[28] simulations on complexation of two oppositely charged polymers.

We have shown in the previous section that counterion adsorption on isolated polyelectrolytes is common, especially at large Γ. Also plotted in Figure 3.3 are the evolutions in the number of adsorbed counterions and polycation-polyanion pairs during the complex formation between two oppositely charged chains. At Γ=2.0, there are about 30 adsorbed counterions on each chain at the start of complexation. During complexation, these counterions are progressively displaced by polycation-polyanion pairs. The final complex is deprived of any counterion of both signs. This counterion release phenomenon is more prominent at even larger Γ, i.e., Γ >3 where over 70% of counterions are associated with polyelectrolyte chains before complexation. Counterion release has been indirectly measured from complexation in solutions,[18] and a complete exclusion of counterion was observed inside a multilayered film made by alternative

adsorption of oppositely charged polyelectrolytes. In the following sections, we will examine the enthalpy and entropy consequences of such ionic exchange processes.

The internal structure of a polyelectrolyte complex after it reaches the equilibrium state (see discussions below) is characterized by radial distribution function between oppositely charged monomers as shown in Figure 3.4(a). The correlation between oppositely charged monomers within a polyelectrolyte complex is weak and broad at small Γ =0.3 where two oppositely charged chains are seen to undergo dynamical complexation-dissociation throughout simulation. The sharp peak of radial distribution function at $\sigma=1.0l_0$ (the diameter of polymer bead used in simulations) at larger Γ >1.0 reflects a close pairing between oppositely charged monomers. Direct visualizations of the complex from simulations reveal a collapsed interpenetrating globule. This is consistent with the general observation in experiments where the so-called scrambled egg morphology of polyelectrolyte complexes is typically found. More complicated structures such as toroids and folded chains may result from stiff polyelectrolytes such as dsDNA.[11,46]

Overall, thanks to the intrinsic flexibility of polyelectrolyte chains in the current modeling, a polyelectrolyte complex formed at Γ >1.0 is a collapsed globule with interpenetrating chains that are closely paired locally between two oppositely charged monomers. Figure 3.4(b) depicts the time evolution of Coulomb energy of the system for Γ =2.0 and Γ =4.0. In both cases, the Coulomb energy of the system levels off after the formation of polyelectrolyte complexes and the autocorrelation functions of the plateau regime (see inset) clearly indicate that the fluctuation of Coulomb energy at this

stage is completely random, that is, polyelectrolyte complexes are in their equilibrium states.

3.3.2.2 Coulomb energy change of polyelectrolyte complexation

According to the model described in Sec. II, the total internal energy of a system consists of three parts: bond stretching energy, Lennard-Jones excluded volume interaction, and Coulomb interaction. As an example, Figure 3.5 compares the contributions from all the three parts during the complex formation at Γ =2.0. All but Coulomb energy show little change in going from the isolated to the complexed state. This is due to the fact that we are simulating freely jointed chains which could adjust their conformations to accommodate close pairing without significant monomer overlapping or bond distortion. Thus, the enthalpy of polyelectrolyte complexation is directly equal to the Coulomb energy difference ΔE between that before and after complexation [see Figure 3.4(b)]. Figure 3.6 shows $\Delta E/T$ at different Γ along with the respective Coulomb energies before and after complexation. Similar to the shape of R_g in Figure 3.1, the Coulomb energy of the system before complexation is a nonmonotonic function of Γ, going through a maximum before rapidly decreasing when the attraction between counterions and polyelectrolytes becomes stronger. ΔE is negative and small in the very low limit of Γ, e.g., Γ <0.3, when the net attractive energy between two oppositely charged chains is small. This attractive energy becomes larger with Γ, resulting in a more negative ΔE of complexation. The Coulomb energy change is the most negative around Γ =1.0, after which it gets less negative, and at Γ >2.5, starts to

turn positive. This positive Coulomb energy change, however, does not increase infinitely with Γ; it starts to level off at the highest Γ studied. It is expected that at even higher values of Γ, Coulomb energies of isolated and complexed states shall converge since all the charges in the system, either monomers or counterions, will be completely neutralized by ion pairing. We have not been able to explore even higher range of Γ because at that stage, nearly all the counterions are adsorbed on polyelectrolyte chains and isolated polyelectrolyte chains are significantly compacted, making it impossible to observe complexation (if it does happen) between two collapsed chains within reasonable simulation time.

The fact that negative Coulomb energy change ΔE reaches its minimum around Γ =1.0 is closely related to the amount of adsorbed counterions shown in Figure 3.1. At Γ <1.0, only a few percent of total counterions adsorb on a chain and leave most of polymer charges un-neutralized. Such highly charged state is alleviated when two oppositely charged chains complex in such a fashion that most of their charges are now neutralized, resulting in a net Coulomb energy gain. At large Γ, such favorable Coulomb energy change (negative ΔE) is diminished when more and more chain charges are already neutralized by adsorbed counterions before complexation, and it is energetically less favorable to displace counterions-monomers interaction by polycation-polyanion interaction. Γ for commonly investigated polyelectrolytes is in the range of 2–4 (e.g., for sodium polystyrene sulfonate and dsDNA, Γ is 2.8 and 4.1, respectively, in aqueous solutions at room temperature.). As seen in Figure 3.6, in this range, ΔE can be either negative or positive depending on the Coulomb interaction

strength of a particular system, as found in complexation of DNA with different cationic copolymers.[14,17] Matulis *et al.* have applied electrostatic binding model to study the energetics and its temperature dependence for DNA complexation with multivalent cationic species and found a small positive enthalpy that is increasing with temperature.[50] This could be explained by an increase of Γ with temperature in aqueous solutions, e.g., for dsDNA, Γ increases from 4.2 at 20 °C to 4.8 at 70°C, which leads to a more positive ΔE of polyelectrolyte complexation, as revealed in Figure 3.6.

We must point out that the enthalpy of complexation measured in experiments is often complicated by unknown contributions from hydrogen bonding, hydrophobic interaction, and hydration force, making it difficult to discern the significance of electrostatic contribution that is of most interest to a charged system. Our simulations on simple polyelectrolyte systems have clearly demonstrated an intriguing behavior of Coulomb energy change accompanying polyelectrolyte complexation across different electrostatic interaction strength regimes.

3.3.2.3 Counterion release entropy of polyelectrolyte complexation

In complexation with another oppositely charged chain, the configuration, translational, and rotational entropies of a polyelectrolyte chain are reduced, the extent of which depends on how compact the chain is within the complex. More important, as evident in Figure 3.6, the complex formation is accompanied by a concomitant release of adsorbed counterions, increasing the system entropy. To quantify these entropy changes upon complexation, we have resorted to two different approaches:

(1) Free energy of polyelectrolyte complexation is first obtained by Eq. (3.8), and the entropy of complexation is then calculated by subtracting the free energy from the enthalpy of complexation, $T\Delta S=\Delta E-\Delta F$.

$$\frac{\Delta F}{T} = -\int_{T_{\text{ref}}}^{T} \frac{\Delta E}{T'^2} dT', \tag{3.8}$$

where T is the temperature of interest and T_{ref} is the reference temperature which in the current study is taken to be the temperature when Γ is the smallest (e.g., 0.01). To carry out the above integration, $\Delta E/T$ in Figure 3.6 was first fitted by a smooth fifth order polynomial function of Γ, $\Delta E/T=f(\Gamma)=\sum_{i=1}^{5} A_i \Gamma^i$ where A_i is the coefficient for the ith power term. Next, dT'/T' and the limits of integration in Eq. (3.8) need to be expressed in the Γ space. From its definition in Eqs. (3.4) and (3.5), the relation between Γ and T is specific to the solvent (and T dependence of ε) and the charge separation l_0 on the polymer. However, the practical range of Γ available for a specified solvent is very narrow, as already pointed out after Eq. (3.5). Therefore, we adopt the procedure of changing Γ over a wider range by tuning the charge separation length (i.e., the "charging" procedure) but by fixing T for a given solvent. This is performed by defining $\Delta F/T$ as $\Gamma\Delta F'$,

$$\Gamma\Delta F' = -\ln\left[\text{Tr}\exp\left(-\frac{1}{T}\mathcal{H}\right)\right] = -\ln[\text{Tr}\exp(-\Gamma\mathcal{H}')], \tag{3.9}$$

where $\mathcal{H}$ is the Hamiltonian of the system and **Tr** gives the partition sum. Now, we get exactly

$$\frac{\Delta F}{T} = \int_{\Gamma_{ref}}^{\Gamma} \frac{f(\Gamma')}{\Gamma'} d\Gamma' \qquad (3.10)$$

This is a general result valid for any solvent at a given temperature.

(2) By using a mean-field lattice model [see Figures 3.7 (a) and 3.7 (b)], we can explicitly write down the formulas for the entropy of the system before and after complexation. At each Γ, based on counterion adsorption results in Figure 3.3, a certain number of counterions are assigned to each chain. Since these adsorbed counterions are strongly attracted to the chain, their mobility is highly retarded and much smaller than that in the free states. So we did not include the configuration entropy of adsorbed counterions in the following calculations. From Figure 3.7(a), the entropy for the isolated polyelectrolytes and their counterions is

$$\begin{aligned} S_0 = {} & n_{+,p} \ln \phi_{+,p} + n_{-,p} \ln \phi_{-,p} \\ & + (1 - \alpha_+) n_{+,c} \ln(1 - \alpha_+) \phi_{+,c} \\ & + (1 - \alpha_-) n_{-,c} \ln(1 - \alpha_-) \phi_{-,c}. \end{aligned} \qquad (3.11)$$

where $n_{+,i}$ and $n_{-,i}$ are the numbers of positive and negative species i (chain, $i=p$; counterion, $i=c$), respectively. Similarly, $\phi_{+,i}$ and $\phi_{-,i}$ are the volume fractions of positive and negative species i (chain, $i=p$; counterion, $i=c$) and α_+ and α_- are the fractions of adsorbed counterions for positive and negative counterions. The first two terms in Eq. (3.11) are the configuration entropies for positive and negative charged chains and the last two terms represent the translational entropies of unadsorbed counterions of both

signs. In a similar fashion, the entropy of the system after the complex formation can be approximated by

$$S_1 = n_{\pm} \ln \phi_{\pm} + n_{+,c} \ln \phi_{+,c} + n_{-,c} \ln \phi_{-,c}. \tag{3.12}$$

where $n_{\pm}$ and $\phi_{\pm}$ are the number and volume fraction of the complex, respectively. Here, we treated the polyelectrolyte complex of oppositely charged chains as a new chainlike object with $\phi_{\pm}$ volume, and the released counterions are free to explore the whole volume. From Eqs. (3.11) and (3.12), the net entropy change resulting from polyelectrolyte complexation is

$$\begin{aligned} \Delta S &= S_1 - S_0 \\ &= -\left\{ n_{\pm} \ln \frac{2}{\phi_p} + 2N \ln \phi_c - 2(1-\alpha)N \ln \alpha\phi_c \right\}, \end{aligned} \tag{3.13}$$

where we have used the following equalities: $\phi_{-,p} = \phi_{+,p} = \phi_p = 0.5\phi_{\pm}$, $n_{+,p} = n_{-,p} = n_{\pm} = 1$, $\phi_{-,c} = \phi_{+,c} = \phi_c$, $n_{+,c} = n_{-,c} = N$, and $\alpha_- = \alpha_+ = \alpha$. In Eq. (3.13), when the fraction of adsorbed counterions, α, approaches 1 at a high Coulomb interaction strength (see Figure 3.3), the second term in Eq. (3.13) with its N dependence dominates over the first term, i.e., counterion release entropy contributes the most to the entropy of polyelectrolyte complexation.

Figure 3.8 compares the results from the above two approaches. Entropies calculated by two independent ways are in good agreement with each other across a large range of Γ . The entropy of complexation is negligible at lower range of Γ, e.g., $\Gamma<1.0$, but quickly increases afterwards. The biggest discrepancy between the two

approaches appears at the highest value of Γstudied; while the entropy from approach (1) starts to go down, that from the mean-field calculation continues to increase. The difference can be attributed to the assumption used in the mean-field approach, that is, released counterions can explore the whole solution volume to maximize their entropy, which is not particularly true at high Coulomb interaction strengths where ion pairing is prevalent. Except for this minor discrepancy at very large values of Γ, the agreement of these two approaches throughout most of Coulomb interaction strengths demonstrates that counterion release entropy is the dominant contribution to the entropy of polyelectrolyte complexation for $\Gamma>1.0$.

Taking Coulomb energy change and counterion release entropy together, free energy of polyelectrolyte complexation takes on a concave-up function of Γas shown in Figure 3.8. It closely follows the decreasing negative ΔE for $\Gamma<1.0$, and at $\Gamma=1.0$ the entropy contribution kicks in and continually lowers free energy until $\Gamma=2.5$. At $\Gamma\geq2.5$, the magnitude of negative free energy of complexation starts to reduce due to the fact that the Coulomb enthalpy now becomes increasingly positive. If we define Γ^* as the Coulomb interaction strength where the magnitudes of the enthalpy ΔE and the entropy $T\Delta S$ equal each other, Figure 3.8 can be divided into two regimes at $\Gamma^*=1.5$: Below Γ^*, polyelectrolyte complexation is driven by the negative Coulomb energy change derived from electrostatic attraction between two oppositely charged polymers, while the counterion release entropy only plays a subsidiary role; above Γ^*, the counterion release entropy contributes significantly. Especially at the high range of Γwhere the Coulomb energy change is positive and opposes polyelectrolyte complexation, it is the large

counterion release entropy that actually drives polyelectrolyte complexation. As already mentioned above, for highly charged polyelectrolytes, e.g., NaPSS and dsDNA in aqueous solutions, Γ is in the range of 2.0–4.0 where, according to Figure 3.8, the counterion release entropy is expected to contribute significantly to the driving force of complexation involving these polyelectrolytes. This is not to rule out the possible contributions of nonelectrostatic origin, such as hydrophobic interaction and hydration force, but to denote the critical role of counterion release entropy played in the free energy change of complexation by highly charged polyelectrolytes.

3.3.3 Polyelectrolyte complexation in the presence of salt

The presence of salt is ubiquitous in most experiments on polyelectrolyte complexation. Salt ions screen the electrostatic interaction among charged particles, and depending on salt concentrations used, the ionic strength of a solution can be readily tuned. In this section, we seek to understand the effect of varying ionic strength on the energetics of polyelectrolyte complexation, i.e., the effects on the Coulomb energy change and counterion release entropy. Three different salt concentrations have been used: $0.1M$, $0.25M$, and $0.5M$. Simulations on even larger salt concentrations are presently hindered by the prohibitively long computational time required for large Coulomb systems. Also, only monovalent salt is considered in the current study.

3.3.3.1 Salt effect on Coulomb energy change of polyelectrolyte complexation

Polyelectrolyte complexation between two oppositely charged polymers is carried out in three salt concentrations, and Figure 3.9 compares their respective Coulomb energy change ΔE with the one in the salt-free solution. The salt effect on ΔE manifests itself very differently in different Coulomb interaction strength ranges. At $\Gamma<3.0$, ΔE in the solution with a salt concentration, e.g., 0.1M, either becomes less negative ($\Gamma<2.0$) or even changes from negative to positive ($2.0<\Gamma<3.0$), in comparison with that in salt-free solutions. In other words, at $\Gamma<3.0$, polyelectrolyte complexation in the presence of salt has a less favorable ΔE than that in the salt-free solution. By contrast, at $\Gamma>3.0$, ΔE in salty solutions is always less positive than the one in salt-free solutions, suggesting that in this high Coulomb interaction strength range, the energy barrier (positive ΔE) is lower for polyelectrolyte complexation in the presence of salt. Also, in the weak Coulomb interaction range, $\Gamma<2.0$, $|\Delta E|$ decreases notably with salt concentrations, but it becomes almost invariant to the changes in salt concentrations at $\Gamma>2.0$ where experiments on highly charged polyelectrolytes in aqueous solutions are of interest. Such a weak dependence of ΔE on salt concentration in high Coulomb interaction strength range has been observed in experiments on DNA binding with cationic polymers,[14,16] oligometric lysines and arginines,[19] multivalent cationic species,[15] as well as proteins.[20] Despite the fact that ΔE only weakly depends on salt concentrations in those experiments, the free energy of polyelectrolyte complexation would decrease readily with the salt concentration used. This suggests that in these strongly interacting

systems, ionic screening effect alone cannot adequately explain the reduction of the driving force for polyelectrolyte complexation due to the addition of salt.

To elucidate the salt effects on ΔE in different Coulomb interaction strength regimes, it is instructive to understand how the salt addition influences the interactions among charged groups in the system. There are three pairwise interactions that make up the Coulomb energy of the system: polyion-polyion, polyion-counterion, and counterion-counterion. If we further differentiate the polyelectrolyte chains together with their adsorbed counterions from the free counterions, these pairwise interactions can be artificially grouped into two distinct contributions: Contribution I which includes both the interactions among polyions (with adsorbed counterions) and the interaction between these polyions and free counterions, and contribution II that only involves the interaction among free counterions. The salt effects on these two distinct contributions to the overall Coulomb energy are illustrated at Γ =2.0 and 4.0 in Figure 3.10, as examples for polyelectrolyte complexation in two different Coulomb interaction strength regimes. Let E_1 and E_2 be these two contributions prior to complexation. After complexation, the corresponding values are E_{1c} and E_{2c}. The values of these energies are computed by taking the time average in the isolated and complexed states.

For Γ =2.0, the values of E_1 and E_{1c} are –250 and –300, respectively, for the salt-free case, while E_2 and E_{2c} are essentially zero. In the presence of 0.5M monovalent salt, the values of E_1 and E_{1c} are –400 and –350, respectively. E_2 and E_{2c} are essentially about –600 for 0.5M salty solution. Thus, the energy of complexation, dominated by contribution I, is exothermic and endothermic for the salt-free and salty cases,

respectively. The exothermicity for the salt-free case implies that for complexation at Γ =2.0, the replacement of polyion-counterion interactions by polycation-polyanion interactions is favorable in energy, as already shown in Figure 3.9. By adding salt ions to the system before complexation, polyion-counterion interaction is strengthened (by screening the repulsion among those un-neutralized chain charges), and consequently E_1 is significantly more negative in comparison with the salt-free case. Since E_{1c} is essentially the same in the final complexed states, the complexation process is less exothermic in the salty case. In fact, for the values of the parameters used here, the process is actually slightly endothermic. It is to be noted that E_{1c} is slightly more negative for the salty case in comparison with the salt-free case. This is due to the interaction of the polyelectrolyte complex with the surrounding counterions of both signs, although the interior of the complex is essentially deprived of counterions.

For Γ=4.0, E_1 and E_{1c} are −1100 and −650, respectively, for the salt-free case. The corresponding values for the solution of 0.5M monovalent salt are −1150 and −750. The second contribution is around zero and −750 for the salt-free and salty cases without any significant change during complexation. So, at Γ =4.0, the endothermicity of polyelectrolyte complexation is reduced in the presence of 0.5M salt. The calculated endothermicity for both salt-free and salty cases at Γ =4.0 is due to the fact that the polyelectrolyte chains are already neutralized by counterion adsorption before complexation at these high Γ values. In general the role of salt is to make the complexation process more endothermic, as is evident in Figure 3.10. Furthermore, our simulation results, at Γ ~0.1 show that complexes dissociate at higher ionic strengths. It

is therefore envisaged that complexes at higher Γ values may require much higher salt concentrations to lose their stability.

3.3.3.2 Salt effect on counterion release entropy of polyelectrolyte complexation

Counterion release entropy of polyelectrolyte complexation at different salt concentrations is calculated from approach (1); the result is compared with that in salt-free solutions in Figure 3.11. In the lowest salt concentration, counterion release entropy does not deviate much from that in salt-free solutions until Γ =1.8 after which the reduction in entropy is very significant. There is also a big difference in ΔS for low and high salt concentrations. At Γ =1.8, ΔS in salt concentration of 0.5M is about 40% smaller than that in salt concentration of 0.1M. Such a large difference in ΔS persists into the higher range of Γ. We have also monitored the fraction of adsorbed counterions at different salt concentrations; in the range of ionic strength studied here, the number of adsorbed counterions only slightly increases from that in salt-free solution, e.g., at Γ =4.0, α is 0.80 and 0.87 for salt-free solutions and salt concentration of 0.5M, respectively. So, the large reduction of counterion release entropy in the presence of salt cannot be attributed to the changes in the number of adsorbed counterions but rather to the counterion osmotic pressure changes induced by increasing salt concentration. The entropy gain for adsorbed counterions to be released from polyelectrolyte chains is reduced when there are already plenty of free counterions present in the solution. The suppression of counterion release entropy ΔS by the addition of salt is consistent with what has been observed in studies of DNA binding with cationic species.[14, 16,19,20,50]

Combining ΔS and ΔE, it is clear that the addition of salt decreases the free energy for polyelectrolyte complexation as shown in Figure 3.12. Such reduction, however, takes on very different origins at low and high Coulomb interaction strengths. As an example, in solutions with salt concentration of $0.1M$, at $\Gamma < 1.8$ the reduction of ΔF is mainly due to the fact that ΔE is now much smaller than that in salt-free solutions, while at higher range of Γ, especially when $\Gamma > 3.0$, polyelectrolyte complexation is actually helped by a less positive Coulomb energy change compared to that in salt-free solution, and the reduction in ΔF is brought about by a strong suppression of counterion release entropy as shown above. There are ongoing debates in literature on the salt effect on polyelectrolyte complexation.[19,20] A predominantly entropic effect in salt-dependent electrostatic contribution to the free energy of polyelectrolyte complexation is inferred from the counterion adsorption theory.[20] It is also argued that addition of salt mainly acts to screen the Coulomb interaction in the system, resulting in a weaker tendency for polyelectrolyte complexation. Our systematic simulations on polyelectrolyte complexation at different salt concentrations and Coulomb interaction strengths have shown that the exact nature of salt effects on the driving force of polyelectrolyte complexation has to do with the strength of Coulomb interaction at which the complexation is carried out. In the weakly interacting regime, ionic screening effect is manifested in a strong reduction in Coulomb energy change of complexation. In the strongly interacting regime, the strong suppression of counterion release entropy results in a weaker driving force for polyelectrolyte complexation.

3.4 Conclusions

The energetics of complexation by two oppositely charged polymers were studied in both weakly and strongly interacting Coulomb systems and at different salt concentrations. Using a simple model of polyelectrolyte with explicit counterions and salt ions, the Coulomb energy change and entropy of polyelectrolyte complexation were clearly defined. Distinct energy and entropy contributions to complexation of oppositely charged polyelectrolytes were differentiated at weak and strong Coulomb interaction strengths. In a weakly interacting system, polyelectrolyte complexation is driven by negative Coulomb energy change derived from electrostatic attraction between two oppositely charged chains. Because of the weak Coulomb interaction strength, there are only a small amount of counterions adsorbed on a polyelectrolyte chain, and consequently a less counterion release entropy is obtained. In a strongly interacting system, polyelectrolyte chains attract a large number of counterions. As such, the complex formation is driven by a large entropy gain due to counterion release upon complexation while opposed by a positive Coulomb energy change.

Addition of monovalent salt is found to strongly affect the energetics of complex formation. Compared to salt-free solutions, the Coulomb energy change of polyelectrolyte complexation, negative or positive, is reduced by ionic screening effect across all the Coulomb interaction strengths studied. The counterion release entropy of complexation decreases with salt concentration as well, but significant reduction only appears at strong Coulomb interaction strength. Taken together, at the weak interaction strength, the decreases of both negative Coulomb energy change and positive entropy result in a weaker tendency for polyelectrolyte complexation. At the strong interaction

strength, a less positive Coulomb energy change in the presence of salt actually decreases the positive Coulomb energy change for complexation but this is counteracted by an even stronger suppression of counterion release entropy. Overall, the driving force for complexation weakens with salt concentration at all Coulomb interaction strengths. Also, in the range of Coulomb interaction strength of interest in experiments (Γ=2–4), the Coulomb energy change of complexation is only a weak function of salt concentration, which is in contrast to the large variations in counterion release entropy as a function of salt concentrations. Our result leads to the notion that the salt effect on polyelectrolyte complexation in those highly charged systems is of entropic origin. Our simulation study on a simple model of polyelectrolyte complexation is in qualitative agreement with many available experimental observations and provides insight into fundamental forces behind complexation among polyelectrolytes.

3.5 References

1. Macromolecular Complexes in Chemistry and Biology, edited by P. Dubin, J. Bock, R. Davis, D. N. Schulz, and C. Thies (Springer-Verlag, New York, 1994).

2. V. A. Bloomflied, Curr. Opin. Struct. Biol. 6, 334 (1996).

3. V. Vijayanathan, T. Thomas, and T. J. Thomas, Biochemistry 41, 14085 (2002).

4. G. Decher, Science 277, 123 (1997).

5. B. Philipp, H. Dautzenberg, K.-J. Linow, and W. Dawydoff, Prog. Polym. Sci. 14, 91 (1989).

6. A. F. Thunemann, M. Muller, H. Dautzenberg, J. F. O. Joanny, and H. Lowne, Adv. Polym. Sci. 166, 113 (2004).

7. N. Karibyants, H. Dautzenberg, and H. Colfen, Macromolecules 30, 7803 (1997).

8. T. Schindler and E. Nordmeier, Polymer 40, 7019 (1999).

9. A. N. Zelikin, A. I. Natalia, and I. A. Vladimir, Macromol. Chem. Phys. 202, 3018 (2001).

10. H. Dautzenberg and W. Jaeger, Macromol. Chem. Phys. 203, 2095 (2002).

11. G. Maurstad, S. Danielsen, and B. T. Stokke, J. Phys. Chem. B 107, 8172 (2003).

12. U. Rungsardthong, T. Ehtezazi, L. Bailey, S. P. Armes, M. C. Garnett, and S. Stolnik, Biomacromolecules 4, 683 (2003).

13. J. DeRouchey, R. R. Netz, and J. O. Radler, Eur. Phys. J. E 16, 17 (2005).

14. T. Bronich, A. V. Kabanov, and L. A. Marky, J. Phys. Chem. B 105, 6042 (2001).

15. D. Matulis, I. Rouzina, and V. A. Bloomfield, J. Mol. Biol. 296, 1053 (2000).

16. T. Ehtezazi, U. Rungsardthong, and S. Stolnik, Langmuir 19, 9387 (2003).

17. C. K. Nisha, S. V. Manorama, M. Ganguli, S. Maiti, and J. N. Kizhakkedathu, Langmuir 20, 2386 (2004).

18. D. P. Mascotti and T. M. Lohman, Proc. Natl. Acad. Sci. U.S.A. 87, 3142 (1990).

19. D. P. Mascotti and T. M. Lohman, Biochemistry 36, 7272 (1997).

20. T. Lundback and T. Hard, J. Phys. Chem. 100, 17690 (1996).

21. H. Dautzenberg, Macromolecules 30, 7810 (1997).

22. H. M. Buchhammer, G. Petzold, and K. Lunkwitz, Langmuir 15, 4306 (1999).

23. V. Yu. Borue and I. Yu. Erukhimovich, Macromolecules 21, 3240 (1988).

24. A. Kudlay and M. O. de la Cruz, J. Chem. Phys. 120, 404 (2004).

25. P. M. Biesheuvel and M. A. C. Stuart, Langmuir 20, 2785 (2004).

26. R. Zhang and B. T. Shklovskii, Physica A 352, 216 (2005).

27. D. Srivastava and M. Muthukumar, Macromolecules 27, 1461 (1994).

28. R. G. Winkler, M. O. Steinhauser, and P. Reineker, Phys. Rev. E 66, 021802 (2002).

29. Y. Hayashi, M. Ullner, and P. Linse, J. Chem. Phys. 116, 6836 (2002).

30. Y. Hayashi, M. Ullner, and P. Linse, J. Phys. Chem. B 108, 15266 (2004).

31. R. S. Dias, A. A. C. C. Pais, M. G. Miguel, and B. Lindman, J. Chem. Phys. 119, 8150 (2003).

32. Y. Hayashi, M. Ullner, and P. Linse, J. Phys. Chem. B 107, 8198 (2003).

33. R. Messina, C. Holm, and K. Kremer, Langmuir 19, 4473 (2003).

34. V. Panchagnula, J. Jeon, and A. V. Dobrynin, Phys. Rev. Lett. 93, 037801 (2004).

35. P. Ewald, Ann. Phys. 64, 253 (1921).

36. M. Fixman and J. Skolnick, Macromolecules 11, 863 (1978).

37. T. Odijk, Macromolecules 12, 688 (1979).

38. M. Muthukumar, J. Chem. Phys. 105, 5183 (1996).

39. F. J. Solis and M. O. de la Cruz, J. Chem. Phys. 112, 2030 (2000).

40. A. V. Dobrynin, R. H. Colby, and M. Rubinstein, Macromolecules 28, 1859 (1995).

41. C. Y. Shew and A. Yethiraj, Phys. Rev. Lett. 77, 3937 (1996).

42. S. Förster and M. Schmidt, Adv. Polym. Sci. 120, 51–133 (1995).

43. V. M. Prabhu, M. Muthukumar, G. D. Wignall, and Y. B. Melnichenko, Polymer 42, 8935 (2001).

44. M. Stevens and K. Kremer, J. Chem. Phys. 103, 1669 (1995).

45. S. Liu and M. Muthukumar, J. Chem. Phys. 119, 1813 (2003).

46. Z. Ou and M. Muthukumar, J. Chem. Phys.123, 074905 (2005).

47. S. Liu and M. Muthukumar, J. Chem. Phys. 116, 9975 (2002).

48. G. S. Manning, Q. Rev. Biophys. 11, 179 (1978).

49. M. Muthukumar, J. Chem. Phys. 120, 9343 (2004).

50. D. Matulis, I. Rouzina, and V. A. Bloomfield, J. Am. Chem. Soc. 124, 7331 (2002).

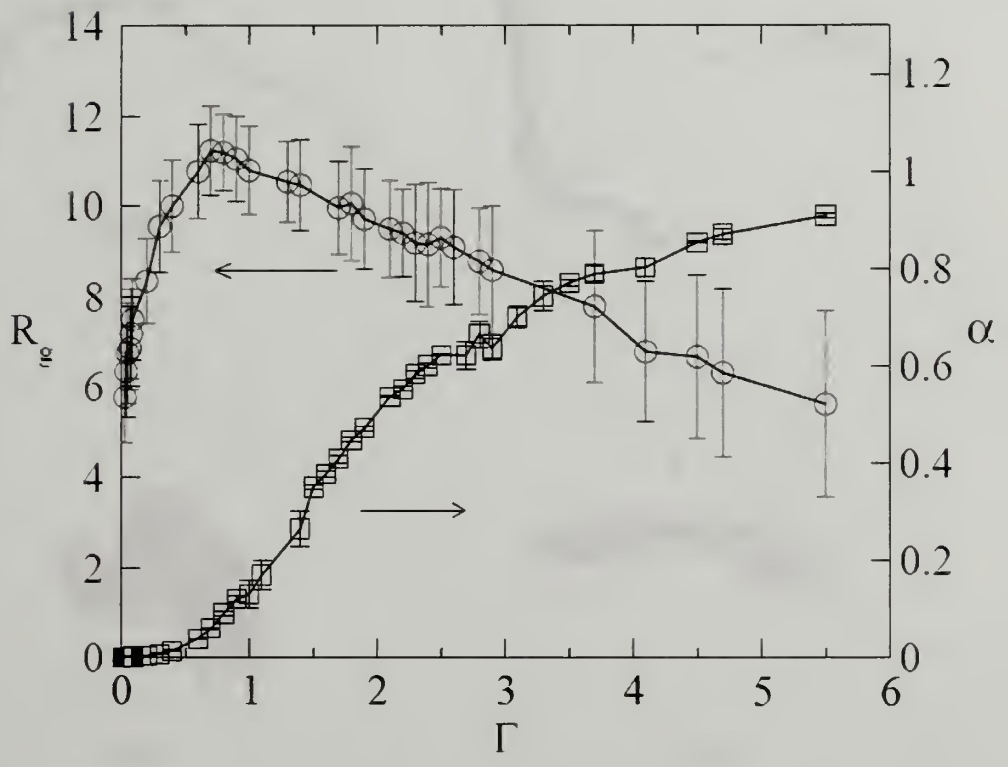

Figure 3.1 Radius of gyration R_g and fraction of adsorbed counterions α as functions of Coulomb interaction strength Γ in salt-free solutions. Chain length N=60 and counterion valency Z_c=1.

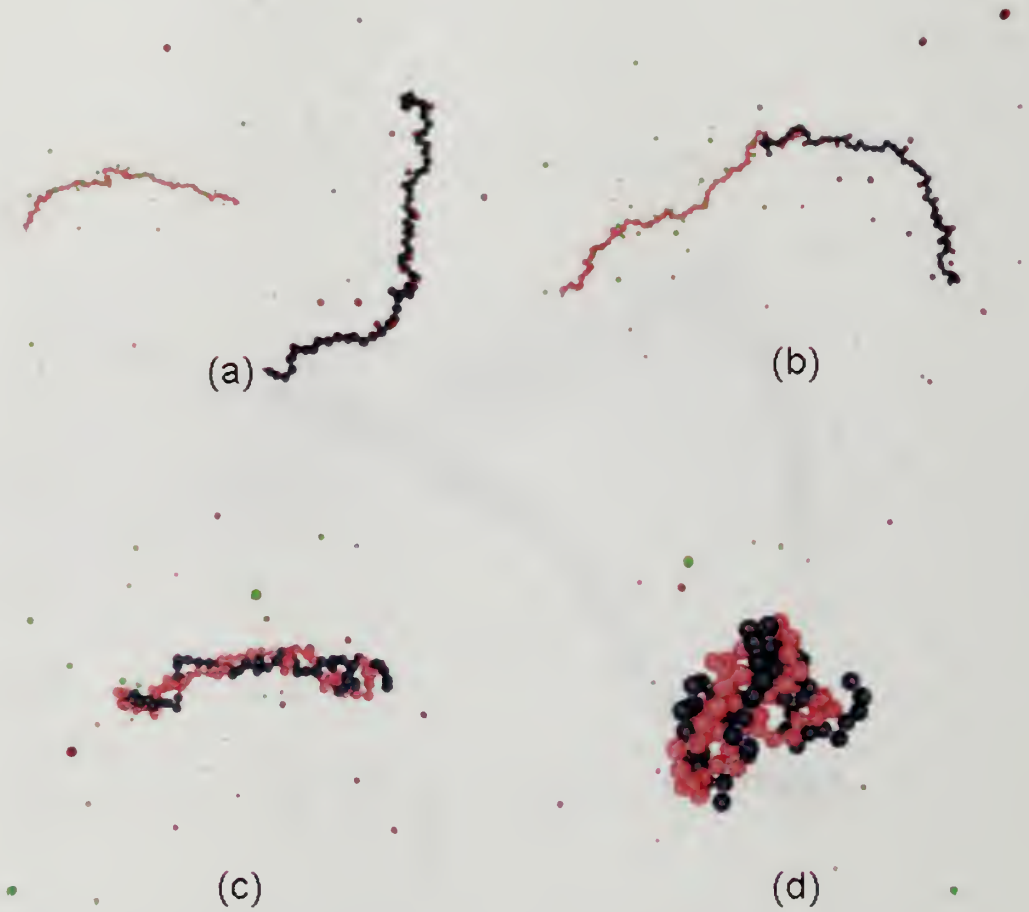

Figure 3.2 Snapshots of chain configurations at different stages during the complexation between two oppositely charged polymers in salt-free solutions. The gray bead represents a positively charged chain and the dark one is a negatively charged chain. Positive and negative counterions are shown as gray and dark dots, respectively. Chain length N=60, counterion valency Z_c=1, and Γ=2.0. (a)–(d) represent simulation time units of 71, 501, 811, and 966, respectively.

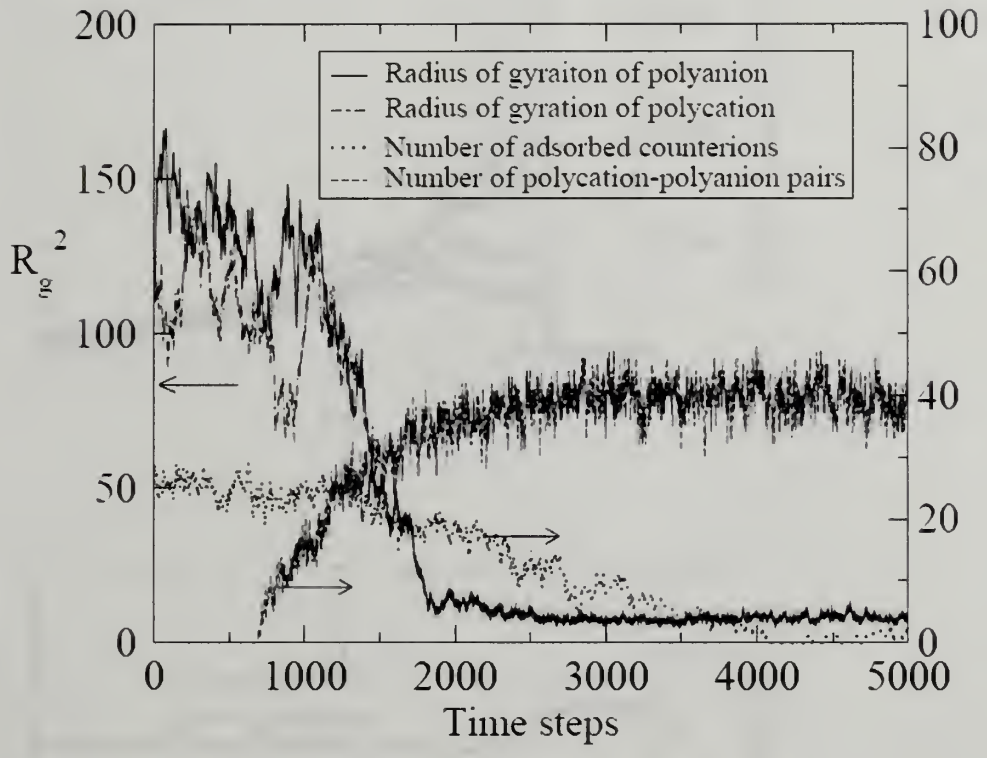

Figure 3.3 The time evolution of the radii of gyration for positively and negatively charged chains during the complex formation and the time evolution of the numbers of adsorbed counterions and polycation-polyanion pairs during the complex formation. Chain length N=60, Z_c=1, and Γ=2.0.

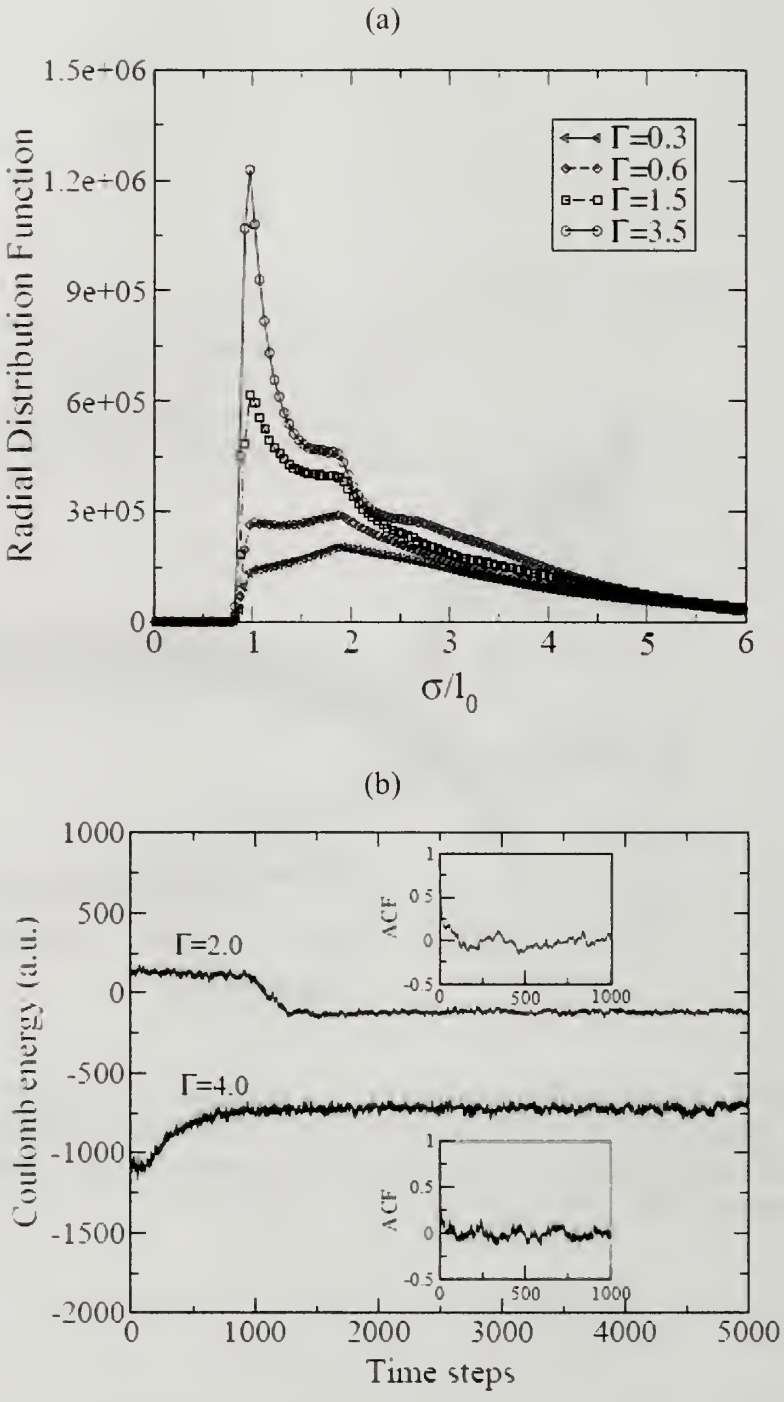

Figure 3.4 (a) Radial distribution function of two oppositely charged chains within a polyelectrolyte complex at different Coulomb interaction strengths. (b) The time evolution of Coulomb energy of the system during the complex formation at Γ=2.0 and 4.0. Autocorrelation functions for the plateau regimes are plotted in the inset. Chain length N=60 and Z_c=1.

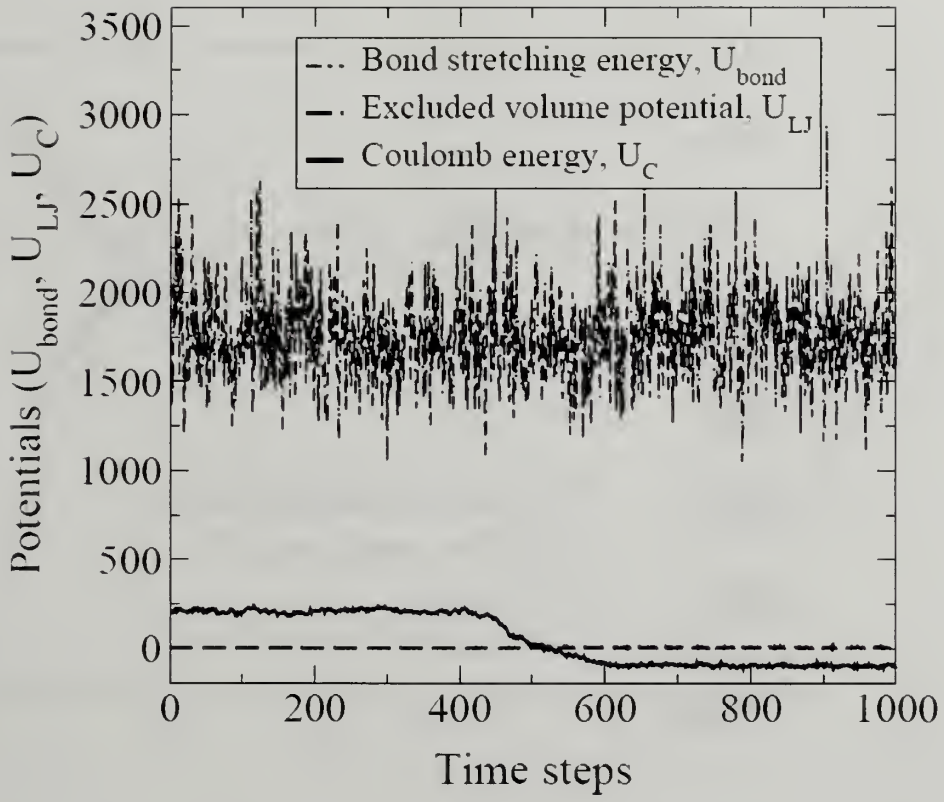

Figure 3.5 The changes in bond stretch energy, Lennard-Jones interaction, and Coulomb energy during the complex formation between two oppositely charged polymers. Chain length N=60, counterion valency Z_c=1, and Γ=2.0.

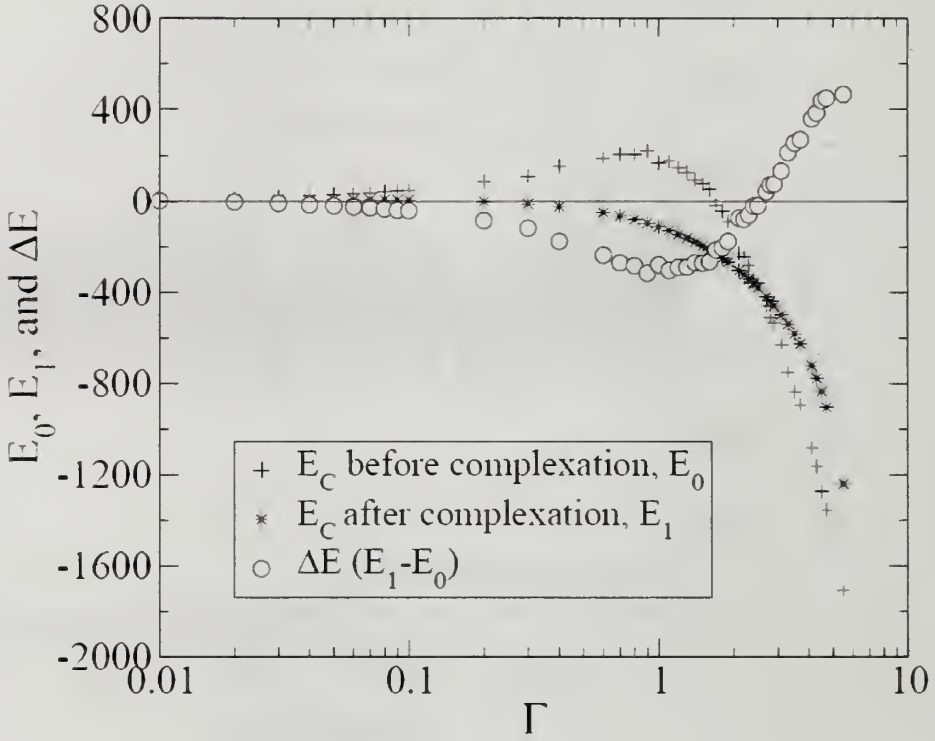

Figure 3.6 Coulomb energy of a system before complexation and after complexation and net Coulomb energy gain for the complex formation between two oppositely charged polymers at different Γ values. Chain length N=60 and counterion valency Z_c=1.

(a)

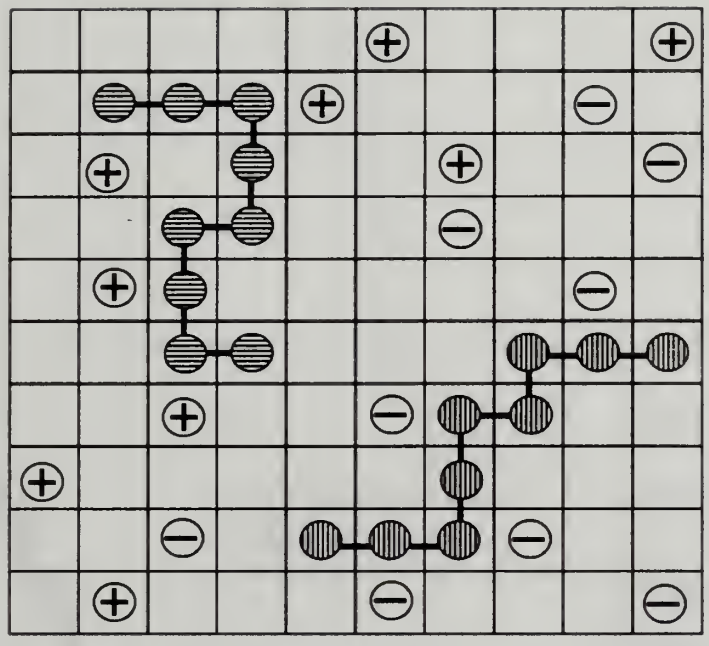

(b)

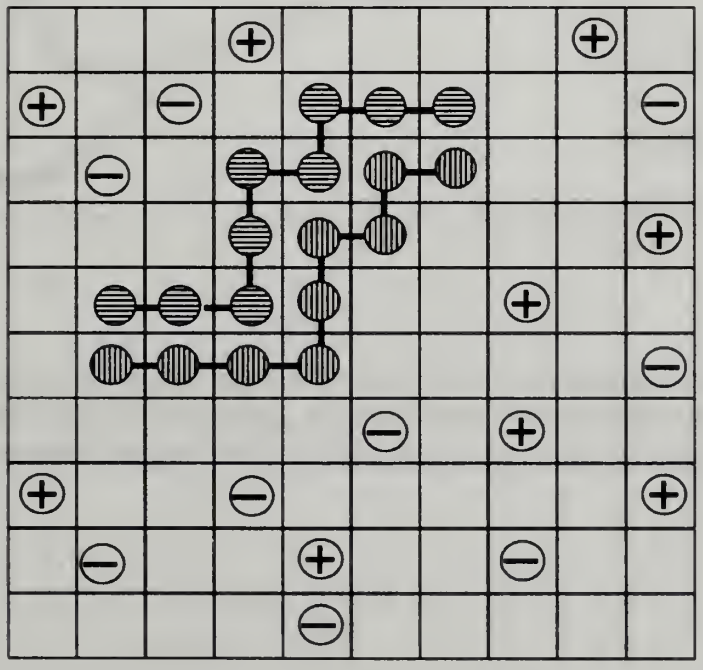

Figure 3.7 Lattice model representations of polyelectrolyte chains and counterions. (a) before polyelectrolyte complexation and (b) after polyelectrolyte complexation. The chain with beads of vertical stripes is positively charged, and the chain with beads of horizontal ones is negatively charged.

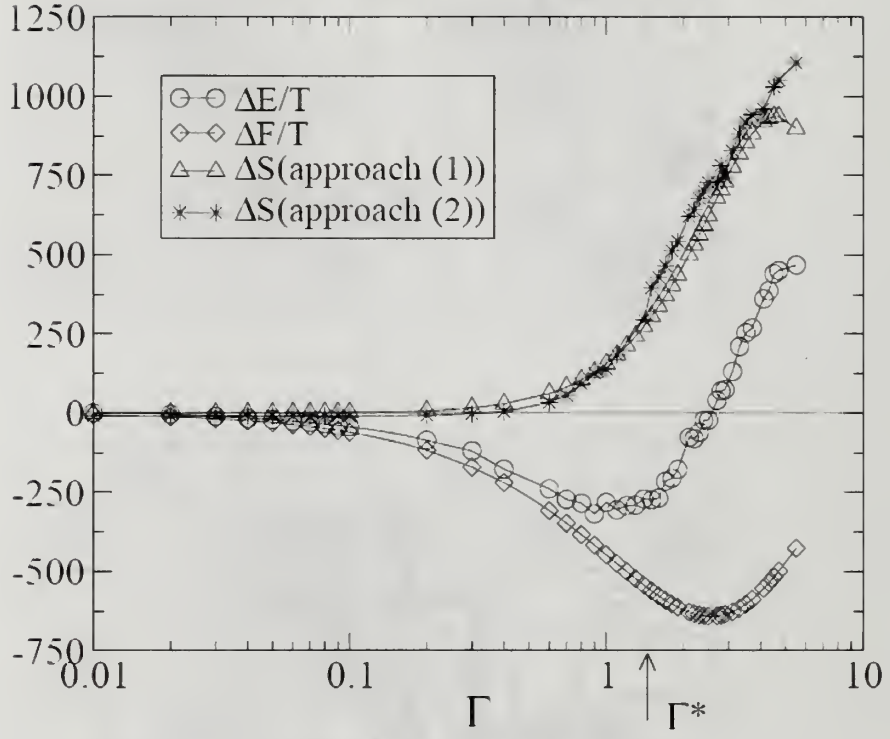

Figure 3.8 Comparison of the counterion release entropy of polyelectrolyte complexation determined by two different approaches defined in the text. Approaches 1 and 2 use Eqs. (3.1) and (3.6), respectively. Chain length N=60 and counterion valency Z_c=1.

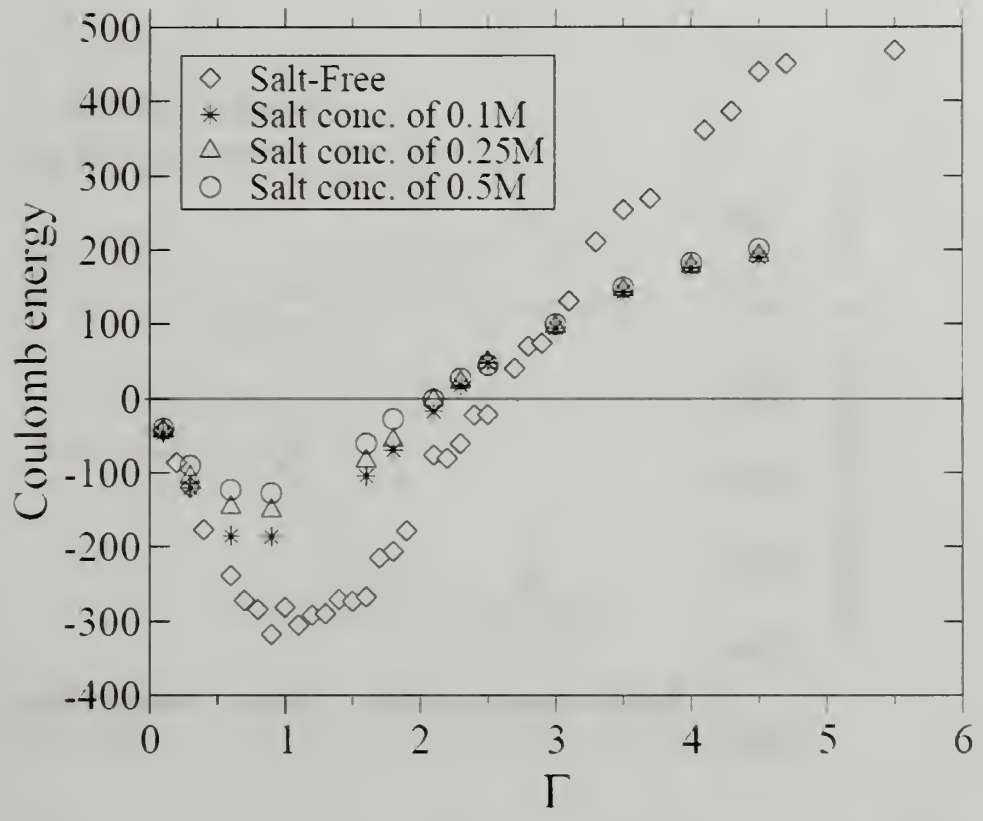

Figure 3.9 Salt effects on the Coulomb energy change of polyelectrolyte complexation. Three different salt concentrations are studied, 0.1*M*, 0.25*M*, and 0.5*M*. Monovalent salt is used. Chain length N=60 and counterion valency Z_c=1.

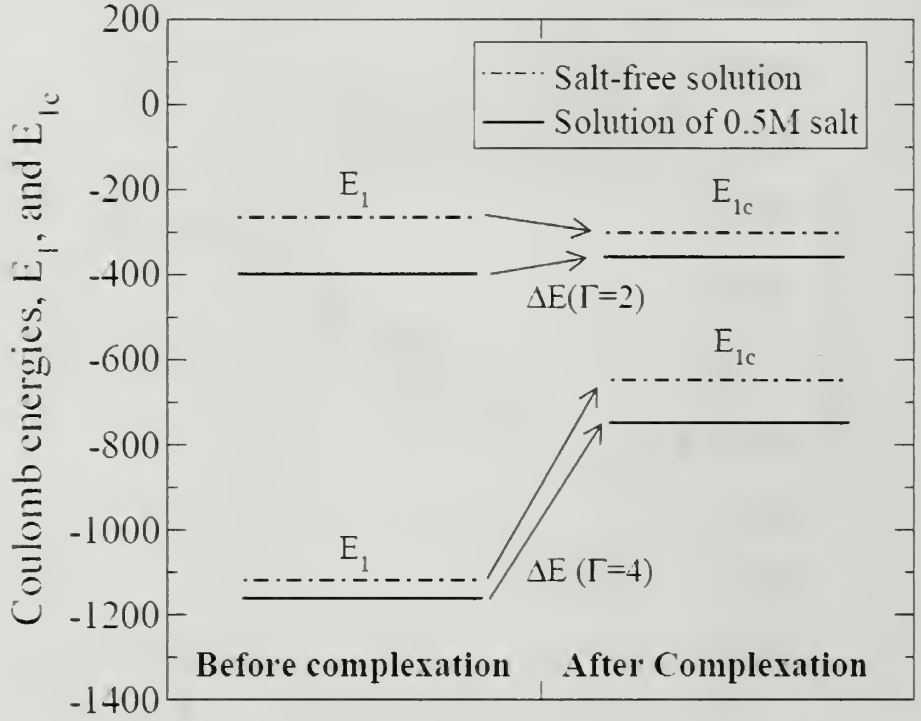

Figure 3.10 Salt effects on energy of complexation at Γ=2.0 and Γ=4.0. The salt concentration is 0.5*M*. Chain length N=60 and Z_c=1.

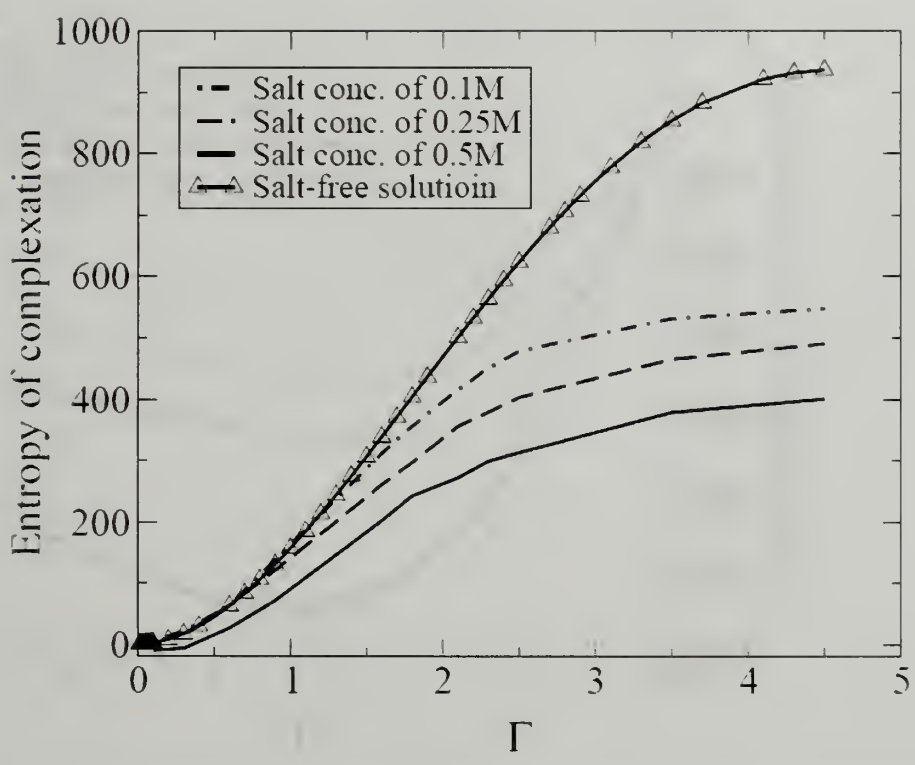

Figure 3.11 Salt effects on the counterion release entropy of polyelectrolyte complexation. Three different salt concentrations are studied, 0.1*M*, 0.25*M*, and 0.5*M*. Chain length N=60 and Z_c=1.

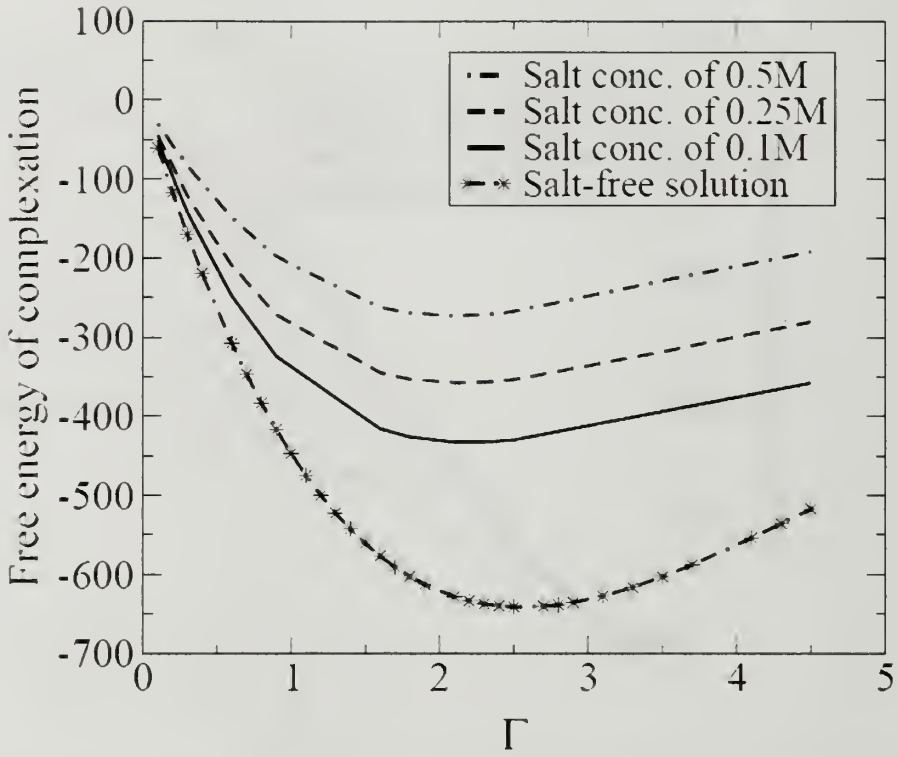

Figure 3.12 Salt effects on the free energy of polyelectrolyte complexation. Three different salt concentrations are studied, 0.1*M*, 0.25*M*, and 0.5*M*. Chain length N=60 and Z_c=1.

CHAPTER 4

COMB POLYELECTROLYTES AND COMPLEXES

4.1 Introduction

Comb polyelectrolyte refers to an intriguing class of polymer whose backbone is grafted with charged side chains in a regular fashion. The best example of comb polyelectrolyte is probably proteoglycan (Figure 4.1),[1] one of the major components in extracellular matrix (ECM). Proteoglycan's structure features long negatively charged polysaccharide chains (chondroitin sulphate and keratan sulphate, see Figure 4.1) chemically linked onto a linear polypeptide backbone, with its overall conformation mimicking a rigid molecular "bottlebrush".[1] In recent decade, advances in controlled polymerizations have enabled an increasingly larger number of different functional charged polymers to be grafted into comb architecture.[2-21] Besides the benefits of having choices over many types of side chains to be incorporated, synthetic comb polyelectrolyte also offers unprecedented controls over such structural parameters as side chain graft density and molecular weight. As demonstrated in proteoglycan, the important consequence of having many highly charged side chains is the extended conformations afforded on the neutral main chain backbone which is intrinsically flexible otherwise. The stretching of main chain backbone in a comb polyelectrolyte can be attributed to two major effects: (1) steric crowding of side chains; (2) electrostatic repulsion among charged units of side chains. Previous studies of neutral comb polymers have shown that steric crowding from densely-grafted chains overcomes the

entropic restoring force of a flexible main-chain backbone and forces it to adopt a rigid conformation with a persistence length much larger than that of a flexible chain.[22-28] When side chains in comb polymers also carry electric charges, it naturally follows that the stretching of main chain backbone should be more significant due to long-ranged electrostatic repulsion within side chains, in addition to their steric effects. A molecular "bottlebrush" is envisaged with both side chains and main chain in comb polyelectrolyte highly extended.[2,29-32] The steric crowdness of side chains in comb polyelectrolyte, in analogue with planar polymer brushes, stems from localized entropic interactions between nearest-neighboring side chains, each occupying a spherical space defined by its radius of gyration (R_g) and separated by a fixed distance (inversely proportional to brush grafting density). The higher the grafting density (shorter distance) and/or the longer the side chain (larger R_g) is, the stronger the steric repulsion and the stiffer the main-chain backbone becomes. In contrast with the short-ranged steric repulsion, electrostatic interaction is inherently long-ranged, potentially affecting both nearest-neighboring and next-nearest neighboring chains. It is also strongly mitigated by the presence of counterions and external salt ions. It is well known in single linear polyelectrolyte[33-37] that when the charge density of a polyelectrolyte chain, characterized by the spatial separation distance of two neighboring charged monomers along the chain, l_0, is increased to such that l_0 becomes smaller than l_B, the Bjerrum length of surrounding medium (typically water), a fraction of the polyelectrolyte's counterions will start adsorbing on the polyelectrolyte chain, in effect screening the electrostatic repulsion among charged monomers and reducing the stiffness of the polyelectrolyte chain as a whole. The critical l_B/l_0 (=1) was first defined in the

celebrated Manning condensation theory,[38,39] which was refined recently by a more realistic and sophisticated description of polyelectrolyte model.[36] In comb polyelectrolytes, electrostatic repulsion between two neighboring side chains is expected to be much stronger than that between two charged monomer units in a linear polyelectrolyte. As a result, the inception of counterion condensation in a comb polyelectrolyte could happen at a critical l_B/ l_0 ratio that is much lower than unity found in linear polyelectrolytes. The rigidity of a comb polyelectrolyte would then very much depend on when this critical l_0/ l_B ratio appears, which is in turn determined by side chain density and side chain molecular weight.

The high rigidity of a comb polyelectrolyte bottlebrush makes it a very attractive template for nanostructure fabrications. [40-42] As an example, negatively charged $HAu(Cl)_4$ ions was brought to complex with Core-shell cylindrical brushes with a PVP core and PS shell, and after subsequent reduction, one-dimensional gold phase was produced within the macromolecular brush.[40] It is also of great interest to understand the connection between bottlebrush conformation of naturally occurring proteoglycan to its important physiological roles in maintaining a hydrated and resilient cartilage under extreme pressures.[1] Due to the unique spatial arrangements of side chains in comb polyelectrolyte, understanding its conformational properties is also essential to studies on binding of comb polyelectrolyte with oppositely charged molecules, e.g. proteins and polyelectrolytes.[43-46]

This chapter will contain three sections. The first one deals with static and dynamic light scattering studies of conformational properties of oligopeptide-grafted polyocycloctenes in water. Following the solution studies of single oligopeptide-grafted

polycyclooctenes, the second section reports the formation and characterization of pentalysine-*g*-polycycloocene complexes with dsDNA in water. This study aimed to establish fundamental knowledge on the DNA-complexation behaviors of this new class of comb-shaped cationic polyelectrolytes, with the ultimate goal of utilizing these polyelectrolytes as novel effective and efficient non-viral gene carriers in gene therapy. The third section provides a systematic computer simulation study on electrostatic-mediated rigidity of comb polyelectrolytes, in efforts to unraveling the intriguing effects of side chain graft density, side chain length, and electrostatic coupling strength ($\Gamma = l_B/l_0$) on the stiffness (quantified by persistence length parameter, l_p) of main chain backbone. The simulation results will also be compared to theoretical predictions from a mean-field model for a comb polyelectrolyte in the weak electrostatic coupling limit (small Γ by either a small l_B or a large l_0).

4.2 Conformational Properties of Oligopeptide-Grafted Polycyclooctenes In Water

4.2.1 Experimental

4.2.1.1 Materials

Oligopeptide-grafted polycyclooctenes (Figure 4.2) were synthesized by Rebecca B. Breitenkamp in Professor Todd Emrick's group in University of Massachusetts at Amherst. Briefly, oligolysine-grafted cyclooctene monomers were prepared by Fmoc-based SPPS on a 2-chlorotrityl chloride resin, cleaved from the solid state resin under mildly acidic conditions, and characterized by ^{1}H and ^{13}C NMR spectroscopy, FTIR spectrometry, elemental analysis, mass spectrometry, and/or GPC. Detailed information on structural characterizations of monomers can be found in a recent publication.[47] Oligolysine-grafted cyclooctene monomers were polymerized by Ring Opening Metathesis Polymerization (ROMP) using the bromopyridine-functionalized Grubbs Generation III catalyst. The molecular weight and molecular distribution of polymers **1-3** (Figure 4.2) were determined by organic and/or aqueous GPC and the results were collected in Table 4.1.

4.2.1.2 Sample Preparation and Static and Dynamic Light Scattering

NaCl solutions with concentration of 0.1M and 0.5M were made by dissolving suitable amounts of NaCl pellets (Fisher) in water purified by a Mill-Q UF system with a resistance of 18.2 mΩ.cm. To adjust the pH of a solution, HCl (diluted from concentrated solution.) or NaOH (1M) solution was used. Stock solutions were prepared by dissolving the polymer in the NaCl solutions and were then allowed to equilibrate at room temperature for at least 24 hours prior to dilution.

Light scattering studies were performed with an ALV light scattering apparatus equipped with an ALV-5000 board. A green laser (COHERENT) with a wavelength of 514.5 nm was used as incident light source, and the temperature of the sample holder was held constant at 25±0.1°C by a circulating water bath. For static light scattering experiments, the scattering intensity of a toluene solution was first measured as the standard. Polymer solutions were directly filtered into pre-cleaned curettes by a syringe equipped with a membrane filter of diameter 0.22 um (Millipore, hydrophilic PVDF membrane). Static light scattering was carried out in the angle range of 35° to 135° with three repeats at each angle. In dynamic light scattering studies, the scattering intensity autocorrelation function, $g^2(t)$, was recorded and analyzed by CONTIN algorithm to generate a relaxation spectrum where a dominant peak was identified, and its corresponding relaxation time, $1/\tau$, was plotted against scattering vector square, q^2. The slope of a linear fit of $1/\tau$ *vs.* q^2 yielded the diffusion coefficient of the polymer molecule at that concentration (c), D(c). The polymer diffusion coefficient at zero concentration, D_0, was obtained by extrapolating the D(c) *vs.* c curve to c=0 with a linear fit with the equation $D(c) = D_0(1 + kc)$ where k is a constant. To determine the hydrodynamic radius, R_h, the Stoke-Einstein equation, $D_0 = k_B T/6\pi\eta R_h$ was applied where k_B is the Boltzmann constant, T represents temperature, and η is the solvent viscosity at T.

4.2.2 Results and Discussion

Table 4.2 summaries the molecular weight, second viral coefficient A_2, and radius of gyration (R_g), and hydrodynamic radius for poly 1, poly 2 and poly 3 in solutions of different pH and ionic strength. The first three quantities were results from static light scattering with Zimm analysis. Hydrodynamic radius was obtained through CONTIN[48,49] analysis of intensity autocorrelation function in dynamic light scattering.

4.2.2.1 Salt Effects on Size and Shape of Pentalysine-g-Polycyclooctene in Water

Poly1 in 0.1 M NaCl aqueous solution. The z-averaged molecular weight of polymer, Mw_z, is given by the inverse of the intercept in the y-axis of Zimm plot where the extrapolated lines from zero concentration(c=0) and zero scattering angle meet (q=0) (**Figure 4.3**). The amine group, NH_2, in a lysine monomer has pKa about 10.5, and thus would be fully protonated and positively charged when they dissolve in neutral aqueous solutions. Assuming that all the lysine groups in the side chains release their chloride counterions when polymer dissolves in water, the M_w of 48.5K puts the degree of polymerization at 66, which is close to the ratio of monomers to resins used in ROMP, 50. If we take into account the polydispersity of the sample, and the fact that some counterions would still be associated with monomers due to so-called "counterion condensation" phenomenon,[36,38,39] it is clear that individual dispersion of single polyelectrolyte molecules is achieved in the concentration range used for light scattering studies; that is, no apparent aggregation by such amphiphilic polymer is taking place in aqueous solutions. The positive second viral coefficient measured in

Zimm plot also shows that the graft polyelectrolyte with hydrophobic backbone is in good solvent regime. The radius of gyration of this polymer is 24.9 nm in 0.1M NaCl solutions. This is much larger than the R_g of 6.6 nm for a Gaussian chain with degree of polymerization of 66 and the length of each monomer unit being 2 nm, and instead, is close to the R_g of 38 nm if the polymer is assumed to have a fully-extended chain conformation.

Size of poly1 in 0.5 M NaCl aqueous solution. To investigate the effect of solution ionic strength on the conformations of the molecule, we have also measured the molecular weight, second viral coefficient, A_2, and the radius of gyration in 0.5M NaCl solutions (Figure 4.4). The slightly decreased A_2 indicates that the solvent quality becomes a little poorer at such elevated ionic strength. Polyelectrolyte molecules, however, seem to remain individually dispersed, with only slightly increased molecular weight. The size of this amphiphilic graft polyelectrolyte strongly shrinks at 0.5M NaCl solution, with the radius of gyration reducing to 15.3 nm, indicating a screening effect by monovalent NaCl salt.

Salt effects on the shape of poly1. It is clear from Figure 4.5 that the relaxation time decreases linearly with scattering angle, and the diffusion coefficient, D and thus, the hydrodynamic radius, R_h calculated with Stoke-Einstein equation, is independent of scattering angle. The hydrodynamic radius changes little going from 0.1M NaCl salt to 0.5M. This is in contrast with the strong salt-dependence of R_g. This suggests that even though the size of this amphiphilic graft polyelectrolyte shrinks significantly with

increasing ionic strength, its hydrodynamic properties are more stable in response to the changes in the solution. As an indication of chain extension, we have also calculated the ratio of R_g/R_h at different salt concentrations. The large R_g/R_h at 0.1M NaCl solution suggests a highly extended chain conformation, which becomes more collapsed when the salt concentration increases to 0.5M with smaller R_g/R_h. Large R_g/R_h has also been observed for other densely-grafted molecules, albeit with neutral side chains, and is correlated with molecules assuming extended conformations in solution.[2,3,5] The extension of the chain backbone in so-called "molecular bottlebrush"[2] originates from a strong excluded volume interaction felt in the crowding side chains, which tends to push the otherwise flexible main chain backbone to extremely elongated conformations. In analogy to current molecules, in addition to steric repulsion, those similarly charged lysine groups in the side chains also electrostatically repel each other, contributing to the main chain extension. This electrostatic repulsion is screened when the solution ionic strength increases, as manifested in the reduced R_g/R_h at 0.5M NaCl solutions.

4.2.2.2 pH Effects on Size and Shape of Oligolysine-*g*-Polycyclooctene in Water

We have observed that in neutral low salt (0.1M NaCl) solutions, poly(cyclooctene-graft-pentalysine) assumes highly extended conformations thanks to the confluences of both steric crowding and electrostatic repulsion among those positively charged lysine side chains. Since the protonation of the amine group of a lysine monomer depends sensitively on environment pH values, it is expected that by tuning the solution pH, the contributions of steric crowning and electrostatic repulsion can be tuned. Towards this

end, we have studied the solutions at both pH=2.0 and pH=12.0 by static and dynamic light scattering.

Poly1 solutions at pH=2.0. Radius of gyration, hydrodynamic radius and the R_g/R_h ratio measured at this low pH low salt (no added NaCl salt. salt only comes from H^+ and OH^-.) conditions are both higher than those in neutral 0.1M NaCl solution (see Table 4.2 and Figure 4.6 for Zimm plot). The conformation of polymer is more extended in this solution, probably due to both a higher percentage of amine protonation (more electrostatic repulsion) at the low pH and less salt screening effect on the lysine groups.

Poly1 solutions at pH=12.0. Both radius of gyration and hydrodynamic radius decrease under such high pH environments, where the lysine side chains would have lost their positive charges (see Table 4.2 and Figure 4.7 for Zimm plot). Such a neutralized polymer, however, retains an extended structure with a large R_g/R_h ratio. This ratio is even higher than that in neutral high salt solutions (0.5M NaCl). It shall be noted that the hydrodynamic radius in solutions of pH=12 is significantly smaller than that in neutral low salt solutions (0.1M NaCl). Since hydrodynamic radius is related to the dimension of the side chains, this shrinkage of R_h indicates that the side chain may have strongly contracted when the positive charges of lysine monomers are removed by high pH. These contracted sides chains could create an even more congested conditions when they are clustered around the main chain which is then forced to remain strongly extended.

4.2.2.3 Conformational Properties of Monolysine-*g*-Polycyclooctene in Water

To further explore the effect of the pendent oligolysine grafts on solution properties, **poly2** was studied by static and dynamic light scattering in 0.1 M and 0.5 M NaCl aqueous solutions at neutral pH (Figure 4.8 and Table 4.2). The R_h of **poly2** was found to be extremely small (on the order of 6.5 and 4.4 nm for 0.1 M and 0.5 M NaCl solutions, respectively). The R_g of **poly2** in 0.1 M NaCl solution was found to be larger than would be expected for a globular polymer conformation. The molecular weight indicated that the polymer was individually dispersed in water. Based on R_g/R_h, **poly2** is viewed as exhibiting highly anisotropic conformation, which was even greater than the anisotropic behavior seen in **poly1**. **Poly2** was in a poor solvent regime at high salt concentrations as indicated by the negative A_2 value measured in 0.5 M NaCl solution. Evaluation of these various parameters suggests that **poly2** behaves as a typical hydrophobic polyelectrolyte. Numerous studies[50-55] have determined that when dissolved in water, strongly-charged hydrophobic polyelectrolytes adopts a "*pearl-necklace*" conformation in which the polymer chain consists of multiple mini-aggregates comprised of several monomer units, or "pearls," connected by a string of uncollapsed monomers. Due to the repulsion between pearls, the pearl-necklace conformation becomes stiff. When the solution ionic strength was increased from 0.1 M to 0.5 M, the electrostatic repulsion among the pearls was screened, and the entire chain collapsed into a globular structure as evidenced by the decrease in R_g and R_h. The values of R_g and R_h changed from 27 nm and 6.5 nm at 0.1 M, to 9.0 nm and 4.4 nm at 0.5 M NaCl. Although these light scattering results for **poly2** are consistent with the pearl-necklace model, more direct observation of "pearls" is desirable. While a direct

observation of pearls formed by a single homopolymer molecule continues to be a challenge, **poly2** appears to be an excellent candidate for future experimental verification of theoretical predictions.

4.2.2.4 Solution Properties of Pentalysine-*g*-*co*-Polyethyleneoxide polycyclooctene in Water

Aqueous solutions of **poly3** were also studied by light scattering at both low and high ionic strengths to explore the effect of charge spacing by the introduction of non-ionic, hydrophilic moieties. Compared to **poly1**, the R_g and R_h of the copolymer were substantially higher (see Figure 4.9 and Table 4.2). Given that the molecular mass of the PEG graft was comparable to that of pentalysine, and that the targeted DP of **poly3** is the same as **poly1**, the expansion of **poly3** was unexpected. Incorporating non-ionic, hydrophilic PEG grafts was expected to reduce the strong electrostatic repulsion among the pentalysine moieties, which was shown to be responsible for the 11 highly anisotropic conformation of **poly1**. Therefore, based on the dilution of the electrostatic repulsion, **poly3** was expected to be smaller. However, the effective molecular weight of **poly3** based on light scattering was measured to be about three times larger than the value obtained from organic and aqueous GPC. Furthermore, the copolymer conformation was stable to the drastic change in the solution ionic strength, in contrast to the behavior of **poly1**. From these observations, the copolymer chains likely formed aggregated structures composed of (on average) three chains. One possible origin of such aggregation could be the hydrophobic nature of the polyolefin backbone. The molecular origin of why such aggregates are comprised of only a finite number of these copolymer molecules remains to be fully investigated. The question of the dependence

of the unimer-to-multimer transition on the PEG content is a fundamental problem in understanding the molecular origin of multimer formation.

4.2.3 Conclusions

In summary, the solution behavior of these polyelectrolytes was tailored by changing the peptide graft length and density. Despite the flexible polycyclooctene backbone, polycyclooctene-graft-pentalysine (poly1) exhibited an extended conformation in low ionic strength aqueous solutions due to combined influences of steric crowding and electrostatic repulsion. Screening of electrostatic repulsion at high ionic strength resulted in a more condensed structure. The R_g/R_h found for the monolysine derivative poly2 is consistent with a pearl-necklace structure, in which the hydrophobic backbone collapses on itself in the aqueous environment. However, with the introduction of only 30 mole percent PEG grafts to the pentalysine derivative, the resulting random copolymer (poly3) no longer adopted an extended conformation based on the R_g and R_h values in solution, instead forming aggregates.

4.3 Complexes of Pentalysine-*g*-Polycyclooctene with dsDNA in Water

4.3.1 Introduction

Synthetic cationic polyelectrolytes have been extensively researched on their potentials to encapsulate anionic nucleic acids (DNA, or RNA) into nanoparticulates which serve carriers to deliver corrective genetic materials into cell nuclei.[56-60] Virus-based gene carriers can deliver nucleic acids very effectively, perfected from millions-of-years' evolution, but could incipit potential fatal immune response from recipients.[61-64] Synthetic polymers are generally non-immunogenetic and versatile in terms of structural and functionality optimization, but suffer from significantly lower delivery efficiency. Many barriers and opportunities have been identified towards improving the delivery efficiency of non-viral polymeric gene carriers, starting from the efficient encapsulation of nucleic acids to the unpacking and transport of the nucleic acids across crowd cell cytoplasm into membrane-enclosed nucleus.[56-60,65-67] Thanks to the advances in polymer synthesis, there is a large proliferation of polymeric structures in the literature that are designed to address the low gene delivery efficiency plaguing polymer-based gene carriers.[68-83] The class of comb-like polyelectrolytes such as the ones under current study offers several distinct advantages over linear-chain polyelectrolytes that potentially allow them to become new versatile efficient gene carriers: (1) Highly tunable cationic charge density along the main-chain backbone by varying side chain grafting density, side chain length, and the degree of ionization of side chains; (2) Easy incorporation of different functionalities through copolymerization of respective macromonomers. In this section, cationic pentalysine-grafted polycyclooctene (**poly1**) was mixed with dsDNA solutions and the resultant polymer-

DNA complexes were characterized by dynamic light scattering (DLS) and Atomic Force Microscopy (AFM). We have explored the effects of polyelectrolyte/DNA mixing ratio and charged density of polyelectrolyte on the size and stability of polyelectrolyte-DNA complexes. AFM was used to directly visualize the morphology of polyelectrolyte-DNA complexes after being deposited on mica surface from solution.

4.3.2 Experimental

4.3.2.1 Materials

The same pentalysine-grafted polycyclooctene as studied in the first section was used in this complexation study. We have used a commercially available double-stranded DNA derived from male and female calf thymus tissue (Sigma-Aldrich product D1501). According to the supplier's specifications, the sample is a highly polymerized DNA which contains predominantly double stranded form of DNA (some minor amount of single stranded form DNA) which has a molecular weight between 10-15 million Daltons.

4.3.2.2 Sample Preparations and Characterizations

For DNA complexation experiments, a dilute solution of **poly1** (1mL of 0.5 mg/mL) was mixed with dsDNA (50 μL; 0.3 mg/mL). Concentrated aqueous NaOH was then added to this mixture to give pH ~11. Subsequently, aqueous HCl was added stepwise in 1-5 μL integrals. Using the same laser light scattering apparatus and software described in the first section, Dynamic light scattering data was collected following solution equilibration at room temperature (~21 °C) for at least 10 minutes. The scattering angle was fixed at 90° and the temperature was 25 °C. For imaging with

atomic force microscopy (Digital Instrument, Nanoscope IIIa), the mixture solution was spin cast (rpm 2000) onto a freshly cleaved mica surface, then transferred to the microscope stage. AFM micrographs were obtained in tapping mode under ambient conditions.

4.3.3 Results and Discussion

4.3.3.1 pH effects

The primary amine group in a lysine unit is a weak base with a pKa around 10. The percentage of charged lysine units in **poly1** can be readily adjusted by tuning the solution pH with added HCl or NaOH. As demonstrated in the first section of this chapter, there is a distinct transition from a rod-like conformation at low pH when **poly1** is fully charged to a more flexible one at high pH when **poly1** essentially becomes a neutral polymer. Apart from effecting this conformational change, the transition from a charged polyelectrolyte to a neutral one will also impact its complexation behavior with anionic DNA molecules. It is known that polyelectrolyte complex is stabilized by a strong electrostatic attraction between two oppositely charged polyelectrolytes. Shown in Figure 4.10 are the autocorrelation function curves from dynamic light scattering as a mixture solution of **poly1** and dsDNA gradually became more acidic by HCl titration. No polymer-DNA complexation was detected at high pH, as expected under conditions at which the lysine residues are predominately neutral. With the addition of HCl to the mixture, and associated charging of the grafts, a progressive increase in solution scattering intensity and hydrodynamic radius (R_h) was seen. The complex size leveled off towards the end of the HCl titration. In this series of

experiments, while DNA molecules always carry their negative charges, the number of positively charged lysine units in **poly1** is controlled by the protonation state of lysine's primary amine units, which increases with decreasing pH. As **poly1** is charging up, there are two significant consequences: (1) the complexation affinity of individual poly 1 molecule to DNA becomes larger; (2) the overall ratio of positive (from **poly 1**) to negative charged units (DNA) increases, meaning that there is a growing competition among **poly1** molecules for complexation with a fixed number of DNA molecules in the solution. Complex formation by two oppositely charged polyelectrolytes is generally a thermodynamically favorable process by itself.[84-87] The spontaneous selection of the size of a polyelectrolyte complex as shown in Figure 4.10 is very intriguing and might have to do with several compounding factors: (1) surface tension between newly-minted polyelectrolyte complexes and solvent; (2) polyelectrolyte translational entropy loss upon its incorporation into a complex; (3) amount of excess charges on the surface of a polyelectrolyte complex; (4) structural mismatches between two oppositely charged polyelectrolytes such as charge spacing, intrinsic stiffness, and molecular weight. At high pH where **poly1** has a small amount of charged lysine units, a **poly1**-DNA complex can not grow bigger due to both a weak attraction between poly1 and DNA and a strong competition for **poly1** molecules by the starving DNA molecules. As **poly1** becomes more charged with decreasing solution pH, a bigger **poly1**-DNA complex can be sustained in the solution by a stronger attraction between **poly1** and DNA. Eventually, when the lysine units in **poly1** are predominantly charged, the equilibrium partition of **poly1** and DNA molecules into relatively uniformly-sized complexes in the solution is probably determined by the stoichiometry ratio as well as by structural

details of participating polyelectrolytes (stiffness, molecular weight, charge distribution, solvation, etc).[82,88-91]

4.3.3.2 Mixing Ratio of Polyelectrolyte and DNA

In the previous section, we have shown that the intrinsic binding affinity between **poly1** and DNA strongly affects the dimension of self-assembled **poly1**-DNA complexes. It was also apparent that there was a spontaneous selection of the size of **poly1**-DNA complexes in the solution at each solution pH condition. In this section, we seek to explore the effects of the stoichiometry ratio between positive charges in poly 1 to negative charges in DNA on the spontaneous size selection of resultant poly 1-DNA complexes. **Poly1** under study was dissolved in neutral salt-free aqueous solutions so that each Poly1 molecule is expected to be completely charged and has the same binding affinity towards DNA. The stoichiometry ratio between positive and negative charges, **P:N**, was varied systematically from where DNA charges were in excess (**P:N**<1) to the limit where **poly1** charges were in excess (**P:N** >1). The hydrodynamic radii of **poly1**-DNA complexes formed at different **P:N** ratios were compared in Figure 4.11. As expected, at **P:N** =1, a macroscopic precipitation was observed due to the complete extrinsic compensation of positive and negative charges. At **P:N** <1 or **P:N** >1, discreet stable **poly1**-DNA complexes with a unique radius were identified. The size of the complex reached its peak value at the ratio of **P:N** ratio closest to 1 (**P:N** =2). The complex size became smaller when there was a greater excess of either DNA or **poly1**. The bell-shaped curve of complex size versus mixing ratio has also been reported in other polyelectrolyte complexes systems. It is not yet well understood why certain

dimension is favored in the course of complex formation when oppositely charged polyelectrolytes are mixed.[90] There exists no universal rule that would predict the size of complex for any particular pair of polyelectrolytes. The factors mentioned in the previous section may all play roles in shaping the unique structure and thermodynamics of polyelectrolyte complexes.

4.3.3.3 Atomic Force Microscopy

We have showed above with dynamic light scattering characterization that there was a spontaneous size selection in the formation of polyelectrolyte complexes. Relaxation spectrum analysis of the autocorrelation curves for polyelectrolyte complexes solutions also indicated that there was generally one population of complexes with a narrow width of size distribution. To complement this finding from dynamic light scattering and to study the morphologies of polyelectrolyte complexes, a mixture solution was spun cast onto a freshly-cleaved mica surface, and examined by Atomic Force Microscopy. Figure 4.12 is the micrograph obtained for the solution in the end of titration study shown in Figure 4.10. The average size of the complexes observed by AFM was smaller than that found by dynamic lights scattering, an expected result of the spinning and drying process during sample preparations. The size across many individual complexes on the micrograph was relatively close to each other, confirming the observations from solution characterization by DLS. Individual complexes were roughly round-shaped, although they all seemed to be deformed in the same vertical direction, a possible artifact stemming from solution shearing during spin-coating.

4.3.4 Conclusions

We have demonstrated in this series of proof-of-principle study that comb-like pentalysined-*g*-polycyclooctene, despite of its unique arrangement of charged units and a rigid chain conformation, was able to complex with DNA effectively, resulting in a stable nanosized polyelectrolyte complexes with a narrow size distribution. The complexation behavior of pentalysined-*g*-polycyclooctene can also be manipulated by adjusting both external solution pH and stoichiometry mixing ratio.

4.4 Conformational Properties of Comb Polyelectrolyte: Computer Simulation

4.4.1 Introduction

The extended rod-like conformation observed in pentalysine-grafted polycyclooctene was very intriguing in two following aspects: (1) pentalysine is a short chain yet very effective in stiffing the flexible polycyclooctene backbone; (2) pentalysine chain can be considered as a weakly charged polyelectrolyte where two neighboring positively-charged primary amine groups are separated by a large spatial distance (see Figure 4.2). Incidentally, in naturally occurring "bottlebrush"-like proteoglycan (Figure 4.1), its CS and KS side chains are also weak polyelectrolytes with a large separation distance between two neighboring units along the chain ≥1nm.[1] The length of side chain, side chain grafting density and the polyelectrolyte nature (strong or weak) of side chain must all contribute to the apparent stiffness of the backbone in a comb polyelectrolyte. This simulation study aims to dissect the compounding effects of many important structural and environmental parameters in shaping the conformational properties of a comb polyelectrolyte, particularly its overall rigidity and counterion distribution.

4.4.2 Simulation Method

We applied the same coarse-grained polyelectrolyte model outlined in the previous chapters (2 and 3), except that a comb-like chain architecture was used instead of a liner one. As shown in Figure 4.13, the backbone of a comb polyelectrolyte has 60 neutral monomer units (green spherical beads). Side chains, shown as silver beads, are

grafted along the backbone with three different grafting densities (GN): GN=14, 29, 59, corresponding, respectively, to the situations where every fourth, every second, and every one of backbone monomers is grafted with a side chain. Each side chain has the same number (GL) of monomer units. Three different molecular weights of side chain were studied, GL=*4, 8* and *16*. Each monomer unit in a side chain carries one positive charge in its center. The electrostatic interaction strength among charged units is again characterized by the coupling parameter, $\Gamma=l_B/l_0$where l_0 is the equilibrium bond length of the side chain and l_B is the Bjerrum length, $l_B = k_b T/4\pi\varepsilon_r\varepsilon_0$. To investigate both the weak and strong polyelectrolyte system, we have systematically varied the value of Γ in simulations over two-order of magnitude, Γ=0.01 - 5. We have used the same form of equations to capture the excluded volume, electrostatic, bond-stretching, and Coulombic interaction. The Langevin dynamics simulation, as detailed in the Chapter 1, was used for this study. To evaluate the rigidity of the backbone of a comb polyelectrolyte, we measured the persistence length (l_p) of the backbone after the whole polyelectrolyte reached its equilibrium conformation state after an extended period of simulation. The methodology for determining l_p from Langevin dynamic simulation was detailed in the Chapter 2.

4.4.3 Results and Discussion

The conformational rigidity of the main chain backbone in a comb polyelectrolyte could be qualitatively understood by considering two synergetic contributions. Firstly, neighboring side chains experience short-ranged excluded volume interactions. Such

mutual exclusion translates into an entropic pressure on the flexible main-chain backbone which stretches out in order to accommodate crowding side chains. The extent of stretching monotonically increases with the crowdness in the side chains. Higher side chain grafting density and longer side chain tend to produce more entropic crowdness, and a stiffer comb polymer. Secondly, same charged side chains repel each other electrostatically. The electrostatic repulsion can be felt across a large distance, depending on what the electrostatic coupling strength (Γ) is. The respective contributions from these two factors can be tuned in an interdependent way by adjusting the parameters of side chain grafting density, the length of side chains and electrostatic coupling strength, Γ. Here, we focused on the changes of main chain stiffness in comb polyelectrolyte when all these three parameters were varied.

4.4.3.1 Grating Length Effects

Main-chain rigidity of a comb polyelectrolyte. One of the most common variations in synthesis of comb polyelectrolytes is the molecular weight of side chain.[2,10,17] We first examined the effects of increasing side chain length on the rigidity of a comb polyelectrolyte. Figure 4.14 compares the persistence length of a com polyelectrolyte with every other monomer grafted with a charged side chain (GN=29). Three different side chain molecular weights were studied, GL=4, 8, and 16. The strength of electrostatic interaction, Γ, was tuned from 0.01 to 1. For each of the three different comb polyelectrolytes (GL=4, 8, and 16), its main-chain rigidity initially increases rapidly with Γ. This is followed by a period of slow incremental of l_p, and eventually l_p

starts to decrease with Γ. The transition to slow growth of l_p happens at a transition Γ_c that shifts to a lower value in polyelectrolytes with a longer side chain, Γ_c =0.4, 0.2, and 0.1, for GL=4, 8, and 16, respectively. The consequences of this non-monotonic increase of l_p with Γ are two-folded: (1) the most stiff comb polyelectrolyte is not necessarily the one with the largest electrostatic coupling strength (Γ); in other words, a comb polyelectrolyte grafted with highly charged side chains may actually appear more flexible than the one with modestly charged ones!; (2) at each Γ studied, polyelectrolyte with longer side chains tends to have a higher rigidity than that with shorter ones, but the biggest difference in l_p between these two cases appears in the weak electrostatic interaction limit, e.g., $\Gamma<\Gamma_c$. In fact, for each of three comb polyelectrolytes in Figure 4.14, its persistence length follows an exponential increase with Γ in the weak interaction range ($\Gamma<\Gamma_c$; see above for values of Γ_c for polyelectrolytes with different side chains.). Figure 4.X provides the least-square power-law fits of l_p as a function of Γ for all the three comb polyelectrolytes in their respective $\Gamma<\Gamma_c$ range. The exponents for three different polyelectrolytes are, with error bar, essentially the same (see Table 4.3) Interestingly, the obtained exponent of 0.33 is also in line with the theoretical predictions from a mean-field model[92] for a comb polyelectrolyte chain in its weak electrostatic coupling strength limit, $l_p \sim l_B^{\frac{1}{3}} GL^{\frac{2}{3}} GN$, where GN and GL is side chain grafting density and side chain length, respectively. To test where the above scaling law will also be valid for the dependence of GL in the $\Gamma<\Gamma_c$ range, we plotted in Figure 4.15 the persistence length of a comb polyelectrolyte as a function of its side chain molecular weight, GL, at different Γ. In order to compare the behaviors of persistence length of a

comb polyelectrolyte across different side-chain molecular weights, the values of Γ in Figure 4.14 were selected to be less than the smallest Γ_c (when GL=16). As shown in Figure 4.15 and Table 4.4, in the lower limit of Γ, the fitting exponents are close to the predicted value of 0.67 by the mean-field model. The exponent for the highest Γ becomes significant smaller (0.4), reflecting the diminishing benefit of having a longer side chain on the rigidity of a comb polyelectrolyte. Both our simulations and the theoretical predications show that increasing the molecular weight of side chains will has its largest impacts on the rigidity of a comb polyelectrolyte when its side chains are within weak electrostatic coupling limit. By the definition of Γ (Eqs. (2.5) and (2.6)), a small polyelectrolyte coupling strength, Γ, can be realized by increasing either the dielectric constant of solvent or the charge separation distance, l_0, of the side chain. In the case where water is used as the medium for polyelectrolyte solutions, weakly charged polyelectrolytic side chains (large l_0) could actually produce a stiffer comb polyelectrolyte than strongly charged ones would.

Counterion distribution. One of the central assumptions of the above mean-field model is that charged side chains do not attract a significant amount of counterions.[92] Therefore, inter-sidechain electrostatic repulsion increases rapidly with Γ, and when combined with entropic exclude volume repulsion, results in significant stretching of the main-chain backbone. To quantify the spatial distribution of counterions around a comb polyelectrolyte, we have determined the percentage of counterions that are closely interacting with a comb polyelectrolyte chain. In Figure 4.13, counterions (red beads) are defined as "condensed" counterions if they are residing within a short cutoff

distance (l_0) to the center-of-mass of a side chain bead. Counterions are defined as "trapped" if they are not within the cutoff distance (l_0) to any side chain beads, but reside within the distance of side chain radius of gyrations (R_s) to the main-chain backbone. Counterions far away from the comb polyelectrolyte do not significantly affect the conformational behavior of the polyelectrolyte since the concentration of polyelectrolyte is very diluted in the simulations. The justification for dividing counterions into two distinct states came from the observations from previous simulations on single polyelectrolytes that counterions in close proximity of monomers (within cutoff length, l_0) are on average significantly less mobile than those away from the monomers, and are hence "condensed."[35,37,93] These condensed counterions help screen the intra-monomer repulsion and the polyelectrolyte itself becomes more flexible. In counterion condensation theory for polyelectrolyte, counterion condensation appears at the electrostatic coupling strength, $\Gamma \sim 1.0$.[36,38,39] Whereas in a linear polyelectrolyte, counterions are only distinguished as either "condensed" or "free", a comb polyelectrolyte could potentially attract a lot of un-condensed within the spatial span (R_s) of its side chains. These trapped counterions play the important role of mediating the inter-sidechain electrostatic repulsion among charged side chains. The importance of dividing counterions populations into these two distinct states will become apparent below. Figure 4.16 compared the relative percentages of different kinds of counterions as a function of Γ for three different comb polyelectrolytes. Significantly, in the range of Γ studied, Γ=0.01-1.0, the percentage of condensed counterions increases very slowly and remains small (<15%) for all three different molecular weights. The percentage of condensed counterions in the comb polyelectrolyte with the shortest side

chains, GL=4, is slightly smaller than those with longer side chains (both GL=8 and GL=16). However, the curves (solid symbols in the figure) for GL=8 and GL=16 are almost the same throughout the Γ range. This indicates that the molecular weight of side chain in a comb polyelectrolyte does not significantly affect the behavior of counterion condensation. This has also been found in studies of single polyelectrolyte systems.[35,37,93] Unlike the behaviors of condensed counterions, the percentage of trapped counterions as a function of Γ shows the significant effects as the side chain grows longer. In the weak electrostatic coupling range, Γ=0.01-0.1, comb polyelectrolyte with the longest side chains, GL=16, already shows a strong increment of trapped counterions. In the Γ range, Γ=0.1-1, the difference in their capability to trap counterions among three comb polyelectrolytes is very significant: at Γ=0.7, over 50% of all its counterions are trapped in a comb polyelectrolyte with GL=16, followed by 35% for GL=8 case and only by 10% for GL=4. At Γ>0.7, the percentage of trapped counterions in all three polyelectrolytes started to peak out and decrease, as trapped counterions became "condensed" ones in the high limit of electrostatic coupling strength. It is very interesting to compare the behavior of l_p as a function of Γ in Figure 4.14 with that for the states of counterions (trapped and condensed) in Figure 4.16. We have shown previously that as Γ increases, there is a transitional Γ_c where the persistence length of a comb polyelectrolyte increases slowly, peaks and eventually starts to decrease with Γ. Γ_c is 0.4, 0.2, and 0.1 for GL=4, 8 and 16, respectively. In Figure 4.16, it becomes clear that the transitional Γ_c also happens to be the point where the percentage of trapped counterions in comb polyelectrolytes starts to quickly increase with Γ. At $\Gamma < \Gamma_c$, a comb polyelectrolyte has only a small percentage of either

condensed or trapped counterions, according to Figure 4.16. In this weak interaction regime, the electrostatic repulsion among charged side chains is unbridled and contributes to the rapid rise of the main-chain rigidity with Γ. This is the situation where the no-counterion assumption in the mean-field theory is applicable.[92] So it is no wonder that the scaling exponents for l_p obtained from simulations match those from the theoretical predictions, as demonstrated above. At $\Gamma>\Gamma_c$, counterions begin to accumulate strongly around charged side chains due to stronger electrostatic attractions. As a result, the electrostatic repulsion among side chains, which has been the primary influence in increasing main-chain rigidity, started to be screened by the presence of trapped counterions residing between charged side chains. A comb polyelectrolyte grafted with longer side chains experiences this screening effects by trapped counterions at a lower Γ_c due to its more electrostatically-congested charged side chains. It shall be noted that condensed counterions also help reduce the inter-side chain repulsion by effectively neutralizing the charges each side chain carries. However, the effect of counterion condensation only appears in the much higher Γ range (Γ~1) where the percentage of condensed counterions increases quickly at the expense of the population of trapped counterions.

Side chain expansion. It is apparent from above results that the expansion (or stretching) of main-chain has, to a large extent, to do with the magnitude of inter-sidechain charge repulsion at different electrostatic coupling strength. What is more subtle and difficult to measure is the contributions from inter-side chain exclude volume interactions.[25,28,94-99] The extent of steric repulsion between two neighboring side chains

can be approximately measured by the *end-to-end* distance of side chains, $<R_e>$. Figure 4.17 shows $<R_e>$ as a function of Γ for GL=8 and GL=16. The changes of $<R_e>$ in GL=4 is only marginal due to its small number of beads. the *end-to-end* distance of side chain, $<R_e>$, continue to increases with Γ in both GL=8 and GL=16. Only at $\Gamma \sim 1$ does $<R_e>$ for GL=16 start to show sign of decrease. This is in stark contrast with the behavior of main-chain rigidity which, after an initial quick increase with Γ, starts to decreases at Γ=0.3, and 0.4 for GL=8 and GL=16 respectively (see Figure 4.14). Since side chains of larger $<R_e>$ would experience a stronger exclude volume effect and in turn contribute more entropic pressure to the stretching of main-chain in a comb polymer, this lack of strong correlation between main-chain stiffness (l_p) and side chain stretching, particularly in the $\Gamma > \Gamma_c$ regime, underscores the critical role of inter-sidechain electrostatic repulsion in producing highly stretched comb polyelectrolytes.

4.4.3.2 Grafting Density Effects

A comb polyelectrolyte (with sixty uncharged monomer units in its backbone) is grafted with side chains of eight-monomers (GL=8) at three different grafting densities: one graft in every fourth monomer (GN=14); one graft in every second monomer (GN=29); one graft in every monomer (GN=59). At the least grafted case(GN=14), the separation distance ($4l_0$) between two neighboring side chains is larger than the radius of gyration of a side chain assumed to have a rod-like conformation ($R_g = 8l_0/\sqrt{12} = 2.3l_0$), while at GN=59, that distance (l_0) is slightly smaller than that of a Gaussian chain ($R_g = \sqrt{8/6}l_0 = 1.2\ l_0$). As with previous results, we have systematically

tuned the electrostatic coupling strength, Γ=0.01-4, and examined the concurrent changes in main-chain rigidity, counterion distribution and side-chain expansion.

Main-chain rigidity of a comb polyelectrolyte. Figure 4.18 illustrates the effects of electrostatic coupling strength on the persistence length of comb polyelectrolytes of different grafting densities. The trend of l_p as a function of Γ is similar to what has been observed before: l_p increases fast with Γ initially, transits to a slow growth period at a transition, Γ_c, and eventually starts to decreases at higher values of Γ.

Γ_c shifts to a smaller value in polyelectrolytes with higher grafting density: Γ_c =0.6, 0.3, and 0.09 for GN=14, 29, and 59, respectively. In general, over all the values of Γ investigated, comb polyelectrolytes with higher degree of grafting density exhibits higher main-chain stiffness. However, due to the bell-shaped function of l_p with Γ, the biggest difference in l_p between that in the least grafted (GN=14) and the most grafted (GN=59) appears at the transitional Γ_c for GN=59. The ratio of l_p(GN59) / l_p(GN14) peaks at Γ=0.09 as shown in Figure 4.18. In the strong electrostatic coupling strength limit, Γ>1.0, the persistence length of a comb polyelectrolyte does not substantially benefit from having a higher side chain grafting density: l_p(GN59) / l_p(GN14) ~2, compared to a peak value of 14 at Γ=0.09. The significant implication is that for the purposes of producing highly extended comb polyelectrolytes (maximum stiffness), changes of side chain grafting density may not yield much benefit if the whole system is situated in the high electrostatic coupling strength regime. In the weak coupling limit ($\Gamma<\Gamma_c$; Γ_c values for different GN were defined above) where l_p is shown to increases

rapidly with Γ, we also applied the power-law analysis[92] to all three comb polyelectrolytes and compared the extracted exponents to the prediction from the mean-field model. In Figure 4.18. the fitted power-law exponents for all three grafting densities are in close proximity to the 1/3 theoretical prediction (see Table 4.5). To test the scaling prediction of l_p in GN, l_p for three different comb polyelectrolytes were plotted a function of GN at reprehensive values of Γ in the weak limits (Γ<0.09). The first-order dependence of l_p over GN is recovered only in the lower G range (G=0.01, 0.02, 0.04), and the exponents at Γ=0.04 and 0.05 starts to deviate from 1 (see Table 4.6). An inspection of l_p in Figure 4.19 shows that the deviation of exponents from 1 at Γ=0.0.4 and 0.05 mainly originates from a slow increment of l_p when side chain graft density GN increases from 29 to 59.

Counterion distribution. Figure 4.20 monitors the percentage changes of "condensed" and "trapped" counterions as a function of Γ. Both "condensed" and "trapped" counterions are insignificant for all grafting densities in lower Γ range, Γ<0.1, that is, side chains are "naked". Passing this "naked" regime, there is a transition window of Γ, where the number of "trapped" counterions increases in a significantly faster rate than that of "condensed" ions; that is, [0.5, 1] for GN=14, [0.2,0.6] for GN=29 and [0.1,0.3] for GN=59. The reason for the faster accumulation of trapped counterions over condensed counterions may be due to the fact that trapped counterions, although confined to the vicinity of a comb polyelectrolyte, still enjoy a large entropic freedom, whereas condensed counterions lost most of their entropy due to strong association with charged monomer units.[35,37,93] This transition window correlates with the Γ range where

main chain persistence length has a slow growth curve with Γ before decreasing with Γ. During such transition window, charged side chains are able to attract and retain a significant amount of counterions, of which only a small percentage closely associate with side chains ("condensed"). The entrapment of counterions is more significant in comb polyelectrolytes with higher grafting density of side chains. This fast accumulation of trapped counterions results in stronger screening of inter-side chain electrostatic repulsion, and counteracts the growth of l_p as Γ increases. In the higher limit of Γ (Γ>Γ_c; Γ_c values as defined above for different comb polyelectrolytes), the decrease of l_p with Γ is obviously correlated with having a significantly larger percentage of condensed counterions. For example, at the highest Γ=4.0, overall 80% of counterions are condensed and 10% remains for GN=29. This is the regime where intra-side chain repulsions are strongly screened and the electrostatic repulsion between two side chains becomes much weaker, hence a more flexible main-chain. In this high Γ regime, excluded-volume repulsion is expected to the predominate interaction contributing to the main-chain rigidity, due to the steric crowdness from side chains together with their closely-associated counterions.

End-to-end distance of side chain. Figure 4.21 plots the averaged end-to-end distance, $<R_e>$ of side chain as a function of Γ for three grafting densities. The size of side chains reaches maximum in the approximate of Γ=1.0: Γ_{max_side} =0.9, 0.8, and 0.7 for GN=14, 29, and 59, respectively. It is interesting that at Γ < Γ_{max_side}, increasing graft density notably enlarges the $<R_e>$ of side chain, but almost has no effects after Γ_{max_side} where

$<R_e>$ for all three grafting densities coincides with each other. $< R_e>$ can be treated as a measure of the extent of stretching in side chains.

Since the stretching of side chain with Γ is mainly due to intra-side chain electrostatic repulsions, it is interesting to compare the Γ-dependence of $< R_e>$ with the persistence length of main-chain (Figure 4.18), whose stretching is, however, dominated by inter-side chain electrostatic repulsion. The difference in their respective dependence on Γ is clearly reflected in the population changes of condensed and trapped counterions shown in Figure 4.X. In the "counterion-free" regime, Γ<0.1, both $<R_e>$ and l_p rise rapidly as electrostatic coupling strength becomes stronger. In the transition window of Γ, (0.1, 1) for GN=14, (0.1, 0.6) for GN=29 and (0.1, 0.3) for GN=59, the accumulation of trapped counterions outpaces that of condensed counterions. This discrepancy results in inter-side chain repulsion being more significantly screened by counterions than intra-sidechain repulsion. Therefore, $<R_e>$ continues its rapid increases while l_p rises with a slower rate, or plateaus out. Passing this transition window of Γ, charged side chains are able to attract and binds with a larger proportion of counterions. The effective charges, after counterion condensation, of side chains reduces and results in continuingly weakening of inter-sidechain repulsion. Both $<R_e>$ and l_p decreases with Γ.

Having discussed the general effects of side chain grafting density, side chain length, and electrostatic coupling strength on the main-chain rigidity of a comb polyelectrolyte, we will attempt to apply the simulation findings to understand the behavior of some real comb polyelectrolytes. Synthetic comb polyelectrolytes with side chains made of strong polyelectrolytes, such as polyvinylpyridine[100] fall in the high

limit of Γ (>3.0). In this regime, as shown in Figures 4.14 and 4.18, side chains in comb polyelectrolyte are strongly neutralized by "condensed" counterions, and the rigidity of main chain is controlled most by steric crowding of side chains and counterions associated with them. As an opposite example, naturally occurring proteoglycans carry weakly charged polysaccharide chains with electrostatic coupling strength in the range, 0.5-1.[1,9] For example, in proteolgycans made of chondroitin sulphate (CS) or keratan sulphate (KS) side chains, the distance between sulfate groups in neighboring repeating units is in the order of 1nm, compared with the Bejrrum length of 7.0Å for water at 25°C. Figure indicates that in this middle range of Γ, comb polyelectrolyte is rigid with a significant population of "trapped" counterions. It is known that proteoglycan plays a critical in maintaining the hydration and compressive modulus of extracellular matrix (ECM). Since counterions will likely lose some or all of their water molecules in hydration shell if they are condensed on a polyelectrolyte chain, the ability of proteoglycan molecule to trap, not condense, a large amount of still-hydrated counterions may prove critical in its biological functions.

4.4.3.3 Counterion and Monomer Density Profiles

Figure 4.22 compares the spatial distribution of counterions away from the center-of-mass of a monomer unit (GN=29 and GL=8) at different Γ. In calculating this distribution, we first identified the closest distance of a counterion to all the monomer units of side chains. This was done for all the counterions and the distribution of the distances were averaged over many different configurations of the system (Figure 4.22(a)). The counterion cloud around a monomer unit is evenly distributed in the lower

range of Γ. Preferential counterion accumulation appears at higher Γ where counterion distribution is strongly skewed towards the vicinity of side chain monomers (see Γ=1.2 and Γ=3.0). Following the norm in defining counterion condensation, we count the number of counterions within an average distance, l_0, to monomers in Figure 4.22(b) as "condensed". Besides these closely-associated condensed counterions, Figure 4.22(b) also indicates that at higher Γ (>0.6), there is a higher density of counterions within a cutoff distance of $<R_c>$ (~4.0; the averaged end-to-end distance of side chains) than the counterion density far away from monomers (considered as *bulk concentration of counterions)*. This population of counterions was the "trapped" counterions that we have defined and discussed above.

Another very interesting measure to characterize the spatial distribution of a comb polyelectrolyte is the density profile away from the central main-chain backbone of the polyelectrolyte. Figure 4.23 depicts counterion and monomer density distribution in the direction perpendicular to main chain backbone. The density was determined by counting the number of counterions, or monomers, in the cylindrical shell volume, $L*2\pi R*dR$ (L is the contour length of a comb polyelectrolyte; dR is the differential incremental of distance, R, away from the center of the main-chain backbone. See Figure 4.23(a) for details), and then dividing the obtained number by the shell volume. All the monomer density profiles across different electrostatic coupling strengths show a parabolic decay from the center of main-chain backbone outward. On the other hand, there are also distinct changes in monomer density profile as the conformation of side chains undergoes expansion and shrinking with Γ (Figure 4.14). When side chains are flexible at lower Γ, there is more entropic freedom for side chain monomer units to fold

back to the interior of a comb polyelectrolyte. Hence, monomer density at Γ=0.09 is high close to the center of main-chain backbone. As side chains expand in response to enhanced electrostatic repulsion at higher Γ(=0.4 and 1.8), monomer densities close to the center reduce while those far away increase. This creates a more spread-out comb polyelectrolyte. At even higher Γ(=3.8), side chains again become more flexible due to strong counterion condensation and monomer density profile resembles that at the lowest Γ (=0.09). The density profile of counterion becomes more pronounced monotonically with Γ as more counterions are drawn to side chains. At higher Γ, counterion density profile also turn parabolic in shape and closely follow the density profile of monomer units (Γ=3.8), reflecting a strong association of counterions with monomers.

Parabolic monomer density profile has previously been shown in solution scattering, computer simulation and theoretical studies of planar polyelectrolyte brushes.[101-108] There have been no similar works for comb-like polyelectrolytes. The systematic simulation study reported here would be of interest for calibrations with future studies on this important class of polyelectrolytes.

4.4.4 Conclusions

We have found in our computer simulation studies that the rigidity of a comb polyelectrolyte is mainly due to inter-side chain electrostatic repulsion. Increasing side chain grafting density or side chain molecular weight generally results in a stiffer comb polyelectrolyte due to stronger the inter-side chain electrostatic repulsion. However, the

benefits of having higher grafting density or longer side chains quickly diminish if side chains are polyelectrolytes of high charge density themselves, and/or comb polyelectrolyte is immersed in strong electrostatics coupling medium, e.g., solvents of low dielectric constant. As grafting density and/or molecular weight of side chains increases, there is a steady accumulation of counterion population inside a comb polyelectrolyte. If the overall electrostatic coupling strength is below some critical value, Γ_c, these counterions predominantly roam between side chains, instead of adsorbing (or condensing) on one particular side chain. Such so-called trapped counterions negate inter-side chain electrostatic repulsion responsible for stiffing main-chain in a comb polyelectrolyte. Γ_c becomes smaller in comb polyelectrolytes with higher side chain grafting density and/or longer side chains. Beyond Γ_c, counterions start to condense on individual side chains. In this regime, a comb polyelectrolyte is essentially a neutral polymer and its rigidity is now dictated by excluded-volume interactions among side chains and their counterions.

4.5 References

1. L. Ng, A. J. Grodzinsky, P. Patwari, J. Sandy, A. Plaas, and C. Ortiz, Journal of Structural Biology 143, 242 (2003).

2. M. Wintermantel, M. Gerle, K. Fischer, M. Schmidt, I. Wataoka, H. Urakawa, K. Kajiwara, and Y. Tsukahara, Macromolecules 29, 978 (1996).

3. P. Dziezok, S. S. Sheiko, K. Fischer, M. Schmidt, and M. Moller, Angewandte Chemie-International Edition 36, 2812 (1997).

4. I. Wataoka, H. Urakawa, K. Kajiwara, M. Schmidt, and M. Wintermantel, Polymer International 44, 365 (1997).

5. M. Gerle, K. Fischer, S. Roos, A. H. E. Muller, M. Schmidt, S. S. Sheiko, S. Prokhorova, and M. Moller, Macromolecules 32, 2629 (1999).

6. K. Fischer and M. Schmidt, Macromolecular Rapid Communications 22, 787 (2001).

7. M. W. Neiser, J. Okuda, and M. Schmidt, Macromolecules 36, 5437 (2003).

8. B. Zhang, S. J. Zhang, L. Okrasa, T. Pakula, T. Stephan, and M. Schmidt, Polymer 45, 4009 (2004).

9. B. Zhang, K. Fischer, and M. Schmidt, Macromolecular Chemistry and Physics 206, 157 (2005).

10. B. Zhang, F. Grohn, J. S. Pedersen, K. Fischer, and M. Schmidt, Macromolecules 39, 8440 (2006).

11. K. L. Beers, S. G. Gaynor, K. Matyjaszewski, S. S. Sheiko, and M. Moller, Macromolecules 31, 9413 (1998).

12. H. G. Borner, K. Beers, K. Matyjaszewski, S. S. Sheiko, and M. Moller, Macromolecules 34, 4375 (2001).

13. S. Rathgeber, T. Pakula, A. Wilk, K. Matyjaszewski, and K. L. Beers, Journal of Chemical Physics 122 (2005).

14. S. Rathgeber, T. Pakula, A. Wilk, K. Matyjaszewski, H. I. Lee, and K. L. .Beers, Polymer 47, 7318 (2006).

15. G. L. Cheng, A. Boker, M. F. Zhang, G. Krausch, and A. H. E. Muller, Macromolecules 34, 6883 (2001).

16. M. F. Zhang, T. Breiner, H. Mori, and A. H. E. Muller, Polymer 44, 1449 (2003).

17. M. F. Zhang and A. H. E. Muller, Journal of Polymer Science Part a-Polymer Chemistry 43, 3461 (2005).

18. Y. Y. Xu, H. Becker, J. Y. Yuan, M. Burkhardt, Y. Zhang, A. Walther, S. Bolisetty, M. Ballauff, and A. H. E. Muller, Macromolecular Chemistry and Physics 208, 1666 (2007).

19. S. S. Sheiko and M. Moller, Chemical Reviews 101, 4099 (2001).

20. H. G. Borner, D. Duran, K. Matyjaszewski, M. da Silva, and S. S. Sheiko, Macromolecules 35, 3387 (2002).

21. M. O. Gallyamov, B. Tartsch, A. R. Khoklov, S. S. Sheiko, H. G. Borner, K. Matyjaszewski, and M. Moller, Macromolecular Rapid Communications 25, 1703 (2004).

22. L. J. Shu, A. D. Schluter, C. Ecker, N. Severin, and J. P. Rabe, Angewandte Chemie-International Edition 40, 4666 (2001).

23. A. F. Zhang, B. Zhang, E. Wachtersbach, M. Schmidt, and A. D. Schluter, Chemistry-a European Journal 9, 6083 (2003).

24. Y. Zhang, X. K. Li, G. H. Deng, and Y. M. Chen, Macromolecular Chemistry and Physics 207, 1394 (2006).

25. M. Saariaho, I. Szleifer, O. Ikkala, and G. ten Brinke, Macromolecular Theory and Simulations 7, 211 (1998).

26. M. Saariaho, A. Subbotin, I. Szleifer, O. Ikkala, and G. ten Brinke, Macromolecules 32, 4439 (1999).

27. A. Subbotin, M. Saariaho, R. Stepanyan, O. Ikkala, and G. ten Brinke, Macromolecules 33, 6168 (2000).

28. E. Flikkema and G. ten Brinke, Macromolecular Theory and Simulations 11, 777 (2002).

29. S. Lecommandoux, F. Checot, R. Borsali, M. Schappacher, A. Deffieux, A. Brulet, and J. P. Cotton, Macromolecules 35, 8878 (2002).

30. H. Schlaad, H. Kukula, B. Smarsly, M. Antonietti, and T. Pakula, Polymer 43, 5321 (2002).

31. S. Jha, S. Dutta, and N. B. Bowden, Macromolecules 37, 4365 (2004).

32. Y. Lu, Y. Mei, R. Walker, M. Ballauff, and M. Drechsler, Polymer 47, 4985 (2006).

33. M. Beer, M. Schmidt, and M. Muthukumar, Macromolecules 30, 8375 (1997).

34. V. M. Prabhu, M. Muthukumar, G. D. Wignall, and Y. B. Melnichenko, Polymer 42, 8935 (2001).

35. S. Liu and M. Muthukumar, Journal of Chemical Physics 116, 9975 (2002).

36. M. Muthukumar, Journal of Chemical Physics 120, 9343 (2004).

37. Z. Y. Ou and M. Muthukumar, Journal of Chemical Physics 123, 9 (2005).

38. G. S. Manning, Journal of Chemical Physics 51, 924 (1969).

39. G. S. Manning, Quarterly Reviews of Biophysics 11, 179 (1978).

40. R. Djalali, S. Y. Li, and M. Schmidt, Macromolecules 35, 4282 (2002).

41. M. F. Zhang, C. Estournes, W. Bietsch, and A. H. E. Muller, Advanced Functional Materials 14, 871 (2004).

42. L. Zhang, W. Li, and A. Zhang, Progress in Chemistry 18, 939 (2006).

43. O. Ikkala and G. ten Brinke, Chemical Communications, 2131 (2004).

44. S. Hanski, N. Houbenov, J. Ruokolainen, D. Chondronicola, H. Iatrou, N. Hadjichristidis, and O. Ikkala, Biomacromolecules 7, 3379 (2006).

45. P. Tsolakis and G. Bokias, Macromolecules 39, 393 (2006).

46. M. O. Gallyamov, S. G. Starodubtsev, T. P. Bragina, L. V. Dubrovina, Potemkin, II, O. Marti, and A. R. Khokhlov, Macromolecular Chemistry and Physics 208, 164 (2007).

47. R. B., Breitenkamp, Z. Y., Ou, M., Muthukumar, and T. Emrick, Macromolecules 40, 7617 (2007).

48. S. W. Provencher, Computer Physics Communications 27, 213 (1982).

49. S. W. Provencher, Computer Physics Communications 27, 229 (1982).

50. A. Kiriy, G. Gorodyska, S. Minko, W. Jaeger, P. Stepanek, and M. Stamm, Journal of the American Chemical Society 124, 13454 (2002).

51. D. Baigl, R. Ober, D. Qu, A. Fery, and C. E. Williams, Europhysics Letters 62, 588 (2003).

52. W. Essafi, F. Lafuma, and C. E. Williams, Journal De Physique Ii 5, 1269 (1995).

53. D. Baigl, M. Sferrazza, and C. E. Williams, Europhysics Letters 62, 110 (2003).

54. U. Micka, C. Holm, and K. Kremer, Langmuir 15, 4033 (1999).

55. A. V. Dobrynin, M. Rubinstein, and S. P. Obukhov, Macromolecules 29, 2974 (1996).

56. D. W. Pack, A. S. Hoffman, S. Pun, and P. S. Stayton, Nature Reviews Drug Discovery 4, 581 (2005).

57. T. Merdan, J. Kopecek, and T. Kissel, Advanced Drug Delivery Reviews 54, 715 (2002).

58. M. E. Davis, Current Opinion in Biotechnology 13, 128 (2002).

59. M. C. Garnett, Critical Reviews in Therapeutic Drug Carrier Systems 16, 147 (1999).

60. D. Luo and W. M. Saltzman, Nature Biotechnology 18, 33 (2000).

61. M. A. Kay, J. C. Glorioso, and L. Naldini, Nature Medicine 7, 33 (2001).

62. K. Benihoud, P. Yeh, and M. Perricaudet, Current Opinion in Biotechnology 10, 440 (1999).

63. P. D. Robbins and S. C. Ghivizzani, Pharmacology & Therapeutics 80, 35 (1998).

64. W. F. Anderson, Nature 392, 25 (1998).

65. C. M. Wiethoff and C. R. Middaugh, Journal of Pharmaceutical Sciences 92, 203 (2003).

66. M. D. Brown, A. G. Schatzlein, and I. F. Uchegbu, International Journal of Pharmaceutics 229, 1 (2001).

67. C. W. Pouton and L. W. Seymour, Advanced Drug Delivery Reviews 34, 3 (1998).

68. U. Lungwitz, M. Breunig, T. Blunk, and A. Gopferich, European Journal of Pharmaceutics and Biopharmaceutics 60, 247 (2005).

69. A. K. Salem, P. C. Searson, and K. W. Leong, Nature Materials 2, 668 (2003).

70. E. S. Lee, H. J. Shin, K. Na, and Y. H. Bae, Journal of Controlled Release 90, 363 (2003).

71. K. Kunath, A. von Harpe, D. Fischer, and T. Kissel, Journal of Controlled Release 88, 159 (2003).

72. K. Rittner, A. Benavente, A. Bompard-Sorlet, F. Heitz, G. Divita, R. Brasseur, and E. Jacobs, Molecular Therapy 5, 104 (2002).

73. H. Petersen, P. M. Fechner, A. L. Martin, K. Kunath, S. Stolnik, C. J. Roberts, D. Fischer, M. C. Davies, and T. Kissel, Bioconjugate Chemistry 13, 845 (2002).

74 M. Ohsaki, T. Okuda, A. Wada, T. Hirayama, T. Niidome, and H. Aoyagi, Bioconjugate Chemistry 13, 510 (2002).

75. D. Luo, K. Haverstick, N. Belcheva, E. Han, and W. M. Saltzman, Macromolecules 35, 3456 (2002).

76. T. Azzam, H. Eliyahu, L. Shapira, M. Linial, Y. Barenholz, and A. J. Domb, Journal of Medicinal Chemistry 45, 1817 (2002).

77. C. Perez, A. Sanchez, D. Putnam, D. Ting, R. Langer, and M. J. Alonso, Journal of Controlled Release 75, 211 (2001).

78. M. Koping-Hoggard, I. Tubulekas, H. Guan, K. Edwards, M. Nilsson, K. M. Varum, and P. Artursson, Gene Therapy 8, 1108 (2001).

79. D. M. Lynn and R. Langer, Journal of the American Chemical Society 122, 10761 (2000).

80. Y. B. Lim, S. O. Han, H. U. Kong, Y. Lee, J. S. Park, B. Jeong, and S. W. Kim, Pharmaceutical Research 17, 811 (2000).

81. L. Dekie, V. Toncheva, P. Dubruel, E. H. Schacht, L. Barrett, and L. W. Seymour, Journal of Controlled Release 65, 187 (2000).

82. J. M. Benns, J. S. Choi, R. I. Mahato, J. S. Park, and S. W. Kim, Bioconjugate Chemistry 11, 637 (2000).

83. D. Putnam and R. Langer, Macromolecules 32, 3658 (1999).

84. Z. Y. Ou and M. Muthukumar, Journal of Chemical Physics 124, 11 (2006).

85. D. P. Mascotti and T. M. Lohman, Biochemistry 36, 7272 (1997).

86. D. Matulis, I. Rouzina, and V. A. Bloomfield, Journal of Molecular Biology 296, 1053 (2000).

87. C. K. Nisha, S. V. Manorama, M. Ganguli, S. Maiti, and J. N. Kizhakkedathu, Langmuir 20, 2386 (2004).

88. T. Reschel, C. Konak, D. Oupicky, L. W. Seymour, and K. Ulbrich, Journal of Controlled Release 81, 201 (2002).

89. H. Q. Mao, K. Roy, V. L. Troung-Le, K. A. Janes, K. Y. Lin, Y. Wang, J. T. August, and K. W. Leong, Journal of Controlled Release 70, 399 (2001).

90. W. T. Godbey, K. K. Wu, and A. G. Mikos, Journal of Biomedical Materials Research 45, 268 (1999).

91. D. Fischer, T. Bieber, Y. X. Li, H. P. Elsasser, and T. Kissel, Pharmaceutical Research 16, 1273 (1999).

92. M., Muthukumar, Unpublished results.

93. M. J. Stevens and K. Kremer, Journal of Chemical Physics 103, 1669 (1995).

94. J. J. Freire, in Branched Polymers Ii (1999), Vol. 143, pp. 35.

95. P. G. Khalatur, D. G. Shirvanyanz, N. Y. Starovoitova, and A. R. Khokhlov, Macromolecular Theory and Simulations 9, 141 (2000).

96. S. Elli, F. Ganazzoli, E. G. Timoshenko, Y. A. Kuznetsov, and R. Connolly, Journal of Chemical Physics 120, 6257 (2004).

97. R. Connolly, G. Bellesia, E. G. Timoshenko, Y. A. Kuznetsov, S. Elli, and F. Ganazzoli, Macromolecules 38, 5288 (2005).

98. A. Yethiraj, Journal of Chemical Physics 125 (2006).

99. M. Hellmann, M. Weiss, and D. W. Heermann, Physical Review E 76 (2007).

100. R. Djalali, N. Hugenberg, K. Fischer, and M. Schmidt, Macromolecular Rapid Communications 20, 444 (1999).

101. H. Ahrens, S. Forster, C. A. Hehn, N. A. Kumar, A. Naji, R. R. Netz, and C. Seidel, Journal of Physical Chemistry B 108, 16870 (2004).

102. F. S. Csajka and C. Seidel, Macromolecules 33, 2728 (2000).

103. P. Guenoun, A. Schlachli, D. Sentenac, J. W. Mays, and J. J. Benattar, Physical Review Letters 74, 3628 (1995).

104. R. Hariharan, C. Biver, J. Mays, and W. B. Russel, Macromolecules 31, 7506 (1998).

105. N. A. Kumar and C. Seidel, Macromolecules 38, 9341 (2005).

106. A. Naji, R. R. Netz, and C. Seidel, European Physical Journal E 12, 223 (2003).

107. J. Ruhe, M. Ballauff, M. Biesalski, P. Dziezok, F. Grohn, D. Johannsmann, N. Houbenov, N. Hugenberg, R. Konradi, S. Minko, M. Motornov, R. R. Netz, M. Schmidt, C. Seidel, M. Stamm, T. Stephan, D. Usov, and H. N. Zhang, in Polyelectrolytes with Defined Molecular Architecture I (2004), Vol. 165, pp. 79.

108. C. Seidel, Macromolecules 36, 2536 (2003).

Table 4.1 Polymerization conditions and data for graft copolymers **1-3**[47]

Polymer	Solvent	Time	M_n	M_w	M_w (abs.)	PDI
poly1	0.5 M 10/90 DCM/TFE	40 min.	87,000[b]	144,000[b]	48,000[c]	1.7
poly2	1.2 M 50/50 DCM/MeOH	3 hrs.	7,500[a]	11,000[a]	36,000[c]	1.5
poly3	0.6 M 50/50 DCM/MeOH	3 hrs	36,000[a]	61,000[a]	200,000[c]	1.7

a = Boc-protected analog analyzed by THF GPC relative to PEG standards
b = determined by aqueous GPC relative to PEG standards (0.5 M acetic acid, 0.3 M sodium sulfate)
c = absolute M_w determined by static light scattering in 0.1 M NaCl aqueous solution (25°C)

Table 4.2 Summary of light scattering studies on polymers **1-3**[47]

Polymer	Conditions	M_w (g/mol)	R_g (nm)	R_h (nm)	A_2 ((mol•dm^3)/g^2)
poly1	0.1 M NaCl*	48,000	25	11	$1.6 \cdot 10^{-6}$
	0.5 M NaCl*	53,000	15	10	$4.7 \cdot 10^{-7}$
	pH 2+	57,000	28	12	$2.9 \cdot 10^{-6}$
	pH 12+	61,000	20	8.8	$6.6 \cdot 10^{-6}$
poly2	0.1 M NaCl*	36,000	27	6.5	$1.3 \cdot 10^{-6}$
	0.5 M NaCl*	28,000	9.0	4.4	$-4.2 \cdot 10^{-6}$
poly3	0.1 M NaCl*	200,000	35	22	$2.2 \cdot 10^{-7}$
	0.5 M NaCl*	220,000	39	23	$2.7 \cdot 10^{-7}$

* pH 7 + salt concentration = 0.1 M NaCl

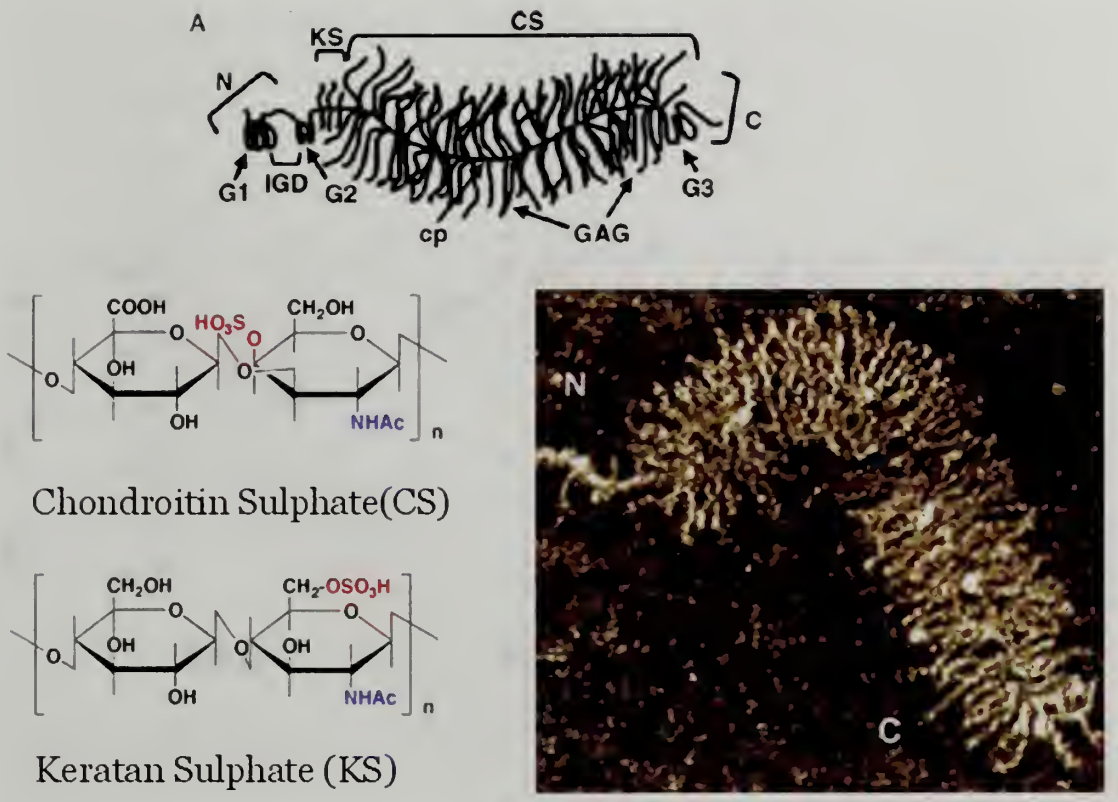

Figure 4.1 Proteoglycan molecular structure and conformation. Top: chemical structure of a proteoglycan; bottom left: chemical structures of chondroitin sulphate and keratan sulphate; bottom right: Atomic Force Micrograph of a proteoglycan on the mica surface[1].

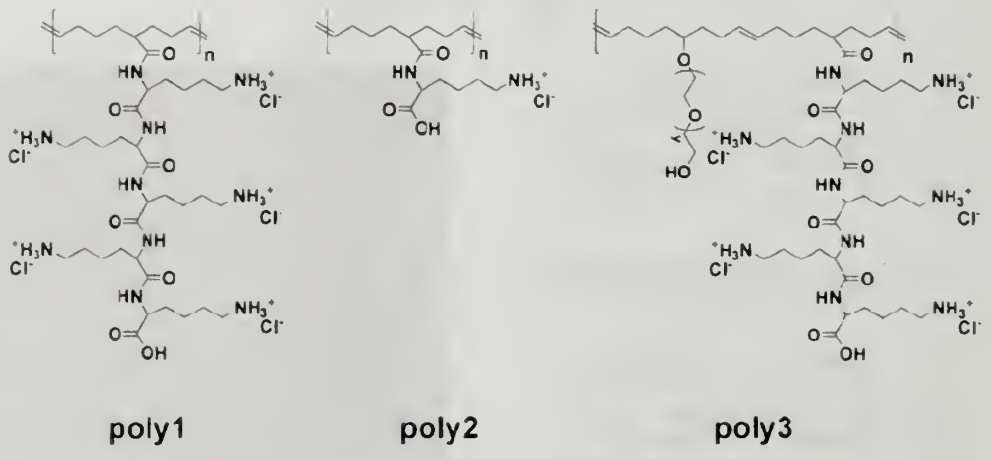

Figure 4.2 Structures of graft copolymers **poly1-3**.

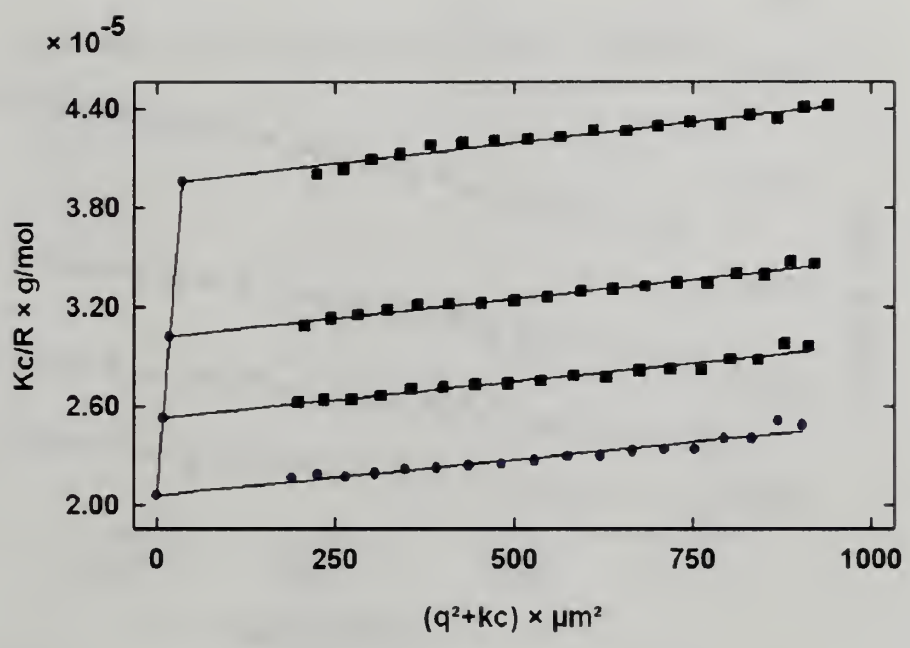

Figure 4.3 Zimm plot for **poly1** in 0.1M NaCl solution. K is the scattering constant, c is the poly 1 concentration and R is relative scattering Raleigh ratio of **poly1** solution. q is the momentum transfer vector and is related with the scattering angle, θ, by $q=4\pi n\sin(\theta/2)/\lambda$. n is the refractive index of polyelectrolyte solution and l is the wavelength of incident laser.

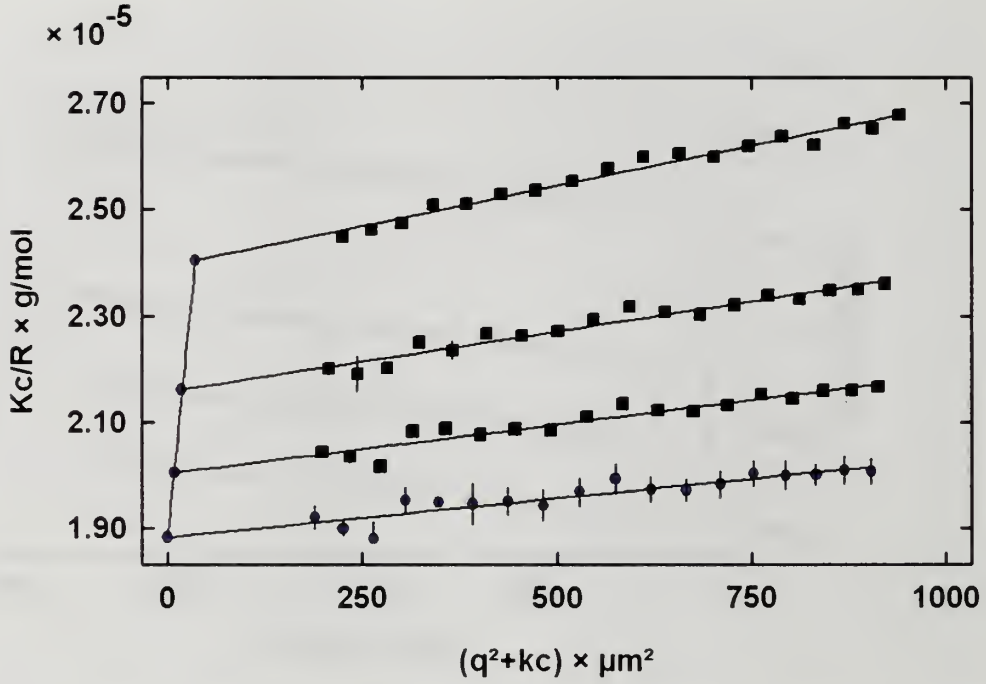

Figure 4.4 Zimm plot for **poly1** solution in 0.5M NaCl solution.

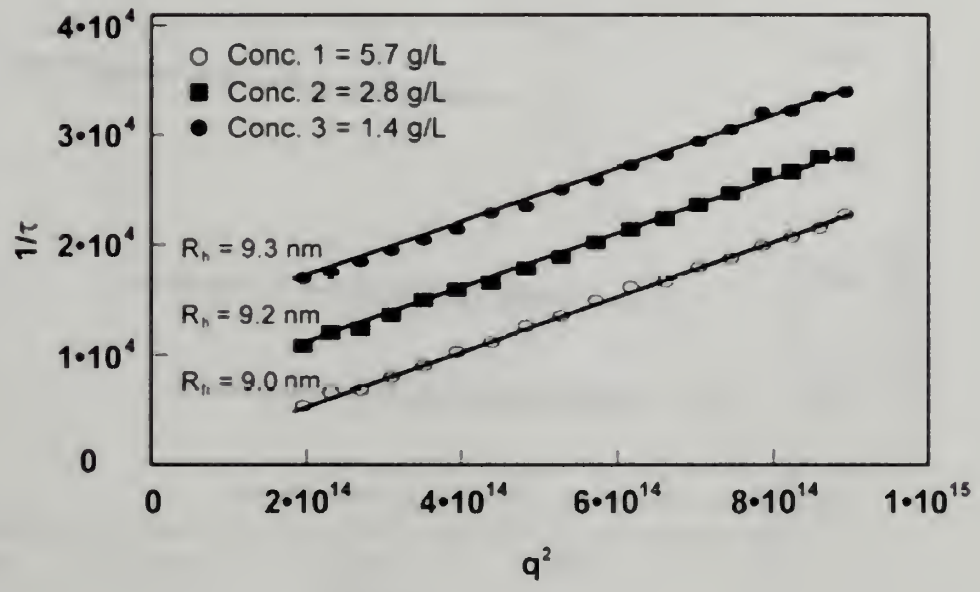

Figure 4.5 Inverse of relaxation time ($1/\tau$) from DLS as a function of q^2 for **poly1** solutions of different concentrations. All $1/\tau$ lines pass through the origin and the top two curves are shifted vertically upward for clarity.

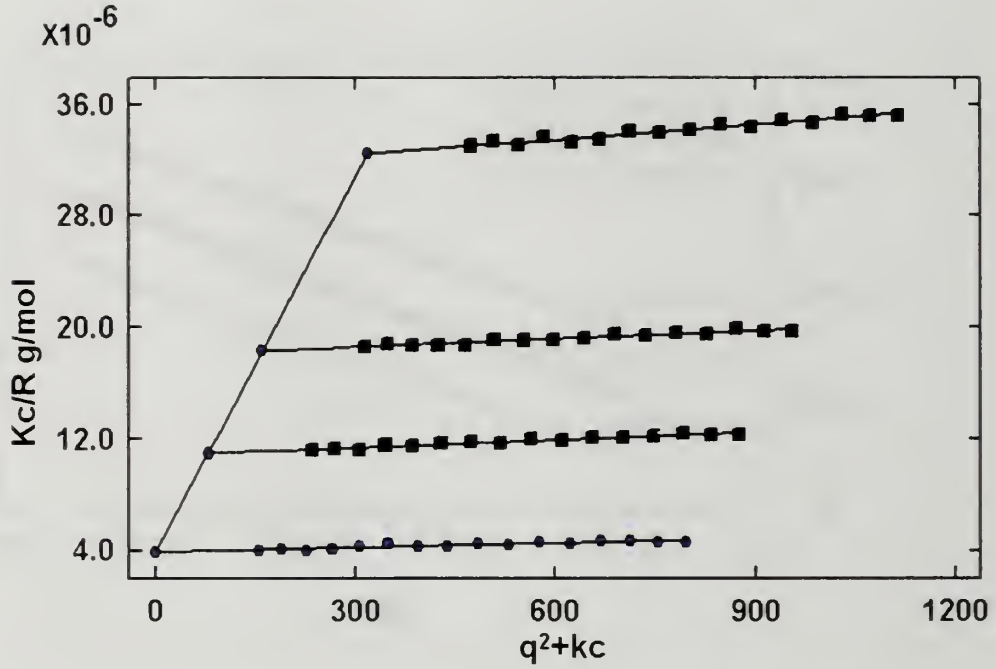

Figure 4.6 Zimm plot for **poly1** in salt-free solutions of pH=2.0

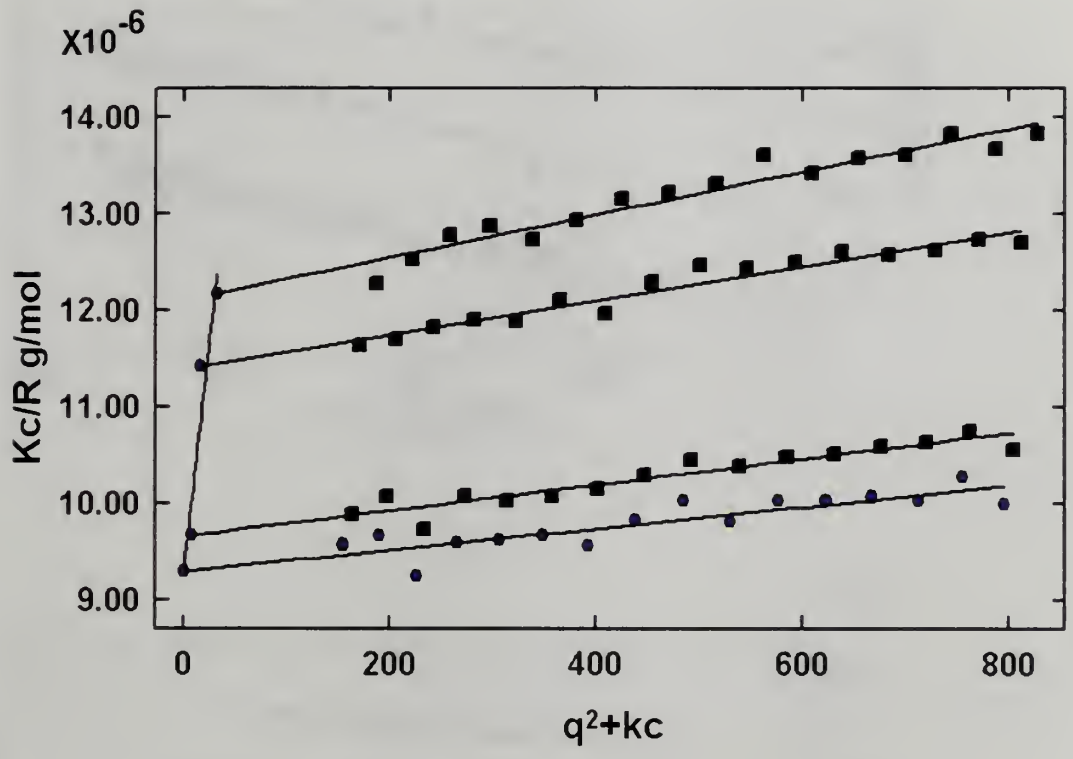

Figure 4.7 Zimm plot for **poly1** in salt-free solutions of pH=12.0.

(a)

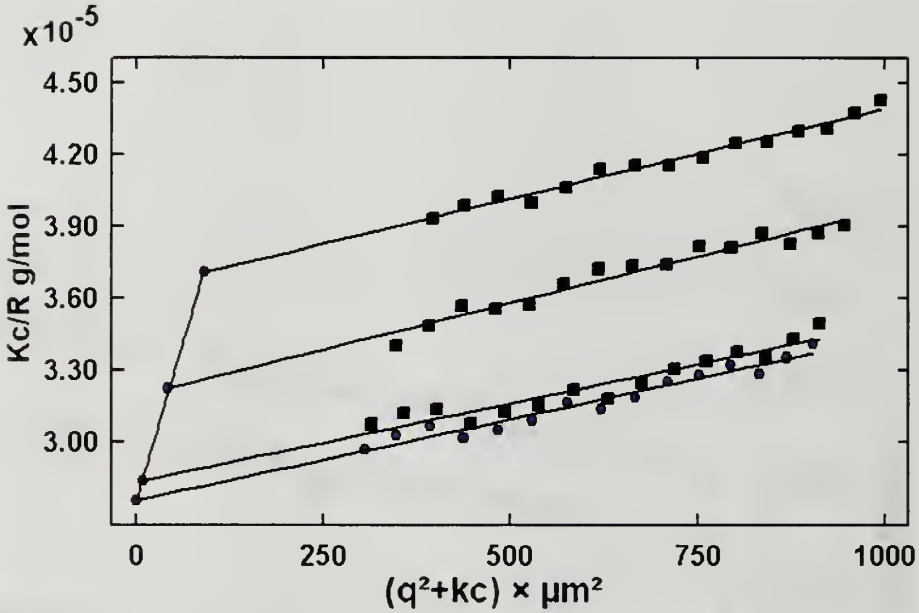

(b)

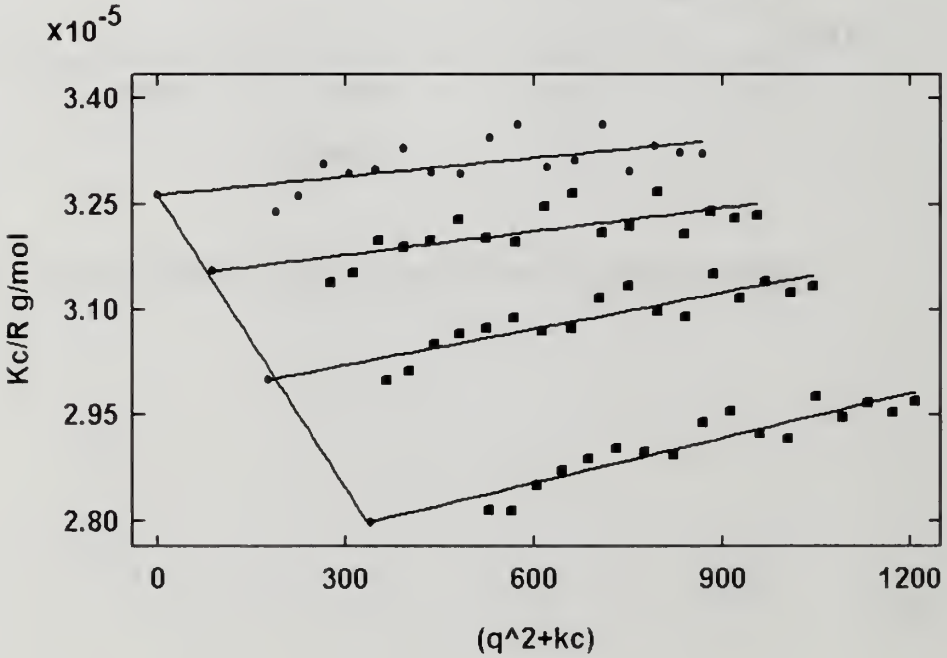

Figure 4.8 (a) Zimm plot for **poly2** in 0.1M NaCl solutions; (b) in 0.5M NaCl solutions.

(a)

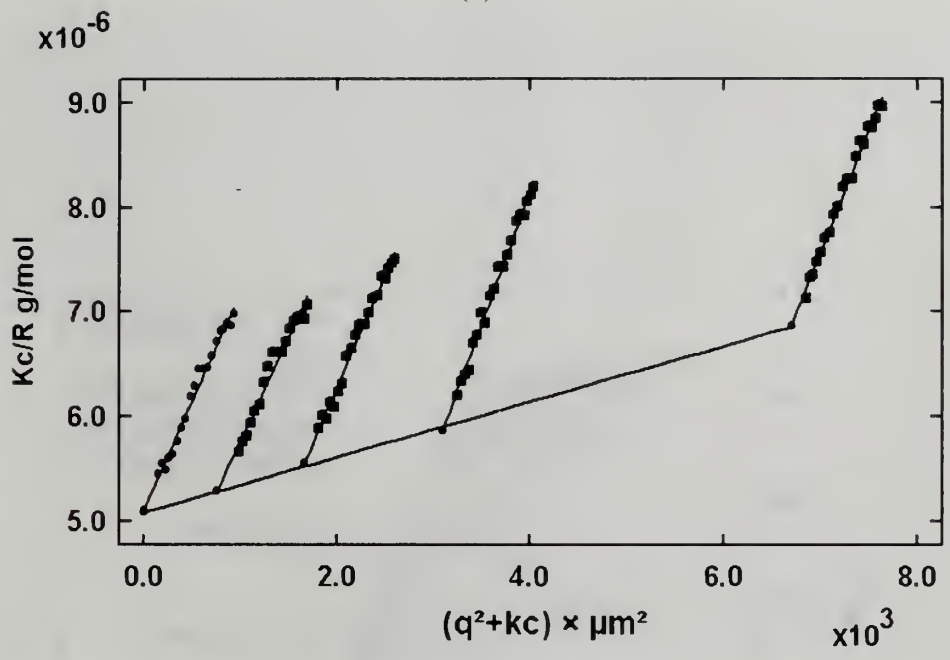

(b)

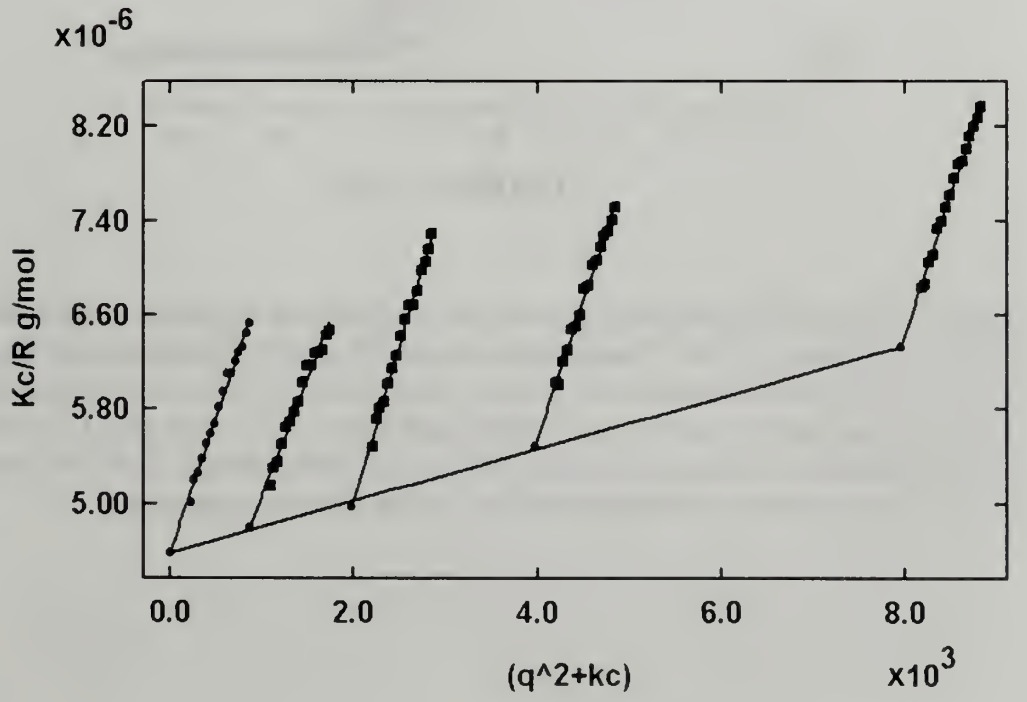

Figure 4.9 (a) Zimm plot for **poly3** in 0.1M NaCl solutions; (b) in 0.5M NaCl solutions.

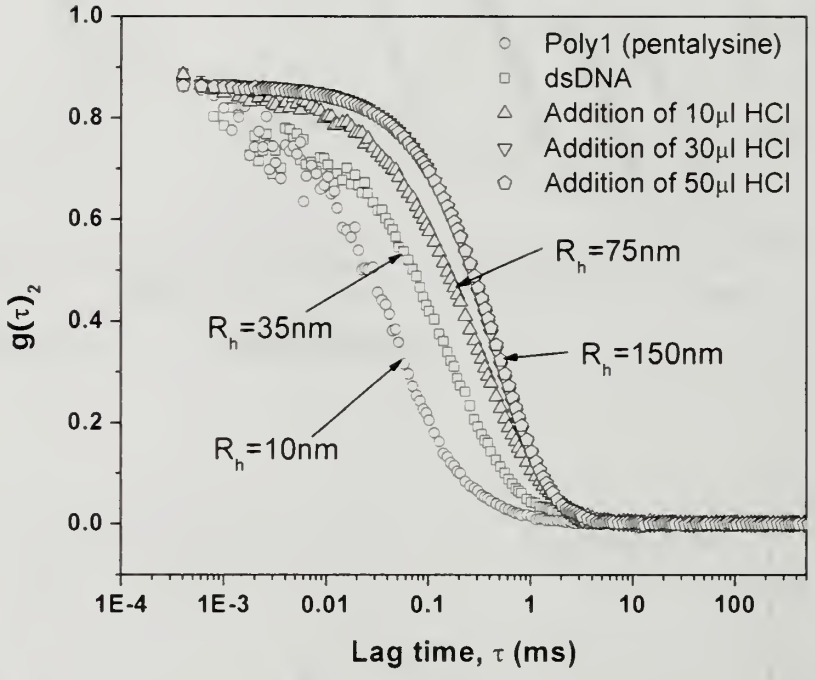

Figure 4.10 Scattering intensity autocorrelation functions for **poly1** (open sphere), DNA (open square), DNA + **poly1** solution with 10 μl HCl added (open up triangle), with 30 μl HCl added (open down triangle), and with 50 μl HCl added (open pentagon). The DNA and poly1 solution was initially held at pH 12, in which **poly1** is neutral, and no complexation was detected by DLS. R_h was calculated from a CONTIN analysis of intensity autocorrelation functions and the Stokes-Einstein relationship.

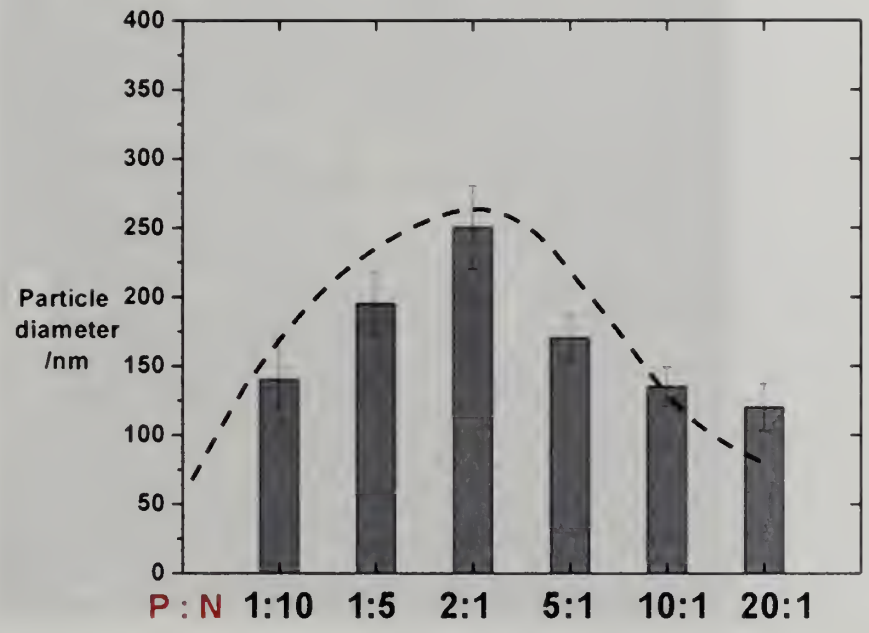

Figure 4.11 The effects of **poly1** and DNA mixing ratio (P: N) on the hydrodynamic radius of the formed **poly1**-DNA complexes in water.

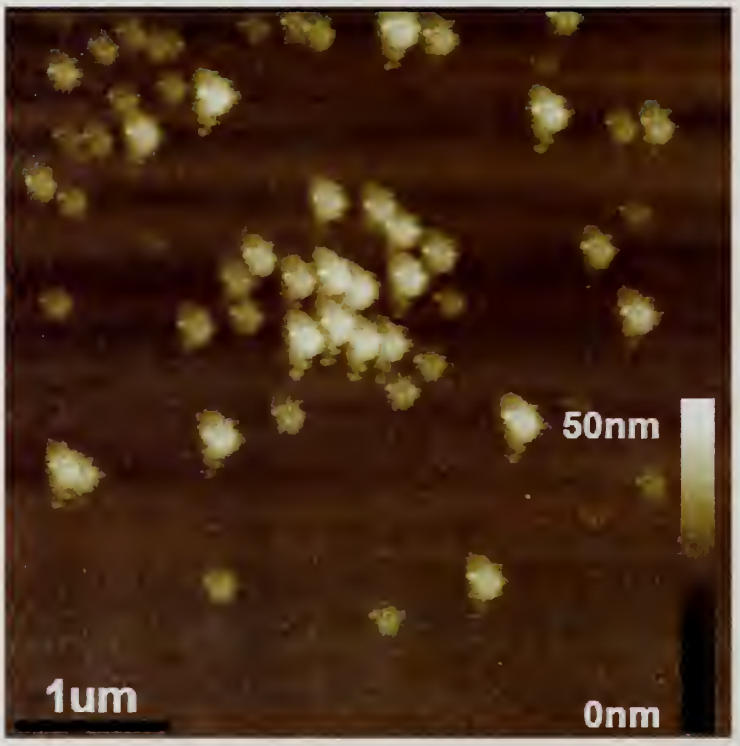

Figure 4.12 Tapping-mode Atomic Force Micrograph of **poly1**-dsDNA complexes spin-cast onto freshly cleaved mica.

(a)

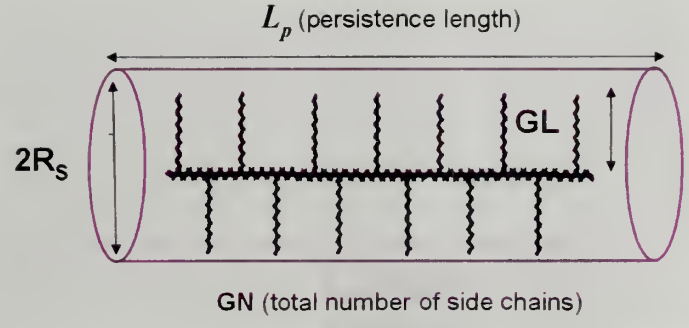

(b)

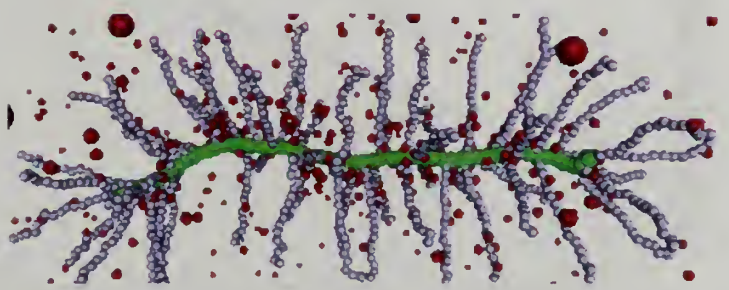

Figure 4.13 Schematic representaions of comb polyelectrolytes in simulation. (a) A schematic representation of a comb polyelectrolyte chain. L_p is the main-chain persistence length, GL is the molecular weigh of side chain, GN is the total number of sides chain per comb polyelectrolyte. R_s is the averaged end-to-end distance of side chains. (b) A snapshot of a model comb polyelectrolyte in simulation. Green beads presents the backbone chain, silver ones are the charged side chains, and red sphere is monovalent counterions. A comb polyelectrolyte is immersed in a medium of dielectric constant, ε.

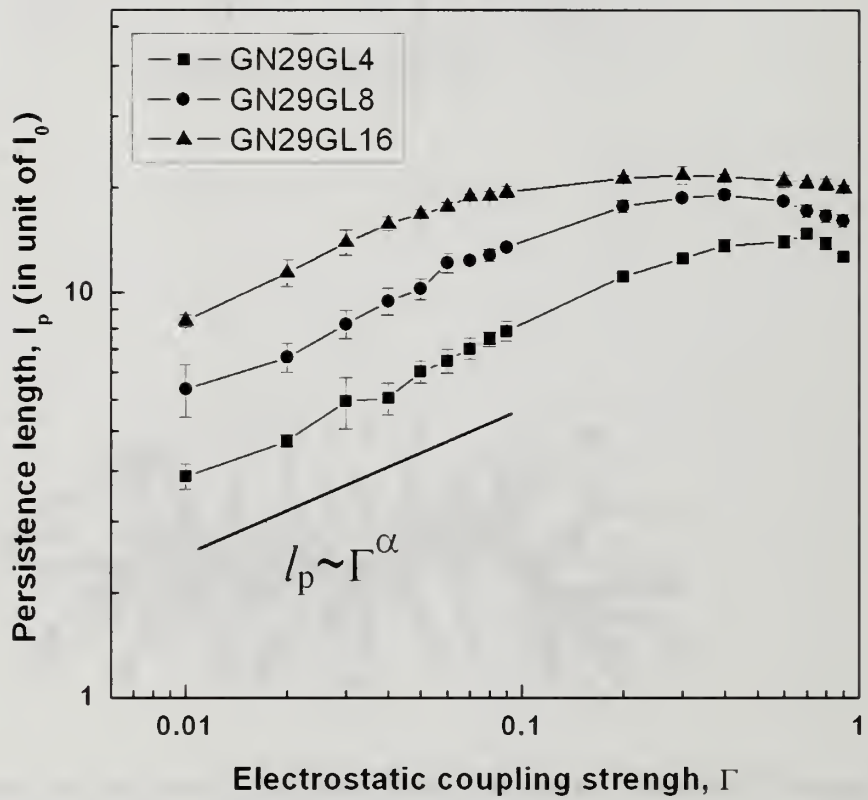

Figure 4.14 The dependence of main-chain persistence length (l_p) on electrostatic coupling strength of comb polyelectrolytes grated with side chains of different molecular weight. Side chain length (GL) varies from 4, 8 and 16 monomers. Every other monomer in the main-chain of comb polyelectrolyte is grafted with one side chain (GN=29). There are 60 monomer units in the main-chain of comb polyelectrolytes. Power-law fitting of l_p vs. Γ is done for Γ<0.1 and the results are tabulated in Table 4.3.

Table 4.3 Power-law exponents for l_p vs. Γ for different GL(Figure 4.14)

	GN=29,GL=4	GN=29,GL=8	GN=29,GL=16	Theory
α	0.34±0.01	0.35±0.01	0.36±0.02	0.33

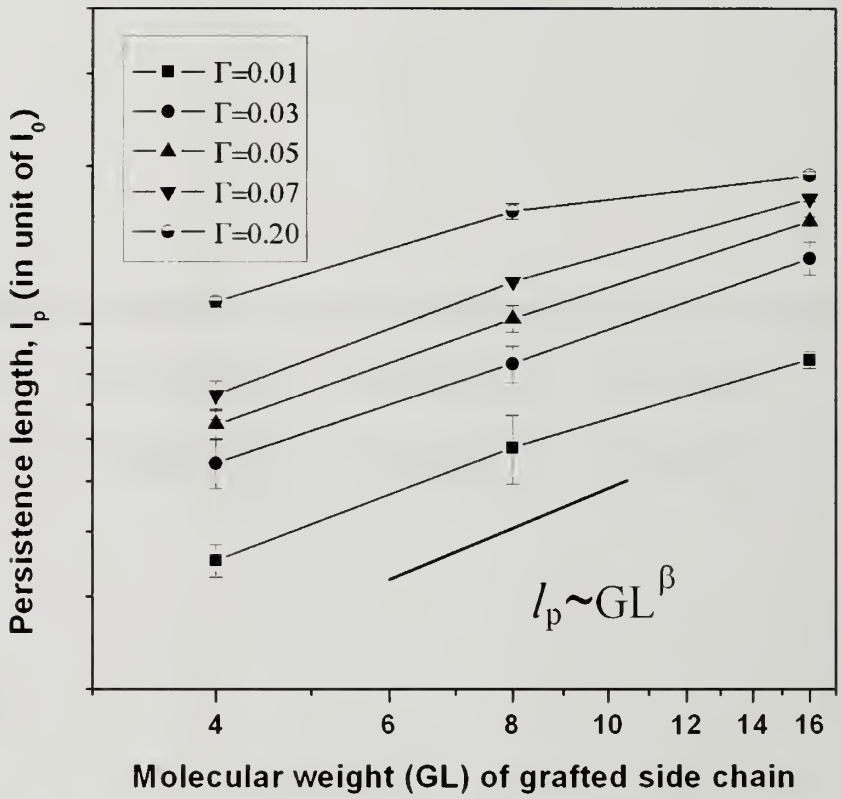

Figure 4.15 The scaling of main-chain persistence length (l_p) on the molecular weight of side chain (GL) in the weak electrostatic coupling strength limit (see Figure 4.14). There are 60 monomer units in the main-chain of comb polyelectrolytes. Every other monomer in the main-chain of comb polyelectrolyte is grafted with one side chain (GN=29). Side chain length (GL) varies from 4, 8 and 16 monomers. Table 4.4 summaries the power-law exponents for l_p vs. GL at different Γ.

Table 4.4 Power-law exponents for l_p vs. GL at different Γ (See Figure 4.15)

	Γ=0.01	Γ=0.03	Γ=0.05	Γ=0.07	Γ=0.20	Theory
β	0.64±0.06	0.65±0.05	0.64±0.04	0.55±0.02	0.4±0.02	0.67

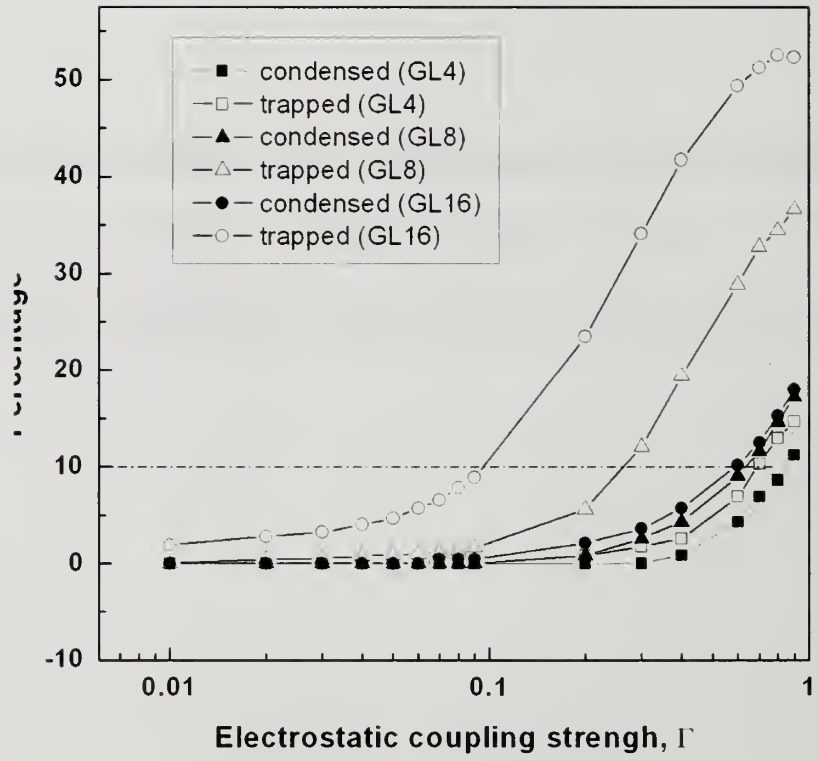

Figure 4.16 The evolutions of the percentages of trapped and condensed counterions in a comb polyelectrolyte as a function of Γ for comb polyelectrolytes of different side chain molecular weight (GL=4, 8, 16). All comb polyelectrolytes have the same number of side chains per chain, GN=29. The definitions for condensed and trapped counterions can be referred to both Figure 4.14(b) and in the text of this thesis.

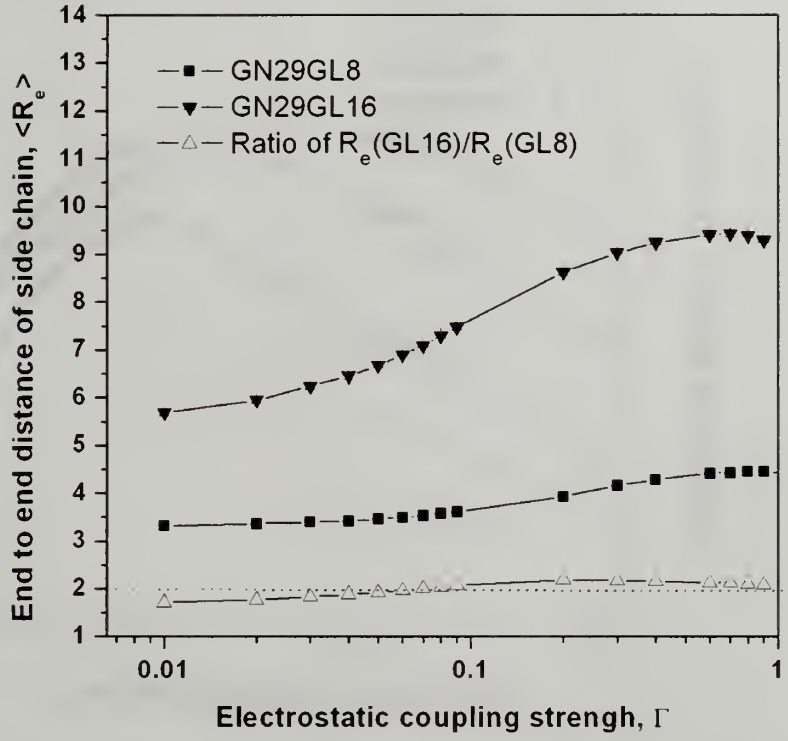

Figure 4.17 The averaged end-to-end distance, $<R_e>$ of side chains (GL=8 and GL=16) as a function of electrostatic coupling strength. The total number of side chain per comb polyelectrolyte is GN=29.

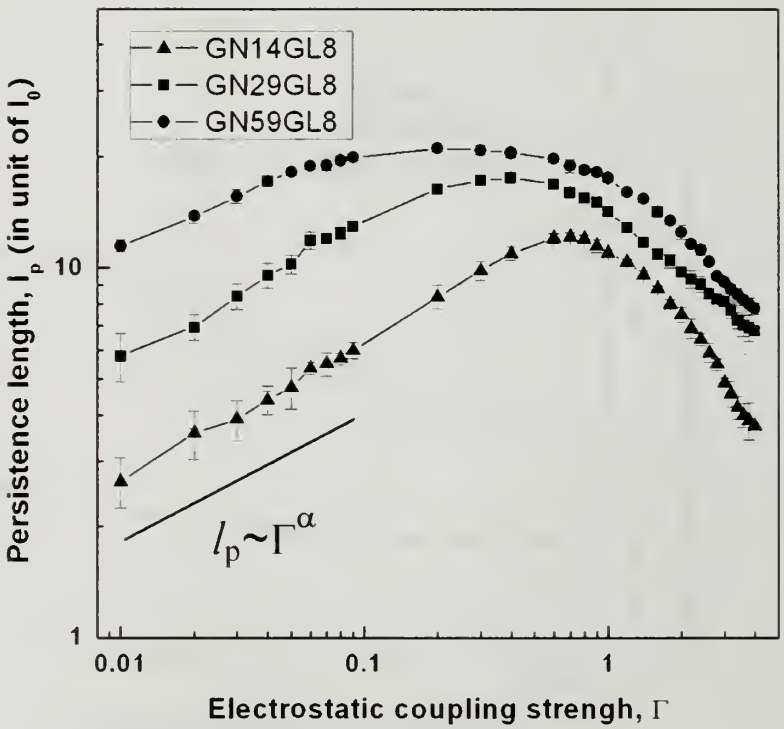

Figure 4.18 The dependence of main-chain persistence length (l_p) on electrostatic coupling strength of comb polyelectrolytes with different grafting densities of side chains (GN=14, 29, and 59). The molecular weight of side chain is fixed, GL=8. There are 60 monomer units in the main-chain of comb polyelectrolytes. Power-law fitting of l_p vs. Γ is done for $\Gamma<0.1$ and the results are shown in Table 4.5.

Table 4.5 Power-law exponents for l_p vs. Γ for different GN (See Figure 4.18)

	GN=14,GL=8	GN=29,GL=8	GN=59,GL=8	Theory
α	0.36±0.02	0.35±0.02	0.29±0.03	0.33

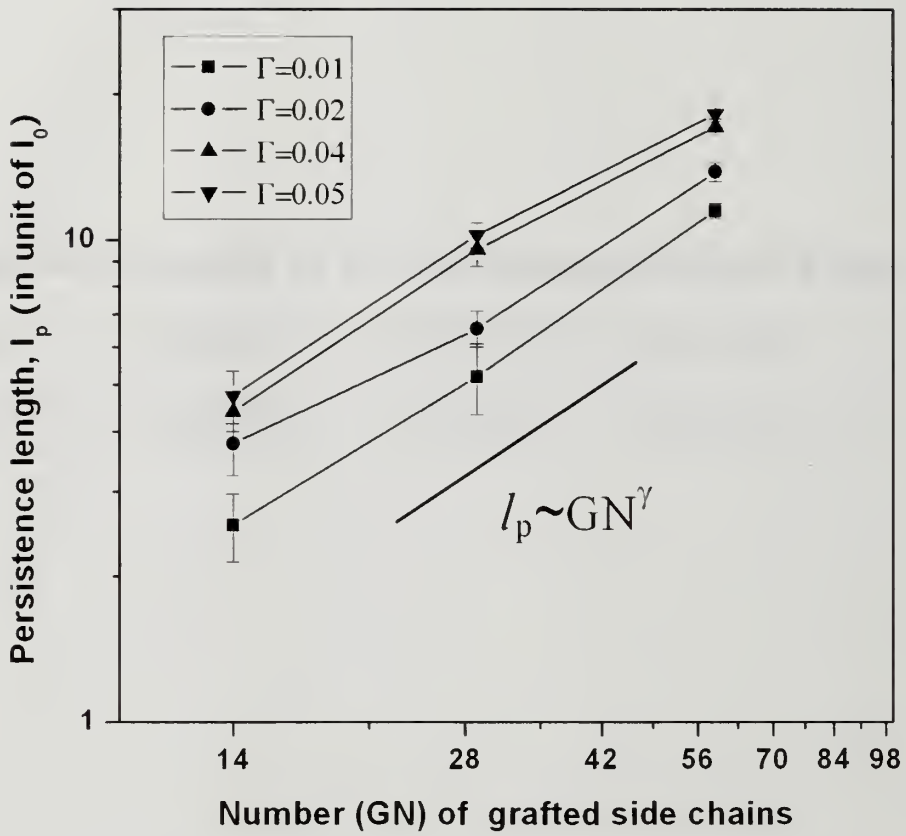

Figure 4.19 The scaling of main-chain persistence length (l_p) on side chain grafting density (GN=14, 29, and 59) in the weak electrostatic coupling strength limit (see Figure 4.18). There are 60 monomer units in the main-chain of comb polyelectrolytes. The length of side chains is fixed at GL=8. Table 4.6 summaries the power-law exponents for l_p vs. GN at different Γ.

Table 4.6 Power-law exponents for l_p vs. GN at different Γ (See Figure 4.19)

	Γ=0.01	Γ=0.02	Γ=0.04	Γ=0.05	Theory
$\overline{\gamma}$	1.06±0.11	0.96±0.09	0.92±0.06	0.87±0.06	1.0

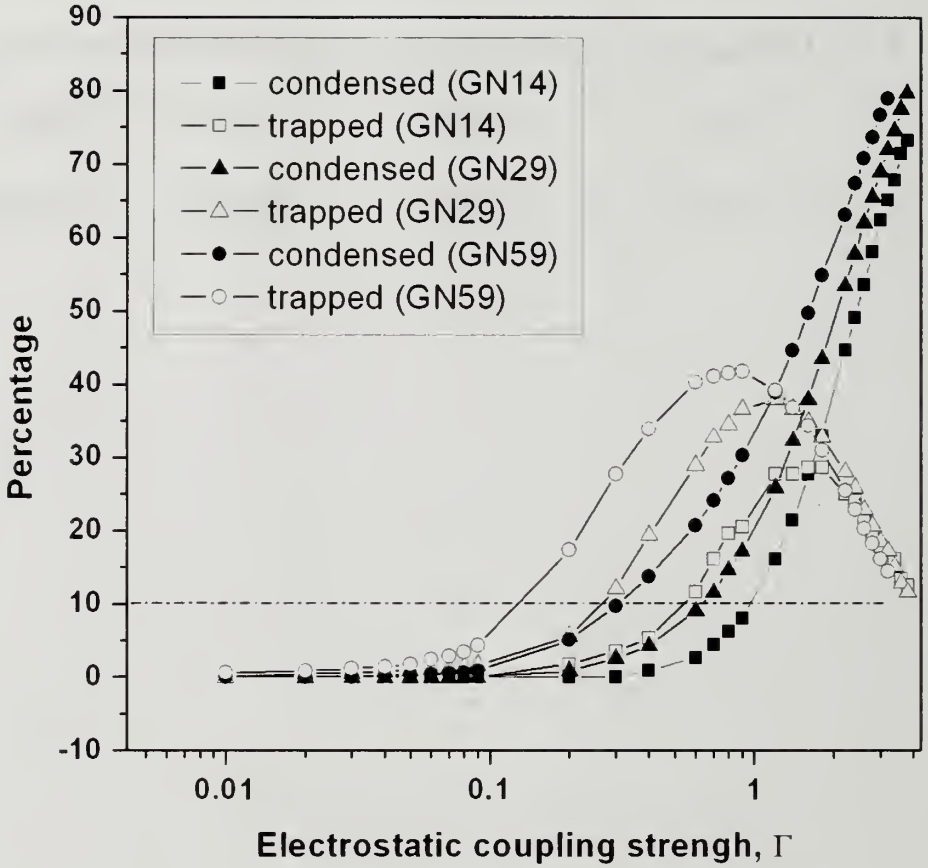

Figure 4.20 The evolutions of the percentages of trapped and condensed counterions in a comb polyelectrolyte as a function of Γ for comb polyelectrolytes with different side chain graft densities (GN=14, 29 and 59). The molecular weight of side chains is fixed at GL=8. The definitions for condensed and trapped counterions can be referred to both Figure 4.14(b) and the text of this thesis.

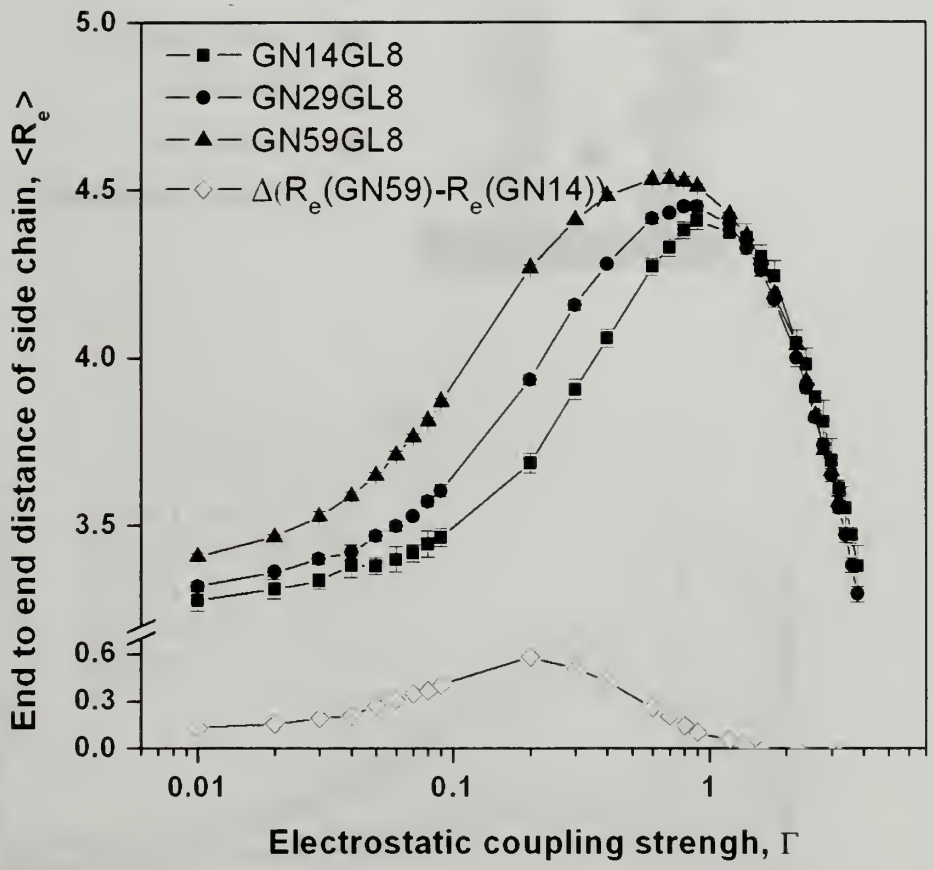

Figure 4.21 The averaged end-to-end distance, $\langle R_e \rangle$ of side chains (GL=8) as a function of electrostatic coupling strength. Three different side chain grafting densities were studied, GN=14, 29 and 59. The total number of beads in the main-chain of a comb polyelectrolyte is 60.

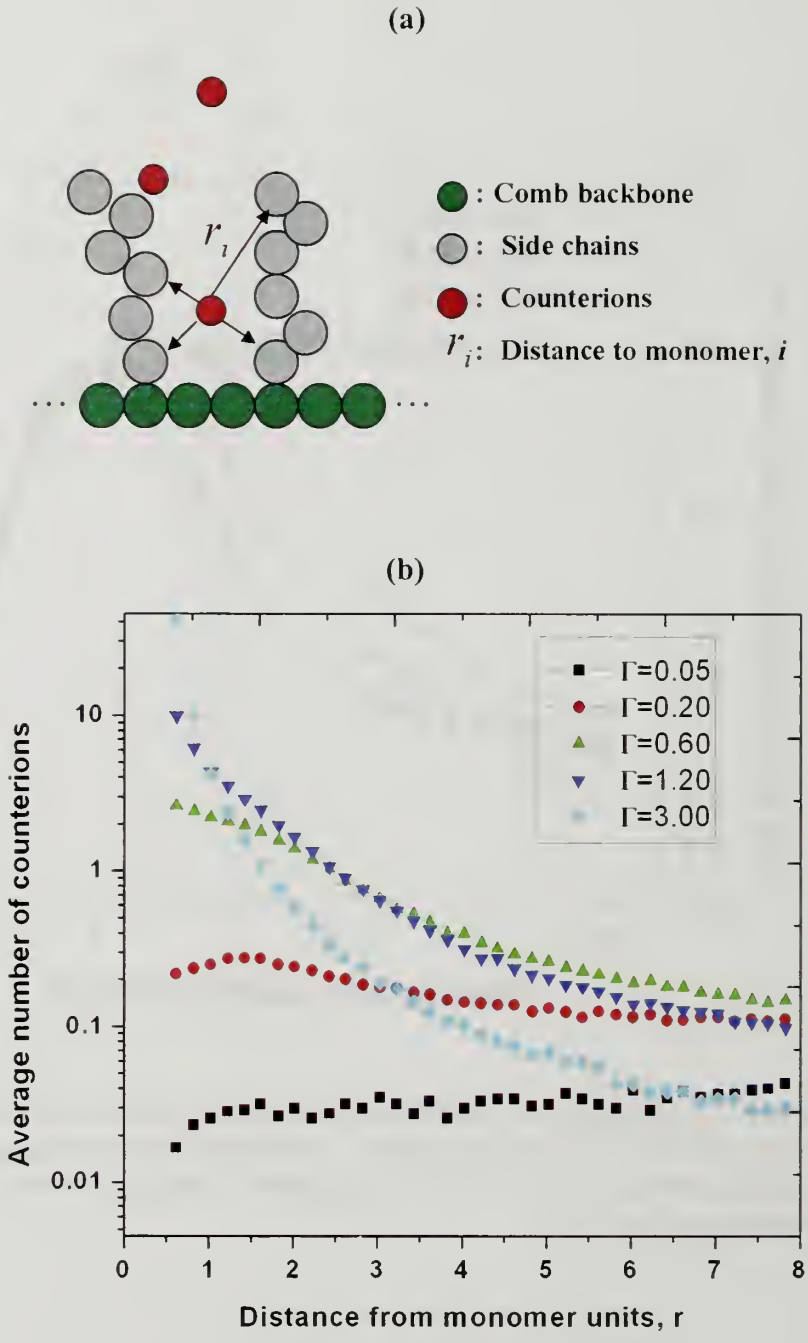

Figure 4.22 Counterion distribution around charged monomers of side chains as a function of Γ. (a) A schematic representation of the definition of the distance, r_i, of a counterion to the i^{th} monomer unit in side chains. The shortest of all r_i, is recorded for that particular counterion. Calculation of such shortest distance to side chain monomers is carried out for all counterions. (b) The distributions of such shortest distances are plotted as a function of the distance from monomer units at difference Γ.

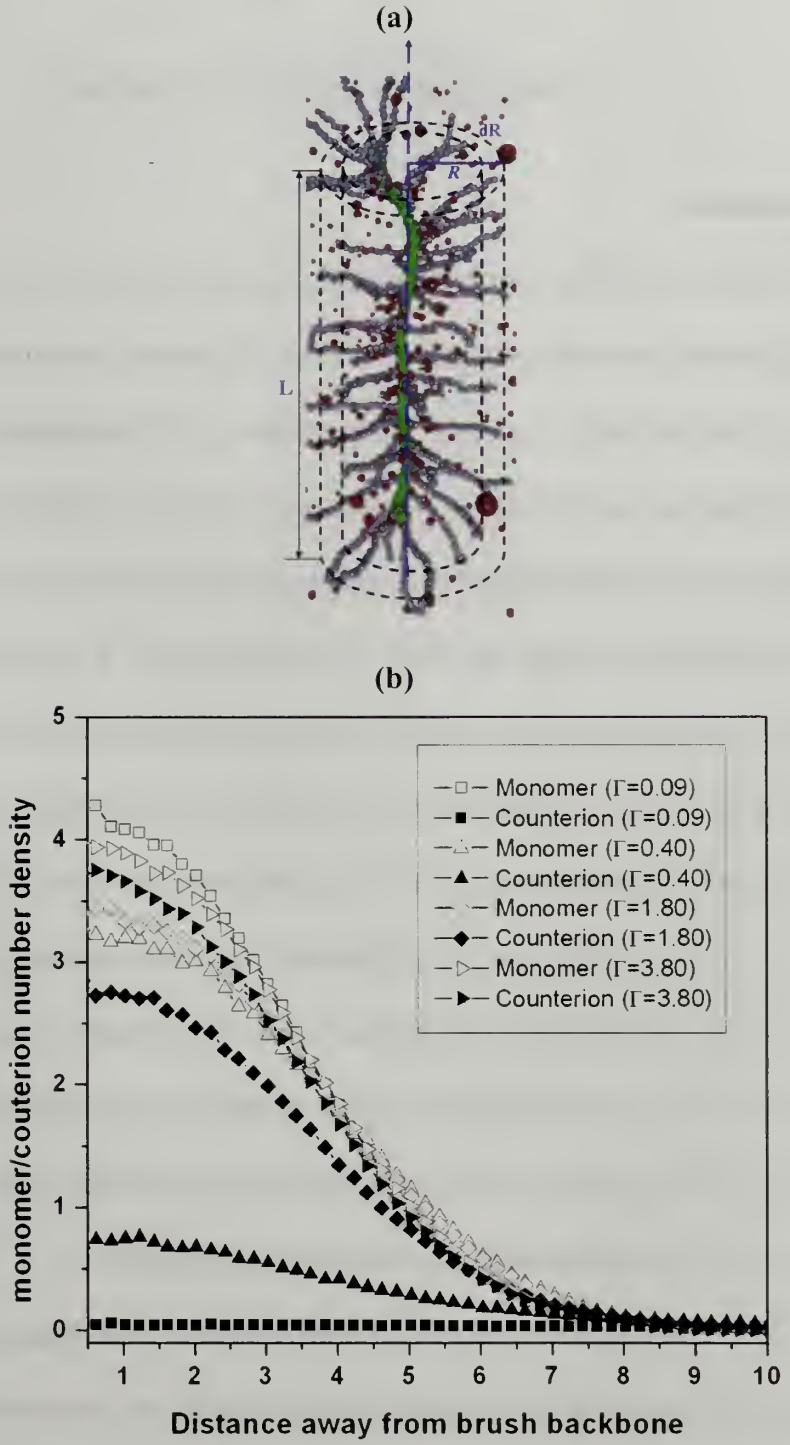

Figure 4.23 Counterion and side chain monomer density distribution of a comb polyelectrolyte as a function of Γ. (a) A schematic representation of how to determine the monomer and counterion density profiles away from the main-chain backbone in a comb polyelectrolyte. (b) Monomer and counterion density profiles away from comb backbone at different Γ.

CHAPTER 5

CONCLUSIONS AND FUTURE WORKS

5.1 Conclusions

In this dissertation, computer simulation has been proven to be a versatile and fruitful approach to fundamental understanding of structure, thermodynamics and kinetics of polyelectrolyte systems. We have shown with simulation that intriguing DNA condensation can be simply understood as the result of a delicate balance between bending a semi-flexible polyelectrolyte chain and electrostatic attraction mediated by multi-valent counterions that adsorb on the polyelectrolyte. We also uncovered in the simulation many kinetic features observed in experimental studies. Moreover, it was shown that non-trivial reorganization of adsorbed counterions plays an important role in determining the equilibrium size of a DNA toroid when the length of DNA increases. Simulation was extended to the complexation of polycations and polyanions, with focus on the enthalpic and entropic contributions to the complexation process. Contrary to the common beliefs, the complexation of highly charged polyelectrolytes is not driven by the mutual attraction between polycation and polyanion, but the large entropy gain from the lease of previously adsorbed counterions on polyelectrolytes.

Experimental characterizations, particularly static and dynamic light scattering, of polyelectrolytes and their complexes have provided many important messages regarding their size, shape and stability in both acquiescent conditions and in response to the changes in external stimuli such as pH and salt ionic strength. Specially, we have uncovered through extensive solution light scattering studies that a novel class of

polyelectrolytes, oligopeptide-grafted polyolefin adopts very intriguing extended "bottlebrush"-like conformations when the grafted oligopeptide side chains are fully charged. Both reducing the amount of charges of oligopeptide side chains through pH changes and increasing the solution ionic strength transforms the bottlebrush polyelectrolyte to a more flexible coil-like polymer. Complexation of such "bottlebrush" polyelectrolytes with dsDNA was demonstrated to produce stable nanosized colloidal dispersion with narrow size distribution. More interestingly, the size of such comb polyelectrolyte-DNA complexes can be finely adjusted by their mixing ratio, or by adjusting the amount of charges of oligopeptide side chains. It is of great interest that *in vitro* cell transfection assay has shown that dsDNA complexes by the comb polyelectrolyte achieved transfection efficiency comparable to those of commercial products, while lowering the cell toxicity at the same time. The unique place of charged side chains and the accompanying extended bottlebrush conformation could be of critical importance.

Motivated by the experimental observations of bottlebrush conformation of oligopeptide-grafted polyolefins, we have applied computer simulation to the electrostatic-mediated rigidity of general comb polyelectrolytes. We have found in our computer simulation studies that the rigidity of a comb polyelectrolyte is mainly due to inter-side chain electrostatic repulsion. Increasing side chain grafting density or side chain molecular weight generally results in a stiffer comb polyelectrolyte due to stronger the inter-side chain electrostatic repulsion. However, the benefits of having higher grafting density or longer side chains quickly diminish if side chains are polyelectrolytes of high charge density themselves, and/or comb polyelectrolyte is

immersed in strong electrostatics coupling medium, e.g., solvents of low dielectric constant.

5.2 Future works

Many interesting works can be envisioned from the standpoints of simulation and experiment on polyelectrolyte systems:

(1) What is the origin of finite-size DNA toroids or bundles? It was not possible to answer this question with the simplest model of bead-spring chain. However, the chirality of biopolymers (DNA, f-actin) may be a key thermodynamic control parameter for the aggregation of biopolymers. Incorporating more structure details (i.e., helix) into simulation is a natural step in furthering the simulation work in this dissertation and would help pave the ways for understanding other interesting biological phenomena.

(2) The equilibrium partitions of polycations and polyanion in a polyelectrolyte complexes. This is a very interesting problem fundamentally and practically, and can be pursued by both simulation and experiment. A large-scale long-time molecular simulation including hundreds of polyelectrolyte chains will be needed to provide both thermodynamics and kinetics of polyelectrolyte complex formation. The disparity in charge density and molecular weight of polycations and polyanions, the mixing ratio of polycations and polyanions, and the solution ionic strength can be systematically explored. A carefully chosen polyelectrolyte, with well-defined molecular characteristics, such as dsDNA, ssDNA and protein, could serve as model systems to experimentally investigate all those effects listed above.

(3) The complexation of comb polyelectrolytes with another polyelectrolyte of opposite charges. The conformational rigidity of comb polyelectrolytes should change how they form ion-pairs with linear-chain polyelectrolytes. A comb polyelectrolyte and a linearized version of it (a polyelectrolyte chain with the same amount of charges as that of the comb polyelectrolyte) will provide very interesting comparisons in their complexation behaviors (the size, stoichiometry, surface charge, and stability of the resultant polyelectrolyte complexes).

BIBILOGRAPHY

1. H. Ahrens, S. Forster, C. A. Hehn, N. A. Kumar, A. Naji, R. R. Netz, and C. Seidel, Journal of Physical Chemistry B 108, 16870 (2004).

2. W. F. Anderson, Nature 392, 25 (1998).

3. P. G. Arscott, A. Z. Li, and V. A. Bloomfield, Biopolymers 30, 619 (1990).

4. P. G. Arscott, C. L. Ma, J. R. Wenner, and V. A. Bloomfield, Biopolymers 36, 345 (1995).

5. T. Azzam, H. Eliyahu, L. Shapira, M. Linial, Y. Barenholz, and A. J. Domb, Journal of Medicinal Chemistry 45, 1817 (2002).

6. D. Baigl, R. Ober, D. Qu, A. Fery, and C. E. Williams, Europhysics Letters 62, 588 (2003).

7. D. Baigl, M. Sferrazza, and C. E. Williams, Europhysics Letters 62, 110 (2003).

8. M. Beer, M. Schmidt, and M. Muthukumar, Macromolecules 30, 8375 (1997).

9. K. L. Beers, S. G. Gaynor, K. Matyjaszewski, S. S. Sheiko, and M. Moller, Macromolecules 31, 9413 (1998).

10. K. Benihoud, P. Yeh, and M. Perricaudet, Current Opinion in Biotechnology 10, 440 (1999).

11. J. M. Benns, J. S. Choi, R. I. Mahato, J. S. Park, and S. W. Kim, Bioconjugate Chemistry 11, 637 (2000).

12. P. M. Biesheuvel and M. A. C. Stuart, Langmuir 20, 2785 (2004).

13. V. A. Bloomfield, Biopolymers 31, 1471 (1991).

14. V. A. Bloomfield, Current Opinion In Structural Biology 6, 334 (1996).

15. H. G. Borner, K. Beers, K. Matyjaszewski, S. S. Sheiko, and M. Moller, Macromolecules 34, 4375 (2001).

16. H. G. Borner, D. Duran, K. Matyjaszewski, M. da Silva, and S. S. Sheiko, Macromolecules 35, 3387 (2002).

17. V. Y. Borue and I. Y. Erukhimovich, Macromolecules 21, 3240 (1988).

18. C. Bottcher, C. Endisch, J. H. Fuhrhop, C. Catterall, and M. Eaton, Journal of the American Chemical Society 120, 12 (1998).

19. O. Boussif, F. Lezoualch, M. A. Zanta, M. D. Mergny, D. Scherman, B. Demeneix, and J. P. Behr, Proceedings Of The National Academy Of Sciences Of The United States Of America 92, 7297 (1995).

20. K. Breitenkamp, J. Simeone, E. Jin, and T. Emrick, Macromolecules 35, 9249 (2002).

21. T. Bronich, A. V. Kabanov, and L. A. Marky, Journal of Physical Chemistry B 105, 6042 (2001).

22. M. D. Brown, A. G. Schatzlein, and I. F. Uchegbu, International Journal of Pharmaceutics 229, 1 (2001).

23. H. M. Buchhammer, G. Petzold, and K. Lunkwitz, Langmuir 15, 4306 (1999).

24. G. L. Cheng, A. Boker, M. F. Zhang, G. Krausch, and A. H. E. Muller, Macromolecules 34, 6883 (2001).

25. G. A. Christos and S. L. Carnie, Journal of Chemical Physics 91, 439 (1989).

26. R. Connolly, G. Bellesia, E. G. Timoshenko, Y. A. Kuznetsov, S. Elli, and F. Ganazzoli, Macromolecules 38, 5288 (2005).

27. C. C. Conwell, I. D. Vilfan, and N. V. Hud, Proceedings of the National Academy of Sciences of the United States of America 100, 9296 (2003).

28. F. S. Csajka and C. Seidel, Macromolecules 33, 2728 (2000).

29. H. Dautzenberg, Macromolecules 30, 7810 (1997).

30. H. Dautzenberg and W. Jaeger, Macromolecular Chemistry and Physics 203, 2095 (2002).

31. M. E. Davis, Current Opinion in Biotechnology 13, 128 (2002).

32. G. Decher, Science 277, 1232 (1997).

33. L. Dekie, V. Toncheva, P. Dubruel, E. H. Schacht, L. Barrett, and L. W. Seymour, Journal of Controlled Release 65, 187 (2000).

34. J. DeRouchey, R. R. Netz, and J. O. Radler, European Physical Journal E 16, 17 (2005).

35. R. S. Dias, A. Pais, M. G. Miguel, and B. Lindman, Journal of Chemical Physics 119, 8150 (2003).

36. R. Djalali, N. Hugenberg, K. Fischer, and M. Schmidt, Macromolecular Rapid Communications 20, 444 (1999).

37. R. Djalali, S. Y. Li, and M. Schmidt, Macromolecules 35, 4282 (2002).

38. A. V. Dobrynin, R. H. Colby, and M. Rubinstein, Macromolecules 28, 1859 (1995).

39. A. V. Dobrynin, M. Rubinstein, and S. P. Obukhov, Macromolecules 29, 2974 (1996).

40. P. Dziezok, S. S. Sheiko, K. Fischer, M. Schmidt, and M. Moller, Angewandte Chemie-International Edition 36, 2812 (1997).

41. S. Elli, F. Ganazzoli, E. G. Timoshenko, Y. A. Kuznetsov, and R. Connolly, Journal of Chemical Physics 120, 6257 (2004).

42. B. D. Ermi and E. J. Amis, Macromolecules 31, 7378 (1998).

43. W. Essafi, F. Lafuma, and C. E. Williams, Journal De Physique Ii 5, 1269 (1995).

44. P. P. Ewald, Annalen Der Physik 64, 253 (1921).

45. D. Fischer, T. Bieber, Y. X. Li, H. P. Elsasser, and T. Kissel, Pharmaceutical Research 16, 1273 (1999).

46. K. Fischer and M. Schmidt, Macromolecular Rapid Communications 22, 787 (2001).

47. M. Fixman and J. Skolnick, Macromolecules 11, 863 (1978).

48. E. Flikkema and G. ten Brinke, Macromolecular Theory and Simulations 11, 777 (2002).

49. S. Forster, I. Neubert, A. D. Schluter, and P. Lindner, Macromolecules 32, 4043 (1999).

50. S. Forster and M. Schmidt, in *Physical Properties of Polymers* (1995), Vol. 120, pp. 51.

51. J. J. Freire, in *Branched Polymers Ii* (1999), Vol. 143, pp. 35.

52. W. B. Fu, X. L. Wang, X. H. Zhang, S. Y. Ran, J. Yan, and M. Li, Journal of the American Chemical Society 128, 15040 (2006).

53. M. O. Gallyamov, S. G. Starodubtsev, T. P. Bragina, L. V. Dubrovina, Potemkin, II, O. Marti, and A. R. Khokhlov, Macromolecular Chemistry and Physics 208, 164 (2007).

54. M. O. Gallyamov, B. Tartsch, A. R. Khoklov, S. S. Sheiko, H. G. Borner, K. Matyjaszewski, and M. Moller, Macromolecular Rapid Communications 25, 1703 (2004).

55. M. C. Garnett, Critical Reviews in Therapeutic Drug Carrier Systems 16, 147 (1999).

56. M. Gerle, K. Fischer, S. Roos, A. H. E. Muller, M. Schmidt, S. S. Sheiko, S. Prokhorova, and M. Moller, Macromolecules 32, 2629 (1999).

57. K. Ghosh, G. A. Carri, and M. Muthukumar, Journal of Chemical Physics 115, 4367 (2001).

58. W. T. Godbey, K. K. Wu, and A. G. Mikos, Journal of Biomedical Materials Research 45, 268 (1999).

59. P. Gonzalezmozuelos and M. O. Delacruz, Journal of Chemical Physics 103, 3145 (1995).

60. P. Guenoun, A. Schlachli, D. Sentenac, J. W. Mays, and J. J. Benattar, Physical Review Letters 74, 3628 (1995).

61. N. Gunari, M. Schmidt, and A. Janshoff, Macromolecules 39, 2219 (2006).

62. S. Hanski, N. Houbenov, J. Ruokolainen, D. Chondronicola, H. Iatrou, N. Hadjichristidis, and O. Ikkala, Biomacromolecules 7, 3379 (2006).

63. H. G. Hansma, R. Golan, W. Hsieh, C. P. Lollo, P. Mullen-Ley, and D. Kwoh, Nucleic Acids Research 26, 2481 (1998).

64. R. Hariharan, C. Biver, J. Mays, and W. B. Russel, Macromolecules 31, 7506 (1998).

65. Y. Hayashi, M. Ullner, and P. Linse, Journal of Chemical Physics 116, 6836 (2002).

66. Y. Hayashi, M. Ullner, and P. Linse, Journal of Physical Chemistry B 107, 8198 (2003).

67. Y. Hayashi, M. Ullner, and P. Linse, Journal of Physical Chemistry B 108, 15266 (2004).

68. S. Q. He, P. G. Arscott, and V. A. Bloomfield, Biopolymers 53, 329 (2000).

69. M. Hellmann, M. Weiss, and D. W. Heermann, Physical Review E 76 (2007).

70. P. Y. Hsiao, Macromolecules 39, 7125 (2006).

71. N. V. Hud and K. H. Downing, Proceedings Of The National Academy Of Sciences Of The United States Of America 98, 14925 (2001).

72. O. Ikkala and G. ten Brinke, Chemical Communications, 2131 (2004).

73. V. A. Ivanov, W. Paul, and K. Binder, Journal of Chemical Physics 109, 5659 (1998).

74. V. A. Ivanov, M. R. Stukan, V. V. Vasilevskaya, W. Paul, and K. Binder, Macromolecular Theory and Simulations 9, 488 (2000).

75. T. Iwaki, Journal of Chemical Physics 125, 6 (2006).

76. T. Iwaki, T. Saito, and K. Yoshikawa, Colloids and Surfaces B-Biointerfaces 56, 126 (2007).

77. S. Jha, S. Dutta, and N. B. Bowden, Macromolecules 37, 4365 (2004).

78. N. Karibyants, H. Dautzenberg, and H. Colfen, Macromolecules 30, 7803 (1997).

79. M. A. Kay, J. C. Glorioso, and L. Naldini, Nature Medicine 7, 33 (2001).

80. P. G. Khalatur, D. G. Shirvanyanz, N. Y. Starovoitova, and A. R. Khokhlov, Macromolecular Theory and Simulations 9, 141 (2000).

81. A. Kiriy, G. Gorodyska, S. Minko, W. Jaeger, P. Stepanek, and M. Stamm, Journal of the American Chemical Society 124, 13454 (2002).

82. M. Koping-Hoggard, I. Tubulekas, H. Guan, K. Edwards, M. Nilsson, K. M. Varum, and P. Artursson, Gene Therapy 8, 1108 (2001).

83. A. Kudlay and M. O. de la Cruz, Journal of Chemical Physics 120, 404 (2004).

84. N. A. Kumar and C. Seidel, Macromolecules 38, 9341 (2005).

85. K. Kunath, A. von Harpe, D. Fischer, and T. Kissel, Journal of Controlled Release 88, 159 (2003).

86. Y. A. Kuznetsov, E. G. Timoshenko, and K. A. Dawson, Journal of Chemical Physics 105, 7116 (1996).

87. S. Lecommandoux, F. Checot, R. Borsali, M. Schappacher, A. Deffieux, A. Brulet, and J. P. Cotton, Macromolecules 35, 8878 (2002).

88. F. D. Ledley, Human Gene Therapy 6, 1129 (1995).

89. E. S. Lee, H. J. Shin, K. Na, and Y. H. Bae, Journal of Controlled Release 90, 363 (2003).

90. Y. B. Lim, S. O. Han, H. U. Kong, Y. Lee, J. S. Park, B. Jeong, and S. W. Kim, Pharmaceutical Research 17, 811 (2000).

91. D. Liu, C. Wang, J. W. Li, Z. Lin, Z. K. Tan, and C. L. Bai, Journal of Biomolecular Structure & Dynamics 18, 1 (2000).

92. S. Liu, K. Ghosh, and M. Muthukumar, Journal of Chemical Physics 119, 1813 (2003).

93. S. Liu and M. Muthukumar, Journal Of Chemical Physics 116, 9975 (2002).

94. Y. Lu, Y. Mei, R. Walker, M. Ballauff, and M. Drechsler, Polymer 47, 4985 (2006).

95. T. Lundback and T. Hard, Journal of Physical Chemistry 100, 17690 (1996).

96. U. Lungwitz, M. Breunig, T. Blunk, and A. Gopferich, European Journal of Pharmaceutics and Biopharmaceutics 60, 247 (2005).

97. D. Luo, K. Haverstick, N. Belcheva, E. Han, and W. M. Saltzman, Macromolecules 35, 3456 (2002).

98. D. Luo and W. M. Saltzman, Nature Biotechnology 18, 33 (2000).

99. D. M. Lynn and R. Langer, Journal of the American Chemical Society 122, 10761 (2000).

100. C. L. Ma and V. A. Bloomfield, Biophysical Journal 67, 1678 (1994).

101. G. S. Manning, Journal of Chemical Physics 51, 924 (1969).

102. G. S. Manning, Quarterly Reviews Of Biophysics 11, 179 (1978).

103. H. Q. Mao, K. Roy, V. L. Troung-Le, K. A. Janes, K. Y. Lin, Y. Wang, J. T. August, and K. W. Leong, Journal of Controlled Release 70, 399 (2001).

104. A. L. Martin, M. C. Davies, B. J. Rackstraw, C. J. Roberts, S. Stolnik, S. J. B. Tendler, and P. M. Williams, Febs Letters 480, 106 (2000).

105. D. P. Mascotti and T. M. Lohman, Proceedings of the National Academy of Sciences of the United States of America 87, 3142 (1990).

106. D. P. Mascotti and T. M. Lohman, Biochemistry 36, 7272 (1997).

107. D. Matulis, I. Rouzina, and V. A. Bloomfield, Journal of Molecular Biology 296, 1053 (2000).

108. D. Matulis, I. Rouzina, and V. A. Bloomfield, Journal of the American Chemical Society 124, 7331 (2002).

109. G. Maurstad, S. Danielsen, and B. T. Stokke, Journal Of Physical Chemistry B 107, 8172 (2003).

110. G. Maurstad and B. T. Stokke, Biopolymers 74, 199 (2004).

111. G. Maurstad and B. T. Stokke, Current Opinion In Colloid & Interface Science 10, 16 (2005).

112. T. Merdan, J. Kopecek, and T. Kissel, Advanced Drug Delivery Reviews 54, 715 (2002).

113. R. Messina, C. Holm, and K. Kremer, Langmuir 19, 4473 (2003).

114. U. Micka, C. Holm, and K. Kremer, Langmuir 15, 4033 (1999).

115. A. Milchev, W. Paul, and K. Binder, Journal Of Chemical Physics 99, 4786 (1993).

116. M. Muthukumar, Journal of Chemical Physics 105, 5183 (1996).

117. M. Muthukumar, Journal Of Chemical Physics 120, 9343 (2004).

118. A. Naji, R. R. Netz, and C. Seidel, European Physical Journal E 12, 223 (2003).

119. M. W. Neiser, J. Okuda, and M. Schmidt, Macromolecules 36, 5437 (2003).

120. L. Ng, A. J. Grodzinsky, P. Patwari, J. Sandy, A. Plaas, and C. Ortiz, Journal of Structural Biology 143, 242 (2003).

121. G. Nisato, R. Ivkov, and E. J. Amis, Macromolecules 33, 4172 (2000).

122. C. K. Nisha, S. V. Manorama, M. Ganguli, S. Maiti, and J. N. Kizhakkedathu, Langmuir 20, 2386 (2004).

123. M. Nishikawa and L. Huang, Human Gene Therapy 12, 861 (2001).

124. H. Noguchi, S. Saito, S. Kidoaki, and K. Yoshikawa, Chemical Physics Letters 261, 527 (1996).

125. H. Noguchi and K. Yoshikawa, Journal of Chemical Physics 109, 5070 (1998).

126. H. Noguchi and K. Yoshikawa, Journal of Chemical Physics 113, 854 (2000).

127. T. Odijk, Macromolecules 12, 688 (1979).

128. M. Ohsaki, T. Okuda, A. Wada, T. Hirayama, T. Niidome, and H. Aoyagi, Bioconjugate Chemistry 13, 510 (2002).

129. F. Oosawa, Biopolymers 6, 1633 (1968).

130. Z. Y. Ou and M. Muthukumar, Journal of Chemical Physics 123, 9 (2005).

131. Z. Y. Ou and M. Muthukumar, Journal of Chemical Physics 124, 11 (2006).

132. D. W. Pack, A. S. Hoffman, S. Pun, and P. S. Stayton, Nature Reviews Drug Discovery 4, 581 (2005).

133. V. Panchagnula, J. Jeon, and A. V. Dobrynin, Physical Review Letters 93 (2004).

134. S. Y. Park, D. Harries, and W. M. Gelbart, Biophysical Journal 75, 714 (1998).

135. V. Percec, C. H. Ahn, G. Ungar, D. J. P. Yeardley, M. Moller, and S. S. Sheiko, Nature 391, 161 (1998).

136. C. Perez, A. Sanchez, D. Putnam, D. Ting, R. Langer, and M. J. Alonso, Journal of Controlled Release 75, 211 (2001).

137. H. Petersen, P. M. Fechner, A. L. Martin, K. Kunath, S. Stolnik, C. J. Roberts, D. Fischer, M. C. Davies, and T. Kissel, Bioconjugate Chemistry 13, 845 (2002).

138. B. Philipp, H. Dautzenberg, K. J. Linow, J. Kotz, and W. Dawydoff, Progress in Polymer Science 14, 91 (1989).

139. C. W. Pouton and L. W. Seymour, Advanced Drug Delivery Reviews 34, 3 (1998).

140. V. M. Prabhu, M. Muthukumar, G. D. Wignall, and Y. B. Melnichenko, Polymer 42, 8935 (2001).

141. V. M. Prabhu, M. Muthukumar, G. D. Wignall, and Y. B. Melnichenko, Journal of Chemical Physics 119, 4085 (2003).

142. S. W. Provencher, Computer Physics Communications 27, 213 (1982).

143. S. W. Provencher, Computer Physics Communications 27, 229 (1982).

144. D. Putnam and R. Langer, Macromolecules 32, 3658 (1999).

145. S. Rathgeber, T. Pakula, A. Wilk, K. Matyjaszewski, and K. L. Beers, Journal of Chemical Physics 122 (2005).

146. S. Rathgeber, T. Pakula, A. Wilk, K. Matyjaszewski, H. I. Lee, and K. L. Beers, Polymer 47, 7318 (2006).

147. T. Reschel, C. Konak, D. Oupicky, L. W. Seymour, and K. Ulbrich, Journal of Controlled Release 81, 201 (2002).

148. K. Rittner, A. Benavente, A. Bompard-Sorlet, F. Heitz, G. Divita, R. Brasseur, and E. Jacobs, Molecular Therapy 5, 104 (2002).

149. P. D. Robbins and S. C. Ghivizzani, Pharmacology & Therapeutics 80, 35 (1998).

150. Y. Rouault and O. V. Borisov, Macromolecules 29, 2605 (1996).

151. J. Ruhe, M. Ballauff, M. Biesalski, P. Dziezok, F. Grohn, D. Johannsmann, N. Houbenov, N. Hugenberg, R. Konradi, S. Minko, M. Motornov, R. R. Netz, M. Schmidt, C. Seidel, M. Stamm, T. Stephan, D. Usov, and H. N. Zhang, in *Polyelectrolytes with Defined Molecular Architecture I* (2004), Vol. 165, pp. 79.

152. U. Rungsardthong, T. Ehtezazi, L. Bailey, S. P. Armes, M. C. Garnett, and S. Stolnik, Biomacromolecules 4, 683 (2003).

153. M. Saariaho, A. Subbotin, I. Szleifer, O. Ikkala, and G. ten Brinke, Macromolecules 32, 4439 (1999).

154. M. Saariaho, I. Szleifer, O. Ikkala, and G. ten Brinke, Macromolecular Theory and Simulations 7, 211 (1998).

155. A. K. Salem, P. C. Searson, and K. W. Leong, Nature Materials 2, 668 (2003).

156. J. M. G. Sarraguca and A. Pais, Physical Chemistry Chemical Physics 8, 4233 (2006).

157. J. M. G. Sarraguca, M. Skepo, A. Pais, and P. Linse, Journal of Chemical Physics 119, 12621 (2003).

158. G. C. Schatz, Proceedings of the National Academy of Sciences of the United States of America 104, 6885 (2007).

159. T. Schindler and E. Nordmeier, Polymer 40, 7019 (1999).

160. H. Schlaad, H. Kukula, B. Smarsly, M. Antonietti, and T. Pakula, Polymer 43, 5321 (2002).

161. B. Schnurr, F. Gittes, and F. C. MacKintosh, Physical Review E 65 (2002).

162. B. Schnurr, F. C. MacKintosh, and D. R. M. Williams, Europhysics Letters 51, 279 (2000).

163. M. Sedlak, Journal of Chemical Physics 105, 10123 (1996).

164. C. Seidel, Macromolecules 36, 2536 (2003).

165. S. S. Sheiko and M. Moller, Chemical Reviews 101, 4099 (2001).

166. L. J. Shu, A. D. Schluter, C. Ecker, N. Severin, and J. P. Rabe, Angewandte Chemie-International Edition 40, 4666 (2001).

167. F. J. Solis and M. O. de la Cruz, Journal of Chemical Physics 112, 2030 (2000).

168. D. Srivastava and M. Muthukumar, Macromolecules 27, 1461 (1994).

169. T. Stephan, S. Muth, and M. Schmidt, Macromolecules 35, 9857 (2002).

170. M. J. Stevens and K. Kremer, Journal of Chemical Physics 103, 1669 (1995).

171. M. R. Stukan, V. A. Ivanov, A. Y. Grosberg, W. Paul, and K. Binder, Journal of Chemical Physics 118, 3392 (2003).

172. A. Subbotin, M. Saariaho, R. Stepanyan, O. Ikkala, and G. ten Brinke, Macromolecules 33, 6168 (2000).

173. M. Takahashi, K. Yoshikawa, V. V. Vasilevskaya, and A. R. Khokhlov, Journal of Physical Chemistry B 101, 9396 (1997).

174. Z. J. Tan and S. J. Chen, Nucleic Acids Research 34, 6629 (2006).

175. Z. J. Tan and S. J. Chen, Biophysical Journal 91, 518 (2006).

176. J. X. Tang, J. A. Kas, J. V. Shah, and P. A. Janmey, European Biophysics Journal With Biophysics Letters 30, 477 (2001).

177. J. X. Tang, S. E. Wong, P. T. Tran, and P. A. Janmey, Berichte Der Bunsen-Gesellschaft-Physical Chemistry Chemical Physics 100, 796 (1996).

178. A. F. Thunemann, M. Muller, H. Dautzenberg, J. F. O. Joanny, and H. Lowne, in *Polyelectrolytes with Defined Molecular Architecture Ii* (2004), Vol. 166, pp. 113.

179. P. Tsolakis and G. Bokias, Macromolecules 39, 393 (2006).

180. M. Ueda and K. Yoshikawa, Physical Review Letters 77, 2133 (1996).

181. I. D. Vilfan, C. C. Conwell, T. Sarkar, and N. V. Hud, Biochemistry 45, 8174 (2006).

182. H. Votavova, D. Kucerova, J. Felsberg, and J. Sponar, Journal of Biomolecular Structure & Dynamics 4, 477 (1986).

183. I. Wataoka, H. Urakawa, K. Kajiwara, M. Schmidt, and M. Wintermantel, Polymer International 44, 365 (1997).

184. Y. F. Wei and P. Y. Hsiao, Journal of Chemical Physics 127, 14 (2007).

185. P. Welch and M. Muthukumar, Macromolecules 31, 5892 (1998).

186. J. Widom and R. L. Baldwin, Journal of Molecular Biology 144, 431 (1980).

187. C. M. Wiethoff and C. R. Middaugh, Journal of Pharmaceutical Sciences 92, 203 (2003).

188. R. W. Wilson, D. C. Rau, and V. A. Bloomfield, Biophysical Journal 30, 317 (1980).

189. R. G. Winkler, M. Gold, and P. Reineker, Physical Review Letters 80, 3731 (1998).

190. R. G. Winkler, M. O. Steinhauser, and P. Reineker, Physical Review E 66 (2002).

191. M. Wintermantel, M. Gerle, K. Fischer, M. Schmidt, I. Wataoka, H. Urakawa, K. Kajiwara, and Y. Tsukahara, Macromolecules 29, 978 (1996).

192. J. K. Wolterink, J. van Male, M. Daoud, and O. V. Borisov, Macromolecules 36, 6624 (2003).

193. Y. Y. Xu, H. Becker, J. Y. Yuan, M. Burkhardt, Y. Zhang, A. Walther, S. Bolisetty, M. Ballauff, and A. H. E. Muller, Macromolecular Chemistry and Physics 208, 1666 (2007).

194. Y. Yamasaki, Y. Teramoto, and K. Yoshikawa, Biophysical Journal 80, 2823 (2001).

195. A. Yethiraj, Physical Review Letters 78, 3789 (1997).

196. A. Yethiraj, Journal of Chemical Physics 125 (2006).

197. A. Yethiraj and C. Y. Shew, Physical Review Letters 77, 3937 (1996).

198. A. N. Zelikin, N. I. Akritskaya, and V. A. Izumrudov, Macromolecular Chemistry and Physics 202, 3018 (2001).

199. A. F. Zhang, B. Zhang, E. Wachtersbach, M. Schmidt, and A. D. Schluter, Chemistry-a European Journal 9, 6083 (2003).

200. B. Zhang, K. Fischer, and M. Schmidt, Macromolecular Chemistry And Physics 206, 157 (2005).

201. B. Zhang, F. Grohn, J. S. Pedersen, K. Fischer, and M. Schmidt, Macromolecules 39, 8440 (2006).

202. B. Zhang, S. J. Zhang, L. Okrasa, T. Pakula, T. Stephan, and M. Schmidt, Polymer 45, 4009 (2004).

203. L. Zhang, W. Li, and A. Zhang, Progress in Chemistry 18, 939 (2006).

204. M. F. Zhang, T. Breiner, H. Mori, and A. H. E. Muller, Polymer 44, 1449 (2003).

205. M. F. Zhang, C. Estournes, W. Bietsch, and A. H. E. Muller, Advanced Functional Materials 14, 871 (2004).

206. M. F. Zhang and A. H. E. Muller, Journal of Polymer Science Part a-Polymer Chemistry 43, 3461 (2005).

207. R. Zhang and B. T. Shklovskii, Physica a-Statistical Mechanics and Its Applications 352, 216 (2005).

208. Y. Zhang, X. K. Li, G. H. Deng, and Y. M. Chen, Macromolecular Chemistry and Physics 207, 1394 (2006).

209. Y. B. Zhang, J. F. Douglas, B. D. Ermi, and E. J. Amis, Journal of Chemical Physics 114, 3299 (2001).